DOCTORAL SCHOOL
MEDITERRANEAN UNIVERSITY OF REGGIO CALABRIA

DEPARTEMENT OF INFORMATION ENGINEERING, INFRASTRUCTURE AND SUSTAINABLE ENRGY (DIIES)

PHD IN
INFORMATION ENGINEERING

S.S.D. ING-INF/07
XXXVI CICLO

BEAMFORMING TECHNIQUE: SENSOR ARRAY/ANTENNA ARRAY SYSTEMS ESSENTIAL FOR SIGNAL PROCESSING: DETECTION, CLASSIFICATION, AND SUPPRESSION

CANDIDATE
John Peter DJUNGHA OKITADIOWO

ADVISOR
Prof. Tommaso ISERNIA, Prof. Aimé LAY-EKUAKILLE

COORDINATOR
Prof. Antonella MOLINARO

REGGIO CALABRIA, APRIL 2024

Finito di stampare nel mese di Aprile 2024

Edizione Centro Stampa d'Ateneo

Università degli Studi *Mediterranea* di Reggio Calabria
Via dell'Università, 25 (già Salita Melissari) - Reggio Calabria

John Peter DJUNGHA OKITADIOWO

BEAMFORMING TECHNIQUE: SENSOR ARRAY/ANTENNA ARRAY SYSTEMS ESSENTIAL FOR SIGNAL PROCESSING: DETECTION, CLASSIFICATION, AND SUPPRESSION

The Teaching Staff of the PhD course in
INFORMATION ENGINEERING

Antonella MOLINARO (coordinator)
Giuseppe ARANITI
Francesco BUCCAFURRI
Claudia CAMPOLO
Riccardo CAROTENUTO
Giuseppe COPPOLA
Mariantonia COTRONEI
Lorenzo CROCCO
Dominique DALLET
Claudio DE CAPUA
Francesco DELLA CORTE
Giuliana FAGGIO
Gioia FAILLA
Fabio FILIANOTI
Patrizia FRONTERA
Sofia GIUFFRÈ
Giorgio GRADITI
Voicu GROZA
Tommaso ISERNIA
Gianluca LAX
Aimè LAY EKUAKILLE
Gaetano LICITRA
Elena Simona LOHAN
Pietro MANZONI
Francesco Carlo MORABITO
Andrea Francesco MORABITO
Giacomo MORABITO
Rosario MORELLO
Gabriel-Miro MUNTEAN
Giuseppe MUSOLINO
Fortunato PEZZIMENTI
Filippo Gianmaria PRATICÒ
Sandro RAO
Maria ROMANO
Domenico ROSACI
Giuseppe RUGGERI
Mariateresa RUSSO
Alexey VINEL
Antonino VITETTA
Maria Gabriella XIBILIA

I. Dedication

The thesis is dedicated to:

To YHWH,
To my parents Pierre DJUNGHA Okitadiowo and Théthé OTETE
To my future family,
To Professor Aimé Lay-Ekuakille,
To professor Tomasso Isernia
To all Professors working in the DIIES Department,
To all friends and colleagues.

John Peter DJUNGHA OKITADIOWO

II. Acknowledgement

I am grateful to Professor Aimé LAY-EKUAKILLE, Professor Tommaso ISERNIA, my thesis supervisors, and Professor Antonella MOLIRANO, PhD school coordinator, for their assistance during my research. This attempt was supported by his availability and wise counsel.

John Peter DJUNGHA OKITADIOWO

III. Abstract

Wireless technology has emerged as a significant domain of research within the field of telecommunications systems over the last ten years. The exponential growth of this domain necessitates the integration of all close disciplines, especially signal processing, with telecommunications. It is obvious that both the technological and natural worlds generate signals in their all aspects; therefore, in order to get a deeper knowledge of these fields, it is imperative that we efficiently interpret their signals. This entails the ability to distinguish, separate, and classify each component of the signal with the objective of eliminating undesired components.

In order to solve this issue, we implemented the beamforming method and its associated algorithms on the sensor array and antenna array in this study. The purpose of this study is to provide a comprehensive illustration of the significant advancements in telecommunication. It is no longer sufficient to merely transmit and receive signals; rather, it is possible to apply telecommunication and its algorithms to environmental signal processing (for monitoring and protection of the environment) and medical signal processing, particularly in the domain of electrocardiography (ECG).

Keywords: Beamforming, Signal, Target, Sensors, Antenna, Measurements for Telecommunication, MUSIC, MVDR, LMS, Technique, Noise, Suppression, Interference, Deviation, Smart Antenna, Adaptive Filtering, Environmental Measurement, Electrocardiography, Noise Zoning.

CONTENTS

IV. List of Figures

V. List of tables

VI. List of abbreviations

3GPP:	3rd Generation Partnership Project
4G:	4th generation mobile network
5G:	5th generation mobile network
AA:	Antenna array
AF:	Array factor
BF:	Beamforming
BS:	Base station
CCET:	Cyclic correlation eigenvalue test
CNN:	Convolutional neural network
D2D:	Device-to-Device
DaS:	Delay and Sum
DB:	Database
dB:	Decibel
DMSSF:	Delay-multiply-sum-to-standard-deviation-factor
DOA:	Direction of arrival of the signal
DP:	Doppler processing
DUE:	Device user end
DWT:	Discrete wavelets transform
ECG:	Electrocardiogram
Enb:	Evolved Node B
ESPRIT:	Estimation of Signal Parameters via Rational Invariance Techniques
E-to-E:	Equipment to equipment
UE:	User Equipment
EWT:	Empirical wavelets transform
fECG:	Foetal electrocardiogram
FIR:	Finite impulse response
gNB:	Signal quality at Node B
GNSS:	Global Navigation Satellite System
i.e:	example provided
IAHS:	International Association of Hydrological Sciences
IC:	Interference cancellation
LCMV:	Linear constraint minimum variance
LMD:	Minimum description length
LMS:	Least mean squares
LTE:	Long-term evolution
MAC:	Medium access control
MCC:	Matthew correlation coefficient
MEC:	Multi-access edge computing
mECG:	Maternal electrocardiogram
MEMD:	Multivariate Empirical Mode Decomposition
MIMO:	Multiple-input and multiple-output
MTI:	Moving target indication
MUSIC:	Multiple Syndicate Classification
MVDR:	Minimum Variance Distortionless Response

NBS:	**Node base station**
NIR:	Noise-to-interference ratio
NR:	New 5G radio
OFDM:	Orthogonal frequency-division multiplexing
PET:	Potential evapotranspiration
PHY:	Physical layer
QRS:	Quick response system
RAN:	Radio Access Network
RBMP:	River Basin Management Plan
ReLu:	Rectified Linear Unit
RF:	Radio frequency
SAR:	Synthetic aperture radar
SGD:	Stochastic gradient descent
SNR:	Signal-to-Noise Ratio
SOT:	Spatial-only therapy
STAT:	Adaptive space-time treatment
STFT:	Short-Time Fourier Transform
SVM:	Support Vector Machine
TDAO:	Time difference of the direction of arrival of the signal
TTD:	True time delay
ULA:	Uniform Linear Array
UWB:	Ultra-wideband
Vm:	Velocity by meter
VNRGC:	Vehicles on roads in good condition
VNPC:	Vehicles on roads in poor condition
WFD:	Water Framework Directive
WGN:	White Gaussian noise
WLAN:	Wireless LAN
WWTPs:	Wastewater treatment plants
WWTP:	Wastewater treatment plant

Part: I
In broad terms

Chapter 1

1. General Information

1.1. Introduction

The field of antenna technology refers to the domain of signal processing. It involves the processing of signals that are received, conditioned, and sampled by sensor arrays including an antenna. When discussing signal processing in the context of antennae, which are made up by sensors, the process involves the optimisation of signal reception downstream of the antennae by emphasising several parameters. It is worth noting that the criteria for differentiating the components of the desired signal from those of undesirable signals may differ within the domain of antennas [1], [2], [3].

Researchers are currently developing novel antenna designs that incorporate advanced signal processing techniques and methodologies. These advancements have resulted in the emergence of new applications in diverse fields that demand enhanced signal precision. Examples of such fields include medical imaging, military applications, communications, navigation, detection (such as radar and sonar), astronomy, space observation, seismography, astrophysics, and more [4], [5].

The discipline of signal modelling has undergone continuous evolution, driven by the objective of achieving greater fidelity to reality within the specific domain of signal processing. As previously said, the objective of signal processing is to extract the pertinent or valuable information from a signal that is combined with noisy information through the utilisation of beamforming (BF) technique and its associated filters. In the contemporary telecommunications industry, the primary objective is to enhance the efficiency of signal transmission between the transmitter and receiver by successfully

reducing interference noise and directing the signal towards where it is intended. The BF strategy has been identified as the most effective approach for resolving this particular issue. The study aims to accomplish two main objectives. The first objective involves the filtration, detection, separation, classification, and removal of the signal components and the characteristics associated with the undesirable signal. The second objective focuses on the regeneration, optimisation, amplification, conduction, and directing of the signal towards the desired target terminal equipment.

The outcomes of BF technique include the estimation of the direction of arrival of the signal (DOA), determination of the time difference of the direction of arrival of the signal (TDOA) detection, suppression of noise, and mitigation of signal interference. The BF technique employs spatial or spatiotemporal filters to align the output of an evaluated transmitting antenna with the intended noisy signal coming from an anomalous axis [6]- [7].

The utilisation of BF technique has become common throughout several fields, encompassing radar, sonar, wireless communications, medicinal imaging, and military domains [8]- [9].

Sensor networks use spatial filtering (BF) to send or receive directional signals. Combining antenna array elements so that signals at certain angles connect constructively and others destructively achieves this. Transmitting and receiving beamforming can accomplish spatial selectivity. Array directivity superiors omnidirectional reception and transmission. BF can transmit radio or sound waves. Radar, sonar, seismology, wireless communications, radio astronomy, acoustics, and biomedicine use it. At the output of a sensor array, adaptive beamforming detects and estimates the signal of interest using optimal spatial filtering (e.g., least squares) and interference rejection.

Beamforming approaches use a variety of highly robust and efficient algorithms, which include the following: MUSIC, LMS and MVDR.

1.2. The Multiple Signal Classification

Multiple Signal Classification (MUSIC) technique is a sophisticated approach for determining the direction of a signal source. It manages this by decomposing the eigenvalues of the sensor covariance matrix at the network level, resulting in an excellent quality prediction. The MUSIC algorithm is included under the family of subspace-based direction-finding algorithms. The sensor data can be successfully linked with signals originating from the source due to the usage of the signal paradigm. Considering $s_d(l)$ is a signal obtained from P independent or partially linked sources. The network-received signals are part of the sensor data $x_m(l)$, together with the noise $n_m(l)$. When T nodes in a network collect data at time l, we call this "taking a snapshot" of the sensor data.

$$x(l) = Ms(l) + n(l) \tag{1-1}$$

$$s(l) = [s_1(l), s_2(l), ..., s_P(l)]' \tag{1-2}$$

$$M = [m(\theta_1 \mid m(\theta_2 \mid ...\theta_P)] \tag{1-3}$$

According to (1.1-1.3) $x(l)$ is a vector T per sensor data samples that contains the signals and additive noise that were received. M is an T-by-P matrix holding arrival vectors. For a single-source plane wave, the relative phase shifts at the various array elements constitute the arrival vector.

The arrival vector of every single source is represented by one of the columns in matrix M, but largely depends on the arrival direction, θ_d. The variable θ_d indicates the angle of arrival for the dth source, which can indicate either the broadside angle for linear arrays or the azimuth and elevation angles for planar or 3D arrays. $s(l)$ is a P-by-1 vector of source signal values from P sources. $n(l)$ is an T-by-1 vector of sensor noise values [10]- [11].

1.3. Least Mean Squares

Least mean squares (LMS) algorithms are adaptive filters that resemble desirable filters by identifying filter coefficients that minimise the difference between the desired and real signal. It is a stochastic gradient descent approach that simply adapts the filter to the current error. The Fig. 1.1 1depicts filter sections [12], [13].

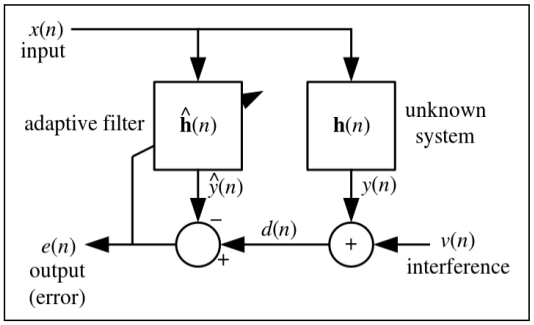

Figure 1-1LMS filter sections

The input signal x is modified by an unknown filter h, which we aim to match with h. Unknown filter output y is interfered with by noise signal ν, resulting in $d = y + \nu$. After computing the error signal $e = y - d = y - y - \nu$, the adaptive filter adjusts its settings to minimise the mean square of the error signal e.

Especially in signal processing, the causal Wiener filter is similar to the least squares estimate. For input matrix X and output vector Y, the least squares solution is: $\beta = (X^T X)^{-1} y$, The FIR least mean squares filter has characteristics comparable to the Wiener filter, except its error criteria does not use cross- or auto-correlations. Converges to Wiener filtering answer. Figure 1 can be used to formulate most linear adaptive filtering problems.

The adaptive filter tries to adapt the filter $h(n)$ to be as near as feasible to $h(n)$ using only visible signals $x(n)$, $d(h)$, and $e(n)$, but not $y(n)$, $v(n)$, or $h(n)$. Wiener filters are similar to its solution. Current input sample number is n, the filters tap quantity is p. $h(n)$ determines filter coefficients after *n* samples.

The fundamental concept underlying the LMS filter is the approximation of ideal filter weights through iterative updates, with the objective of achieving convergence towards the optimal filter weight. The approach utilised in this study is grounded on the principles of the gradient descent method. The procedure initiates by assuming initial weights, typically set to zero or modest values. At each iteration, the gradient of the mean square error is computed, and the weights are subsequently modified. Put simply, when the gradient of the mean squared error (MSE) is positive, it indicates that the error will persistently increase in a positive manner if the same weight is employed for subsequent iterations. Consequently, it becomes necessary to diminish the weights. Likewise, in the event that the gradient exhibits a negative value, it becomes necessary to augment the weights [14]- [15].

1.4. Minimum Variance Distortionless Response

Minimum Variance Distortionless Response (MVDR) algorithm is a commonly used beamforming technique that adjusts a weighting factor in order to achieve an agreed-upon amount of output power while reducing interference and noise [16], [17].

The MVDR approach has the capability to identify and mitigate both interference and noise, but under the condition of a high Signal-to-Noise Ratio (SNR) and low noise levels. Nevertheless, the efficient functioning of MVDR relies on the direction vectors, which are contingent upon the angle of incidence of the signal received from each element of the antenna array. It is imperative to have knowledge of the direction of the intended signal, and to ensure that the output power is limited to unity gain in the direction of the desired signal.

In order to achieve MVDR BF, it is imperative to reduce the energy of the interfering signal while simultaneously maintaining the unaffected characteristics of the source signal.

$$V_{MVDR}(f) = \frac{\arg\min V^H}{V}(f)\Phi_{XX}(f)V(f) \tag{1-4}$$

$$s.j.V(f)^H d(f) = 1 \tag{1-5}$$

In (1.4 – 1.5) establish that the Φ_{XX} denotes the covariance matrix of the noisy Short-Time Fourier Transform (STFT) X inside the frequency range f. The resolution pertaining to the MVDR approach, specifically regarding the choice of the reference channel, can be expressed as equation 6.

$$V_{MVDR}(f) = \frac{\Phi_{RR}^{-1}(f)\Phi_{PP}(f)}{Trace(\Phi_{RR}^{-1}(f)\Phi_{PP}(f))}k \tag{1-6}$$

Φ_{PP}^{-1} and Φ_{PP} are noise covariance matrices, while k is the reference channel vector. The covariance matrix Φ_{PP} of the intended signal can be calculated using the following eq. (1.7):

$$\Phi_{PP}(f) = \frac{\sum_{j=1}^{J}\hat{s}(j,f)P^H(j,f)}{\sum_{j=1}^{J}N_P(j,f)N_P(j,f)} \tag{1-7}$$

$$P(j,f) = N_P(j,f)X(j,f)$$

N_P is the target signal time-frequency mask. Estimating the covariance matrix of Φ_{XX} is similar to replacing the signal mask N_P. Since the signal is not always present in frames, Φ_{PP} is normalised by the sum of mask powers instead of the number of frames j. Estimating of the MVDR becomes estimating the time-frequency masks of the noisy STFT [18]- [19].

The presented thesis has been organised into four distinct parts: The first part concerns in broad terms, it is splitted into two chapters.

The first chapter: We mentioned antenna processing technology, which is signal processing. Signal processing in sensor-based antennas was also examined. Several signal characteristics are used to optimise upstream antenna signal reception. We concluded with parameters for distinguishing desired signal components from antenna-domain unwanted signals.

The second chapter: The second chapter focuses on the specific features of BF technical technique, encompassing its distinctive characteristics, signal

processing and optimisation techniques, as well as its various applications and associated advantages and limits. The second part is dedicated to simulation and data monitoring and comprises the third and fourth chapters. The third chapter concentrates on the antenna sensor, a sensor array designed to detect the quality and quantity of noise pollution. It proposes a simulation and data monitoring of a BF-based antenna sensor for sound direction of arrival (DOA) detection.

The fourth chapter is dedicated to distinguishing and separating noise components, using signals (noise) to deduce invisible events, processing signals to reveal hidden realities in signal envelopes, and using a BF antenna and its associated system with algorithms to distinguish between vehicle noise on a road that is in good shape and one that is in poor condition. The third part is delegated to BF-Processing: detection, suppression, and recovery of signal characteristics.

The fifth chapter: Centres around maintaining a decent signal path during transmission, particularly in radio transmissions employing the BF technique. The BF technique is applied to an antenna array's signal. BF is a technique of tracking and directing the signal path from the antenna transmission to the target (user device) by detecting and removing all interfaces and noise that may deviate the signal from its predefined direction.

The sixth chapter: The emphasis is on the application of the BF technique in the processing of electrocardiogram (ECG) signals. Specifically, the aim is to extract the foetal electrocardiogram (fECG) signals from the raw maternal electrocardiogram (mECG) signals using algorithms based on BF. The fourth part characterises delay and sum motion to derive hydrodynamic signal characteristics and components. The seventh chapter demonstrates how to extract features from a river video using the BF technique and a beamforming approach based on modified sum and delay, such as velocity, water flow, temperature, depth, wave motion, and riverbed recognition.

Chapter 2

2. Concept of Beamforming

2.1 Introduction

Beamforming is an approach within the realm of antenna processing, so it holds significant importance [42], [20]. Its use extends to the identification and mitigation of interference. The aforementioned methodology is also employed for estimation of signals and directions of arrival (DOA). Beamforming is used in various industries, including radar, wireless communications, passive listening, and biomedical imaging, due to its extensive range of applications. The main goal of this technique is finding a spatial filter that produces an output representing an approximation of the desired signal originating from a specific direction, which may be distorted by interference and the presence of Gaussian noise [21]- [22].

This part of this research encompasses an in-depth investigation of the beamforming technique in the linear domain, as well as an assessment of the diverse methodologies employed for optimal conventional linear and adaptive beamforming in the context of stationary and circular signals.

The chapter covers several key components: a comprehensive baseband model, an analysis of the received signals, an examination of their second-order statistics, and an exploration of beamforming techniques and the corresponding filters.

2.2 Approach to narrow band modelling

Within the field of telecommunications, electromagnetic waves propagate through an environment that can exhibit homogeneity, resulting in a constant propagation speed denoted as c.

In certain instances, within a communication system, it is possible for the transmitter to be situated at a considerable distance from the receiving antenna. This occurrence of distance might give rise to the utilisation of a plane wave model, which assumes that the rays seen by sensors are parallel to each other. An antenna array of N sensors pick up a signal focused on a complicated target with a carrier frequency f_0 and bandwidth H.

The complex envelope of the current signal at time p is $s(p)$. Demodulation at the transmitting antenna result indicates the desired signal observation vector without background noise:

$$s(p) = \begin{bmatrix} s(p-P_1)e_X^{i2\pi f_0}P_1 \\ s(p-P_2)e_X^{i2\pi f_0}P_2 \\ \vdots \\ s(p-P_N)e_X^{i2\pi f_0}P_N \end{bmatrix} \qquad (2\text{-}1)$$

Let us denote T_n as the radiation delay pertaining to the resultant signal of sensor n in regard to the reference sensor. When the signal moves inside a narrow band relative to the connection time, the transverse time of the sensor array can be disregarded. The connection time of the signal is equivalent to the negative value of the bandwidth. In essence, it can be postulated that the multidimensional envelope remains constant throughout the network traversal, resulting in (2.1) being modified as follows:

$$S(p) = s(p)\begin{bmatrix} e^{-i2\pi f_0}P_1 \\ e^{-i2\pi f_0}P_2 \\ \vdots \\ e^{-i2\pi f_0}P_N \end{bmatrix},$$

It is important to acknowledge:

$$S = \begin{bmatrix} e^{-i2\pi f_0} P_1 \\ e^{-i2\pi f_0} P_2 \\ \vdots \\ e^{-i2\pi f_0} P_N \end{bmatrix},$$

The directional vector of the target signal, denoted as S, coincides with the intended signal:

$$S(p) = s(p)S.$$

2.3 Traditional received signal prototype

Consider a hypothetical scenario where there exists an antenna with N sensors that operate within a small frequency band. These sensors are designed to receive signals from M different paths originating from multiple directions. Additionally, the received signals are subject to spatially white, Gaussian noise that is centred and follows a circular distribution of second order.

The vector $\times(p)$ represents the complex amplitudes of the signals received at the output of the sensors. Every sensor in the system receives the combined input of the desired signal, together with a composite noise that consists of interference and a Gaussian, concentrated, and circular background noise. Given these specified assumptions and the absence of any carrier residue, the vector of observations denoted as $\times(p)$ can be described in the way that follows:

$$\times(p) = s(p)S + n(p) \qquad (2\text{-}2)$$

In the (2.2); the parameters $s(p)$ and S represent the complex envelope, which is assumed to have a mean of zero, and the directional vector of the desired signal, with a first component equal to 1. The variable $n(p)$ represents the total noise vector, consisting of interference signals and Gaussian noise, with a mean of zero. The noise vector is statistically uncorrelated with the desired signal $s(p)$ and may exhibit non-circularity up to second order.

The second-order statistics of the observation $X(p)$ are fully defined by honouring the first and second covariance matrices $R_x(p,\tau)$ and $C_x(p,\tau)$ such that for all ranges p,τ

$$R_x(p,\tau) \triangleq < E\left[X(p)X(p-\tau)^N \right] > \tag{2-3}$$

however

$$D_x(p,\tau) \triangleq < E\left[X(p)X(p-\tau)^M \right] > \tag{2-4}$$

The requirements for the second-degree stage arrays of the noise $n(p)$ are provided. Using <> to establish equilibrium over a period of time.

$$R_n(p,\tau) \triangleq < E\left[n(p)n(p-\tau)^N \right] > \tag{2-5}$$

however

$$D_n(p,\tau) \triangleq < E\left[n(p)n(p-\tau)^M \right] > \tag{2-6}$$

Once the vector $X(p)$ is considered, the non-circularity of venerate $n(p)$ is maintained under the conditions $D_x(p,\tau) \neq 0$ and $D_n(p,\tau) \neq 0$ for at least one single combination p,τ. Let us rectify the spatial covariance matrices for τ = 0 below.

$$R_x \triangleq < E[X(p)X(p)^N] >= \pi_i ii^N + R_n = R_i + R_n \tag{2-7}$$

$$C_x \triangleq < E[X(p)X(p)^M] >= \pi_i \gamma_i ii^M + D_n = D_i + D_n \tag{2-8}$$

With eq. (2.7-2.8); when $R_n = \pi_i ii^N$, $D_x = \pi_i \gamma_i ii^M$, The initial and second covariance matrix numbers of the intended signal are considered honorary, The equilibrium force exerted by the initial sensor of the target signal is: $\pi_i \triangleq E[|i(p)|^2] >$. The value denoted as $\gamma_i \triangleq \dfrac{< E[i(p)^2] >}{< E[|i(p)|^2] >} \triangleq |\gamma_i| e^{l2\phi i}$ signifies the coefficient, which acts as a representative measure of the intended signal. This is analogous to how the circular phase is represented by ϕi. $R_n \triangleq < E[n(p)n(p)^N] >$ and $D_n \triangleq < E[n(p)n(p)^M] >$ is the covariance matrix

1 and 2 of the global noise. When both matrices R_x and R_n have full ranks, it indicates the presence of background noise.

2.4. Beamforming and signal processing techniques

Signal processing using beamforming, referred to as spatial filtering, beamforming, or channel forming, is used in antenna and sensor arrays for focused transmission or reception. Beamforming uses sensor arrays to boost signals across any number of directions and remove noise and interference across another in a networked signal processing method.

Beamforming improves signal-to-noise ratios, eliminates interference, and concentrates transmitted signals. Beamforming is crucial in sensor network systems, especially 5G, LTE, and WLAN MIMO wireless communication systems.

Wireless applications can utilise MIMO beamforming to boost data flow between base stations and user devices. Wireless communication systems are increasingly using optimization-based beamforming. Hybrid beamforming uses optimisation to efficiently divide base band and RF system topologies to minimise costs [23]- [24].

2.4.1 Beamforming: spatial filtering

Beamforming, often referred to as spatial filtering, is an established technique in signal processing. The aforementioned technique pertains to a signal processing methodology employed for the purpose of transmitting or receiving radio or sound waves in a focused directional manner. Beamforming is a technique that finds applications in various fields such as radar and sonar systems, wireless communication, acoustics, and medicinal devices.

Beamforming and beam scanning are often employed techniques in the field of telecommunications to efficiently guide signals in a specified direction by ensuring that every part of a network receive or send signals that are in phase.

During the process of transmission, beamforming is employed to regulate the magnitude and relative amplitude of the signal sent by each transmitter. This results in the creation of a wavefront design that incorporates both positive and

negative interference, so enhancing the overall effectiveness of the transmission [25].

Beamforming is a well-established technique used to achieve desired antenna radiation patterns by manipulating the transmitted signals towards targeted receivers while reducing interference from other sources [25].

The generation of this can be achieved through the utilisation of a finite impulse response (FIR) filter. Finite impulse response (FIR) filters possess the advantageous characteristic of allowing for flexible manipulation and combination of their weights, hence facilitating the attainment of appropriate beamforming.

As demonstrated in Fig. 1.1, EA is the shown object serves as an electrical amplifier, as seen from visual observation. ,T is how long the carrier frequency will be present, and τ denotes the propagation time.

Fig. 2.1 depicts a network of uniform dimensions. The factor denoted as array factor (AF) in conjunction with true time delay (TTD) is commonly expressed in the following manner, as depicted in (2.9):

$$AF(\theta, f) = \sum_{i=0}^{I-1} A_i \exp\left[l \frac{2\pi fld}{s} (-\sin\theta + \frac{s\tau}{p}) \right] \quad (2\text{-}9)$$

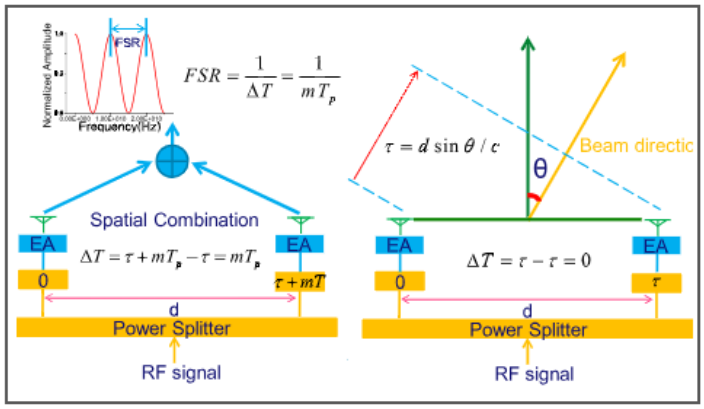

Figure 2-1 The Application of Beamforming for Spatial Filtering [26]

The observation angle denoted as θ in Fig. 2.1, is related to the frequency of the microwave signal, represented by f. The quantity of antenna elements is denoted by I, while p and τ represent the distance and delay between two

adjacent antenna elements. The amplitude weights for antenna element i are represented by A_i, with a value of 1 showing the same linear array. The maximisation of AF can be enhanced by incorporating suitable amplitude weightings.

2.4.2 Application of beamforming

Beamforming is a signal processing technique that is employed to manipulate the direction of an electromagnetic wave by utilising an array of sensors. This approach allows for the steering, shaping, and focusing of the wave towards a specific desired direction.

The utilisation of this technology has been observed in various engineering domains, including radar, sonar, acoustics, astronomy, seismology, medical imaging, and communications.

Beamforming harmoniously aggregates sensor network signals to enhance detection. Conventional beamforming applies set weights, while adaptive uses environment-dependent weights. Beamforming narrow-band signals usually involves multiplying sensor inputs by a complex exponential with the right phase shift.

2.4.2.1 Benefits of beamforming technology

The beamforming technique provides many benefits that find application in many different fields. In this context, we shall outline a few of them, which include:

- BF is useful for millimetre-wave bands. Using unused frequency bands near the millimetre wave range is the only way to increase data prices in the frequency domain for a dense urban cellular connection since most of the spectrum below 5 GHz is licenced. (60 GHz).
- Beamforming must control the signal sent to the customer, in order that only the receiver is able to recover the requested signal from the cover signal,

- Reduced power needs, Low-cost beamforming antennas convey messages to the targeted client and use less power and amplifiers than huge MIMO frames,
- Capability is increased by controlling the power of upward and downward signalling signals, using training sequence information, and developing signal quality with beamforming antenna components,
- Using time division duplexing (TDD) to restore traditional omnidirectional antenna arrays with sectored dynamic cells and beam-steering antenna arrays has improved wireless system traffic implementation,
- Beamforming, instead of omnidirectional antennas at the BS level, improves dynamic cell sectorization efficiency, according to simulations,
- Beamforming must control the signal sent to the customer, so only the receiver can restore the requested signal from the masking signal,

2.4.2.2 Beamforming efficiency

It is essential to note that the very first phases of obtaining the necessary performance of a wireless or radar communications system involve the improvement of beamforming techniques and the assessment of alternative algorithms. Beamforming must be integrated into a system-level model and tested against parameter, direction, and channel combinations. The system-level trade-offs between RF and digital baseband beamforming are another issue. Better to do all these things early in the design phase. The Massive MIMO Hybrid Beamforming with RF Troubles sample shows how RF influences affect beamforming performance.

Part: II
Simulation and Data Monitoring

Chapter **3**

3. Beamforming antenna: framework for the noise environmental detection

3.1 Introduction

Every municipality should restrict noise from vehicle, rail, and air traffic, industrial activity, and recreation. Noise pollution affects human health and activities. However, noise pollution should be monitored using sophisticated sensors that can distinguish noise kinds. Sensor arrays can incorporate the antenna sensor, which measures noise quality and quantity. We design and simulate a beamforming antenna sensor to detect DOA noise.

The most important objective is to reduce noise pollution in cities with or near transportation infrastructure (airport, rail, and road). By building an antenna and calibrating filters to pick up the sound signals released by trucks, trains, and other engines that can reach decibel levels that are harmful to the human ear, using antennas with LF can assist solve the problem of monitoring noise pollution. Sensor antennas have remarkable properties that can be used to solve the problem of noise pollution, with the goal of reducing noise in particular places to protect humans from noise pollution.

The strategy consists of restricting the noise level of cars on highways that pass through protected zones [27] by placing antennae at entry points for collecting noise signals from vehicles, trains, and other destroying engines. The acquired signals are processed in real time in the system's database (DB) using BF algorithms. When a vehicle is moving forward and its engine emits a dB level higher than that calibrated in the antenna filters, the driver will see a message displayed instantly on the road sign "Passing prohibited: follow the left or right

deviation"; if the dB level is lower, a message will display "Continue on the road". The antennae naturally have sensors that detect vehicle sound signals when engine noise exceeds the system's filters' dB level.

Residential areas, schools, hospitals, universities, nursing homes, research centres, and other sites sensitive to dangerous noise that could disrupt peace and quiet, concentration, and smooth operations are targeted for noise reduction. Because its filters let through more noise than intended, the monitoring system is designed in time slots to let through vehicles whose engines interfere in specific areas [28]. Designing complex antenna elements and arrays with intelligent partitioning of the BF systems to collect sound signals and process them in real time to determine if they are below, equal to, or above the zone allowed driving level is crucial. The simulations are executed in MatLab to improve noise pollution monitoring.

3.2 Environment monitoring using beamforming antennas

The transmitter and receiver can use spatial filtering called BF, which comes from pencil-shaped directional antennas. Typically, BF filters signals with overlapping frequencies but different spatial locations. Since transmission is complicated by channel changes, BF requires knowledge of the target signal's DOA or DOA delay and transmission parameters. Since this metric is unknown, we can estimate it using our data. The parameters may change over time; thus, an adaptive FB algorithm sets them.

These algorithms are subdivided into two basic classes which are: block adaptation and continuous adaptation. The block adaptation algorithm estimates the parameters charged from a temporal block of array data, where the continuous adaptation adjusts the parameters upon receipt of the data so that these converge to the optimum solution. Phased array versus delayed array [29], a wavefront arriving at an antenna array under an arrival direction (DOA) introduces an arrival delay to each individual antenna. This delay between two adjacent antennas, ΔT depends on the DOA and the antenna spacing according to $d \sin(DOA) = c\Delta T$ d being the distance between the antennas, and c the speed of light.

Fig. 3.1 illustrates an example of DOA application. The BF is a delay compensatory method that implements an ideal delay element on the reception path, its elements are very difficult to implement, so to cope with this difficulty; it consists of translating the time difference into phase shift in the frequency domain [30]. When the signal we want consists of a single frequency the delay can be replaced with phase shift Δp using

$$\Delta p = 2\pi \Delta T f_0 \tag{3-1}$$

$$\Delta p = 2\pi \frac{d}{c} \sin(DOA) f_0 \tag{3-2}$$

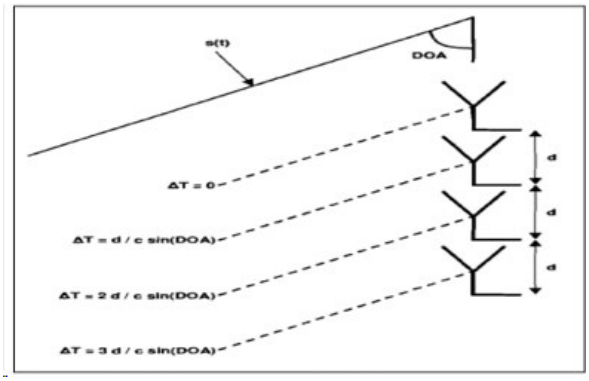

Figure 3-1A relationship between DOA and timing for the linear antenna array.

Calculate a signal phase shift using a single frequency using (3.1-3.2). When the desired signal has a higher bandwidth, (3.3) introduces phase distortion. This distortion will be reduced if the signal bandwidth is narrow compared to the carrier frequency. Signal representation, making use of the relationship between DOA and antenna spacing, a representation of the received signal can be derived, gives the complex envelope of the received baseband signal. In the updated equation, θ_k , is the phase shift caused by the delay of the signal received at the antenna k. If the signal $r_k(t)$ is the signal received at the antenna k under DOA β, θ_k can be expressed as:

$$\theta_k = \theta_1 + (k-1)2\pi \frac{d \sin(\beta)}{\lambda} \tag{3-3}$$

Considering the accelerating development of telecom technologies like 5G, BF antennas are vital. This technology has enormous potential that we must quickly understand and use in other areas, like environmental monitoring.

3.2.1 The development of beamforming

Compared to the previous generations, which could only broadcast and receive [31] on predefined radiation patterns, this new generation of BF antennas produces its main beam and blank beam directions dynamically based on the user's position. New impulse comes from BF antennas. The technology improves telecommunications by reducing interference, signal-to-noise ratio (SNR), and end-user experience. BF antennas come in many configurations and capacities to suit different environments. These antennas may look different, but all BF architectures use an active or passive network structure, digital, analogue, or hybrid BF, and many radio transceivers.

Beam management is a crucial aspect of BF technology, as is understanding it. To support directional communications, the 5G NR specification incorporates a new physical layer (PHY) and medium access control (MAC). In 3GPP terminology, these procedures are referred to as beam management and include four distinct operations: First, beam scanning: the radiation pattern covers a spatial area utilising multidirectional beam scanning and predefined time intervals; second, beam measurement: assessment of the received signal quality at Node B (gNB) or User Equipment (UE); third, beam determination: selection of the appropriate beam(s) at gNB; and fourth, beam report: feedback of beam quality and decision information from the UE to the Radio Access Network (RAN).

3.2.2 Monitoring and beamforming

In the field of wireless communication, BF has evolved as a technology to increase coverage, data rate, and/or signal quality. Future monitoring requires the identical enhancements. BF monitoring simultaneously transmits uncorrelated signals, such as in distinct directions or the same direction with orthogonal polarisations. This enhances the breadth and grade of the received

information. Fig. 3.2 depicts an example of the radiation of three simultaneous beams with BF. In this instance, the total bandwidth of each transmit-receive channel is maintained, so the range resolution of the antenna is not compromised, but the total radiated power is interleaved, i.e., shared. It's entirely under control.

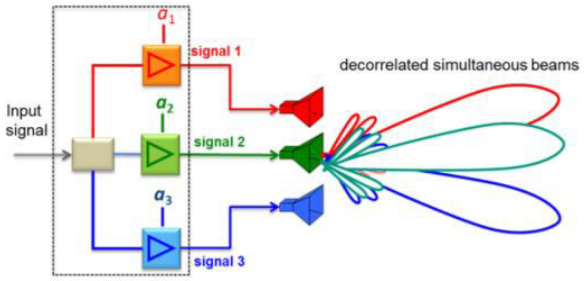

Figure 3-2 Beamforming transmit array with three beams in different direction.

3.2.3 Design and simulation

In this section, Matlab was used to design an area monitoring antenna to detect the high dB level and evaluate its environmental impact; the BF can be used to direct the beam towards the target node. Several methods exist for executing the BF. The following diagrams and figures illustrate the simulation's results: The simulations are conducted under normal vehicle noise conditions, i.e., the vehicle is presumed to be moving along the axis, lifting along the axis, and rotating around the axis, as illustrated in Fig.3.3. The following stages comprise the simulation. First, the vehicle's motion is simulated under the influence of its regular motion, followed by the determination of the parameters measured by the sensors and accelerometers [32].

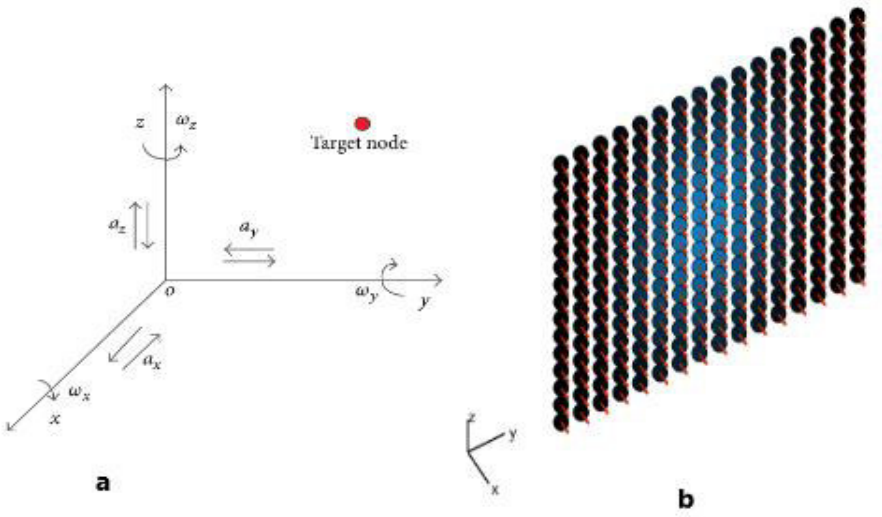

Figure 3-3 (a) Inertial sensor coordinate frame, (b) Array geometry.

Next, the parameters obtained in the preceding phase are used as input to the system, and the Euler parameters are then derived using the orientation filter. Finally, knowing the attitude error and the antenna array pattern after BF allows us to calculate the monitoring power gain over time. Fig.3.4 and 3.5 exhibit the specifications of the other elements.

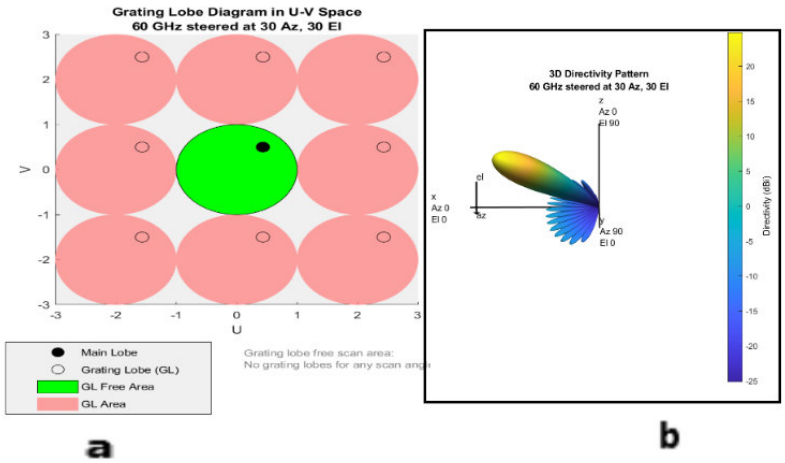

Figure 3-4 (a) Grating lobe diagram with element spacing larger than half a wavelength, (b) Beam pattern and grating lobe diagram element design.

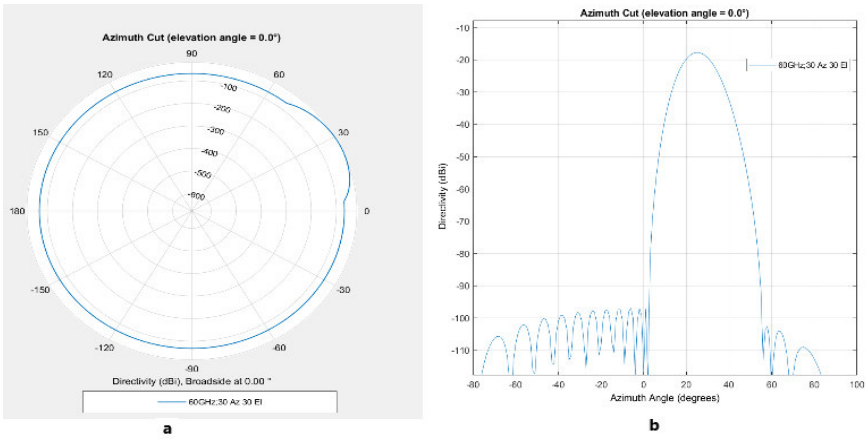

Figure 3-5 (b) Azimuth cross polar coordinate, (b) Azimuth cross rectangular coordinate.

3.2.4 Measure of antenna size

Small substrate depths cause the electric field to be directed along the $\hat{x}$ axis and independent of z. Overall, this is an antenna design process. Initial dimensioning is possible. It can be optimised with an electromagnetic simulator. Electrical permittivity, loss tangent, thickness, and operating frequency are substrate inputs. Substrate depth must meet restrictions. Imagine a perfect, limitless ground plane. Patch width can be calculated as follows in (3.4):

$$W = \frac{\lambda_0}{2}\sqrt{\frac{2}{1+\varepsilon_r}}; \lambda_0 = \frac{c}{F_{res}} \tag{3-4}$$

With (3.4) in which the effective wavelength is λ_e, the effective dielectric constant is ε_e, and the calculation of the patch length extension ΔL is given by (3.5):

$$\Delta L = 0.412h\frac{(\varepsilon_e + 0.3)}{(\varepsilon_e - 0.258)} + \frac{\frac{W}{n} + 0.264}{\frac{W}{h} + 0.8} \tag{3-5}$$

In practice, we find: $0,005\frac{\lambda_e}{2} \le \Delta L \le 0.01\frac{\lambda_0}{2}$ and the calculation of the patch length L is given by eq. (3.6):

$$L = L_e - 2\Delta L = \frac{\lambda_0}{2} 2\Delta L \tag{3-6}$$

Fig. 3.6 illustrates the typical structure applied for the objective to monitor an environmental noise with BF approach.

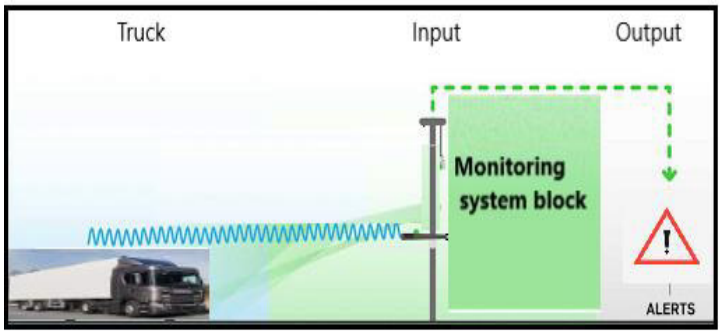

Figure 3-6 Systems block monitoring.

The current findings can be seen in the following figures, illustrating the actual angles and the predicted angles, respectively. Fig. 3.7 displays the trace which corresponds to the computed error in the estimated angles.

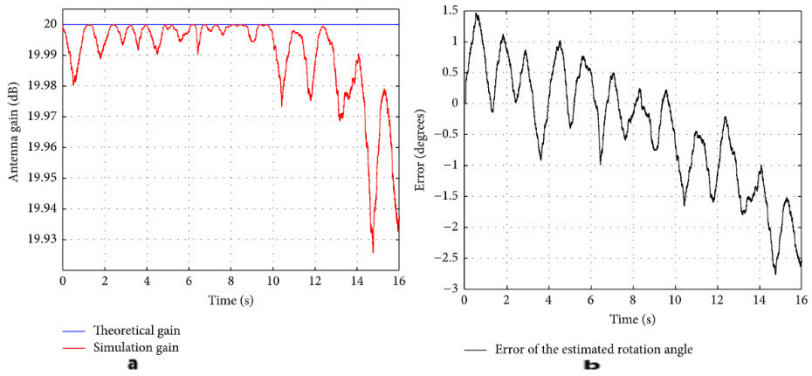

Figure 3-7 (a) Typical results for power gain Monitoring system block, (b)Typical results error.

Based on the analysis of Fig. 3.7 (a)-(b), and Fig. 3.8, it can be observed that the trace denoting the estimated angles of the filter exhibits a strong resemblance to the trace representing the actual angles. Furthermore, the discrepancy between the two traces is within the range of -3 to 1.5 degrees.

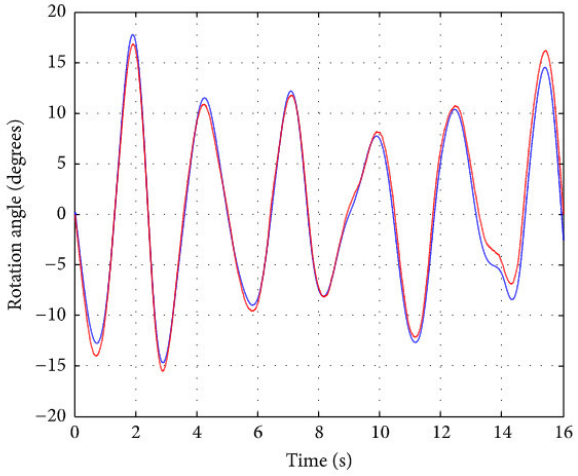

Figure 3-8 Typical results for actual and estimation angle.

3.3 Conclusion

The BF technique has been demonstrated in this chapter as part of enhanced monitoring of environmental protection against noise pollution caused by vehicles, trains, and other equipment. The relative positioning of the target node with regard to the antenna array is computed using the system's real-time attitude. Following that, a method for doing the BF is chosen. Finally, under steady-state conditions, the scheme is tested and verified. The results indicate that BF significantly improves antenna gain [33]. This work is unique in that it employs a method for determining the target node relative direction to an antenna array that is located outside of the array. This allows for improved monitoring of the target area, followed by a channel less BF. The simulation results show that BF can increase power significantly. The same graph shows that the antenna gain, 19.93–20 dB, is larger than that of the antenna without BF. BF improves environmental noise quality and quantity detection.

The collected signals will be processed in the following chapter with the goal of distinguishing the different components contained in a single signal envelope, such as vehicle noise, which contains several noises, such as noise from the engine, tyres, and the wind that the vehicle faces as it moves forward.

Chapter 4

4. Antenna-sensor beamforming: distinguishing external noise

4.1 Introduction

Noise is unpleasant to hear and has negative, sometimes dramatic, repercussions; therefore, cities must limit noise. It's critical to note that environmental noise harms health and human activity [34]. Accordingly, this dangerous environmental pollution from multiple sources must be monitored using specific technology that can distinguish, categorise, and show dB noise levels.

A sensors array is able to be utilised for assessing noise pollution quality and quantity. The design and simulation of a BF-based antenna sensor for noise DOA detection and signal envelope noise differentiation are reported in the chapter. The system records and stores noise for processing or real-time.

From the signals (noise), we can deduce that other, invisible events are occurring; when these signals are processed, they disclose the hidden truths. This BF antenna and its associated system and algorithms can differentiate between the noise of a vehicle driving on a road in excellent condition and a road in poor condition. This could have numerous environmental benefits, particularly in terms of pollution, but also financially.

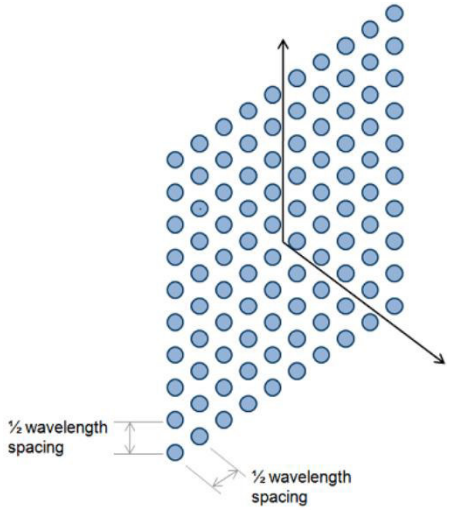

Figure 4-1 Designing an antenna array.

Fig. 4.1 demonstrates antenna array assembly. The image exhibits an antenna array with 100 elements on a grid arrangement in a 10 by 10 rectangle configuration. At the greatest operational frequency, elements are half a wavelength apart to avoid array lobes.

The study major objective is to employ the BF technique and algorithms to separate and categorise vehicle noises in BF antenna signals. In connection with the antenna design, we can calibrate filters to capture and store sound signals from noise sources (vehicles, aircraft, trains, industry, etc.) that exceed the antenna's limits and become damaging to the human ear. Antenna sensors offer extraordinary characteristics that can be utilised to detect noise pollution from multiple sources simultaneously and reduce it in particular circumstances to protect humans [35].

The solution is to limit the decibel level of vehicle noise on roads that pass through residential areas by installing antennas at the entrances to the protected areas to capture sound signals from vehicles, trains, and other harmful engines. The antennas consist of sensors that detect sound signals emitted by vehicles when the engine's noise level exceeds the dB threshold established in the system's filters. The design of complex antenna elements and arrays (see Fig. 4.1) with intelligent partitioning of BF systems to pick up and process sound signals examines if the sound signal picked up has a dB level below the parameters configured in the monitoring system.

The noise that the car makes when it moves is influenced by the condition of the road. When confronted with road regulations, we refer to two sorts of realities: "noise of vehicles on roads in good condition (VNRGC)" and "noise of vehicles on roads in poor condition (VNRPC)". When a vehicle is moving on the first type of road (VNRGC), the noise of the engine and the friction of the tyres on the pavement are not the same as when the vehicle is moving on the second type of road (VNRPC).

Due to increased pollution, traffic noise harms the ecosystem and nearby residents. Noise monitoring can help reduce noise pollution and remind drivers to maintain the road by distinguishing vehicle sounds. The entire system—software and hardware constructed in the road—provides us with an intelligent road, i.e., one that interacts with drivers to protect the environment from noise pollution and to maintain the road [36].

4.2 5G and beamforming capabilities

To adapt the monitoring system to 5G, it is critical to consider the proximity of BF and 5G, as this technology (beamforming) is specifically employed in 5G, and the system will evolve at the rate of 5G. BF was formerly more likely to occur on local WiFi networks. This is set to change, however, with the deployment of 5G networks. 5G makes use of radio frequencies in the 30-300 GHz range.

While these frequencies allow for significantly faster data transmission, they are also far more vulnerable to interference and have a more difficult time penetrating physical thing. Many technologies, like cell size reduction, enormous improvements in MIMO (multiple-input, multiple-output) coverage, including increasing the number of antennas on 5G stations, and, of course, BF, are required to address these issues. If 5G takes off as expected, we'll be using BF on a daily basis without even realising it.

5G offers a quantum leap in network performance compared to 4G, with peak data rates up to 20 times speedier at 20 GB/s and connection densities of 1,000 devices per square kilometre, which is 100 times higher than 4G. This enhanced performance is provided by the new 5G radio (NR), which employs a variety of cutting-edge techniques, such as millimetre waves (between 30 and 300

GHz), frequency transmissions, advanced signal coding techniques orthogonal frequency-division multiplexing (OFDM), multi-access edge computing (MEC), and network slicing.

4.3 Conceptualization and modelling

In the MatLab environment, the monitoring antenna is programmed to detect a high level of dB and evaluate its impact on the environment, keeping in mind that the BF technique has the ability to focus on the targeted node; a variety of schemes can be used to implement the BF technique. The outcomes of the planned simulations are presented in this section. The simulations are done under stable vehicle noise settings to validate the effect of the proposed system, i.e., the vehicle movements are supposed to sway along the axis, lift along the axis, and rotate around the axis, as illustrated in Fig. 3.3 and Fig. 4.4. The following are the simulation steps:

Fig. 4.2 demonstrates the communication between of the system's many components. The noise coming from the various targets (vehicles) is measured by antenna arrays (BF) connected to accelerometers and a specific unit that provides good noise conditioning. The MUSIC algorithm interacts with the antenna arrays to achieve an optimal orientation towards the target, and the power gain over time for control is obtained using the Euler parameters obtained using the orientation filter, knowing the attitude error and the antenna array pattern after beamforming. Fig. 3.7, Fig. 3.8 and Fig. 4.1 show the details of the other elements.

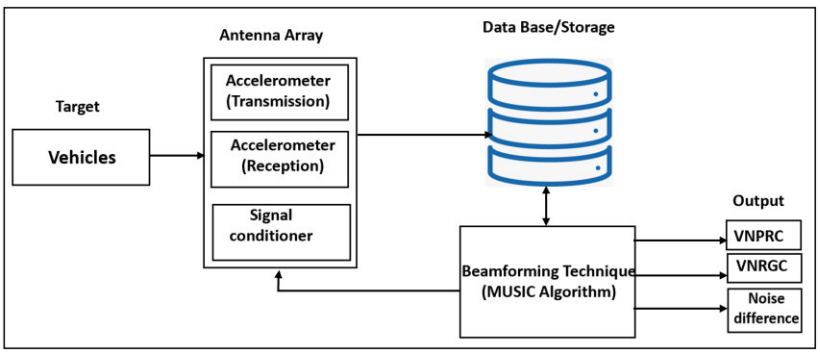

Figure 4-2 System diagram.

The information we collect is saved in a database or storage, which will send them back to the MUSIC algorithm to perform the decomposition and classification of the vehicle noise to give us the outputs (VNRC, VNRGC, noise difference) because the vehicles on the road do not all have the same positioning; this can be seen clearly in Fig. 4.3. These data are subsequently returned to the database's second section for post-processing.

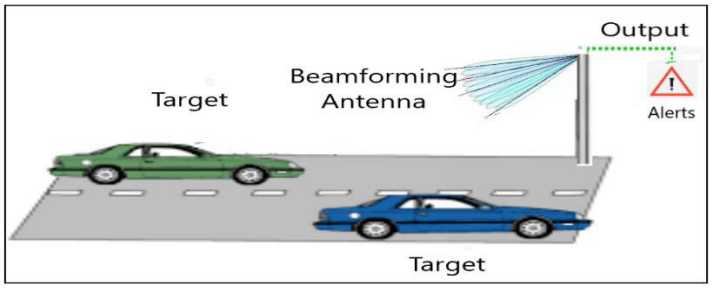

Figure 4-3 A example scenario using an assessment system.

4.3.1 Signal processing

Signal processing is a subfield of electrical engineering that focuses on the analysis, modification, and synthesis of signals such as sounds, images, and scientific measurements [37], [38], [39]. Signal processing techniques can be used to enhance the transmission, storage, and subjective quality of a measured signal, as well as to emphasise or detect its internal components. In order to achieve this objective, we have selected the MUSIC algorithm, which has proven to be superior to other signal processing algorithms.

One of the techniques used for frequency estimation and transmitter localization is MUSIC. Even when the signal-to-noise ratio is very low, this technique can discern the direction of signals occurring on a sensor network. We choose this algorithm because we are going to work with compound signals coming from antennas, and antennas are sensors, and their signals are composed of little signals, each with its own frequency [40], and the MUSIC algorithm is well suited for such operations. Fig. 3.7 and Fig. 4.4 show the results of its work for signal separation or signal categorization separation.

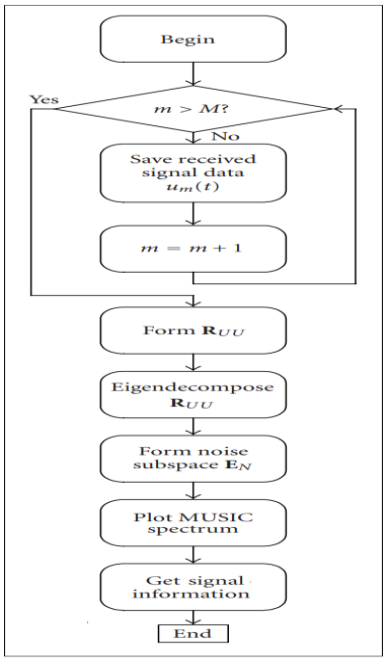

Figure 4-4 MUSIC algorithm flowchart [11].

In order to take advantage of the MUSIC, we used the MUSIC algorithm (Fig. 4.4) for the signal processing part, specifically for signal highlighting, which also has similarities with the maximum method, the likelihood method, and is fundamental with a representation having the one-dimensionality of the maximum entropy.

The MUSIC algorithm's general approach is built on extracting the signal from the noise using the eigenvalue decomposition of the received signal's covariance matrix. The orthogonal property of the signal and noise space is used by the algorithm.

We estimated the noise using a subspace of the signal, considering that the noise and the signal are nearly similar and that the noise of each channel has no association. It is critical to note that the MUSIC method assumes the noise to be uncorrelated, thus the resulting covariance matrix is diagonally natural.

The matrix algebra allows the signal and noise subsets (other internal signals) to be separated and determined to be orthogonal to each other. As a result, the MUSIC algorithm makes use of orthogonality to isolate (separate) the signal and noise components.

4.3.2 The MUSIC algorithm is a tool to process signals in subspace

Noise subspace techniques are widely used for differentiating all of the parameters or components contained within the envelope of a complex signal in the presence of uncorrelated noise, and have applications for modelling signal and noise decomposition. MUSIC is one of the algorithms that can provide solutions to the issue or overcome it. As MUSIC requires an explicit decomposition of the eigenvalues of an autocorrelation signal from an autocorrelation matrix, followed by a linear search in a large space, its computational efficacy is relatively low.

In the MUSIC algorithm, a pseudo-spectrum is generated from the projection of a complex sinusoid onto the entire spectrum of a complex sinusoid on all the eigenvectors of the noise subspace, which define the peaks where the amplitude of this projection is minimal.

We want to make a decomposition of the parameters or components of a composite signal. Let $y(n)$ be the noisy signal, consisting of a deterministic part, $x(n)$, consisting of r real sinusoids and a random noise, $w(n)$. We assume that $w(n) \sim N(0, \sigma^2)$, and that $w(n)$ and $x(n)$ are uncorrelated. The sinusoidal phases ϕ_i are assumed to be i.i.d. (independent, identically distributed) and uniformly distributed

$$\phi_i \sim U(-\pi, \pi) \tag{4-1}$$

$$y(n) = \sum_{i=1}^{r} A_i \cos(\omega_{in} + \phi_i) + \omega(n) \tag{4-2}$$

$$y(n) = x(n) + \omega(n) \tag{4-3}$$

From (4.2) the vector notation, the signal $y \in \mathbb{R}^M$ takes the character $M \times M$ of the autocorrelation matrix $K_y = \mathrm{E}(yy^T)$ As a signal, the autocorrelation matrix coincides with the covariance matrix. Because this matrix is Toeplitz and positively symmetrically defined and see even its eigenvalues are real and non-negative (and positive when $\partial > 0$). We can perform an eigenvalue

decomposition on this matrix to get a diagonal matrix $\wedge$ consisting of the eigenvalues, and an eigenvector matrix **Q**.

The 2_r eigenvectors corresponding to the 2_r largest eigenvalues, Q_x, contain more information about the signal than about the noise, while the remaining $M-2_r$ eigenvectors, Q_w, represents only the noise subspace. Thus, we can have this relationship:

$$K_y = K_x + K_w + \sigma^2 I \tag{4-4}$$

$$K_y = Q \wedge Q^H \tag{4-5}$$

$$K_y = [Q_x Q_w] \begin{bmatrix} \wedge^l & 0 \\ 0 & \sigma^2 I_{M-2_r} \end{bmatrix} \begin{bmatrix} Q_x^H \\ Q_w^H \end{bmatrix} \tag{4-6}$$

Consider a vector of M harmonic (4.6) frequencies written $b(\omega)[1, e^{jw}, e^{2jw} ... e^{(M-1)jw}]^T$ projecting the vector onto Q_ω, let be the subspace occupied by the noise (where there is no signal component); the below spectrum is a function of a set of ω 's:

$$P(\omega) = \frac{1}{b(\omega)^H Q_w^H b(\omega)} \tag{4-7}$$

$$P(\omega) = \frac{1}{\| Q_w^H b(\omega) \|^2} \tag{4-8}$$

For a particular value on (4.8) value of ω which is present in the signal, the sum of the projections of b onto the eigenvectors covering the noise subspace will be zero. This is because the subspace occupied by the signal is orthogonal to that occupied by the noise since they are uncorrelated. Thus, we see that $P(\omega)$ will take a very high value in such cases. In conclusion, we can find peaks of the corresponding frequencies of each element contained in the signal, so peaks that are very close together can be found or will appear thanks to the MUSIC algorithm.

Figure 4.4 depicts the MUSIC algorithm flowchart. The details about the flowchart are: The correlation matrix for the output signals has a similar representation: R_{uu}

$$R_{uu} = E(U(t)U^{U}(t) = \frac{1}{Ns}UU^{H}. \tag{4-9}$$

In (4.9); $E(.)$ is the expected value operator. U without time argument represents discrete samples with a sample block length N_S. The exponent H denotes the conjugate transposition. We assume that all noise components $n_m(t) = 1,...,6$ at each sampling period $\#m$ are independent, identically distributed (i.i.d.) with power σ^2. R_{ss} is then represented as:

$$R_{uu} = [\vec{\alpha}(\phi_1)\vec{\alpha}(\phi_2)...\vec{\alpha}(\phi_K)] \times R_{ss} \tag{4-10}$$

$$\times[\vec{\alpha}(\phi_1)\vec{\alpha}(\phi_2)...\vec{\alpha}(\phi_K)]^{H} + \sigma^2 I_{(6)} \tag{4-11}$$

In (4.11) $I_{(6)}$ is a (6×6) dimensional identity matrix, the correlation matrix of the R_{ss} (4.10) source signal is:

$$R_{ss} = E([s_1(t)s_2(t)...s_k(t)] \times [s_1(t)s_1(t)...s_k(t)]^{H}). \tag{4-12}$$

Based on (4.9), the MUSIC algorithm is executed according to a similar classical procedure see the flowchart of the MUSIC algorithm (Fig. 4.4). The directional vector is used to obtain the MUSIC spectrum, the algorithm requires that the signals are periodic.

a) Construct the signal sample vector given by $U(t) = [u_1,...,u_m(t),...,u_m(t), m = 1,...,6$, which is the signal sample when the antenna is at sampling period $\#m$. With *U(t)*, we form the signal correlation matrix R_{ss}
b) Eigen decompose the signal correlation matrix R_{ss}, and form the noise subspace E_N with eigenvectors corresponding to the small eigenvalues.
c) Evaluate the MUSIC spectrum P_{MU} versus the signal direction ϕ,

$$P_{MU} = \frac{1}{|E_N^H \vec{\alpha}(\phi)|^{2,}} \tag{4-13}$$

In (4.13), where $\vec{\alpha}(\phi)$ is the directional vector that corresponds to the azimuthal viewing direction ϕ.

Data storage for post-processing: As a result of the simulation, the data are saved in the database for post-processing. Once the data is saved, it can be used for a variety of purposes, including examine the data and display it on the screen to get a sense of how the different signal components are decomposed.
The procedure for antenna array characterization and calibration consists of four steps: the first step is to select the appropriate calibration technique based on uncertainty analysis and mutual coupling assessment; the second step is the assessment of the measurement requirements from the calibration technique to define the measurement campaign; the third step is the measurement procedure itself; and the final step is to post-process the measurement results. This approach can be used to determine the suitable calibration technique and the measurement requirements for any antenna array calibration. Furthermore, measurements of active element patterns are included in the automated campaign for mutual coupling performance analysis and characterization.

4.4 Presentation of results and conclusions

In the framework of this research, we have employed BF to enhance environmental monitoring of noise sources (vehicles, trains, aircraft, etc.) in cities and in settings such as research centres, schools, and hospitals; the results of this approach are presented here. The results demonstrate that the BF improves antenna gain. The novel aspect of this research is that it employs a method to obtain the relative direction of the target node with respect to the antenna array installed alone outside the antenna array, which enables better monitoring of the area, the realisation of a channel-less BF, and, most importantly, the differentiation of the various components of a sound signal (noise difference in dB according to VNPRC and VNRGC); in this case, see Fig. 4.5 and Fig. 4.6.
The graph highlights actual and approximate degrees. Fig. 3.7 communicates a trace which reflects the calculated deviation in the estimated angles. In Fig. 3.7 and Fig. 3.8, only the filter estimated angles are considered, which closely

follows the real angles trace, so the error is included in the interval of -3 and 1.5 degrees.

Based on the simulation results, we stress that the BF approach is capable of achieving large power gains. As a result, the same plot shows that the antenna gain, which ranges between 19.93 and 20 dB, is clearly greater than that of the non-beamforming antenna. As a result, beamforming allows for better discrimination of the quality and quantity of environmental noise.

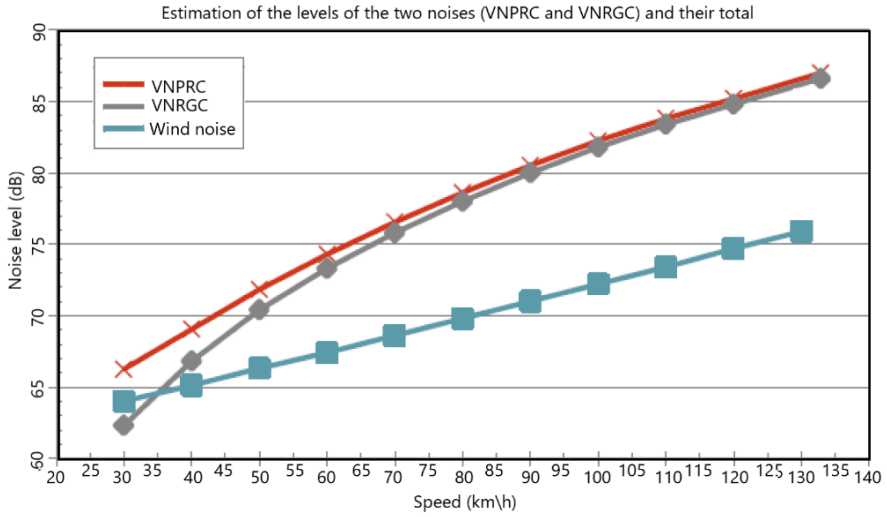

Figure 4-5 Estimation of the levels of the two noises (VNPRC and VNRGC) and their total.

As the vehicle passes near the BF antennas for the environmental monitoring system, the vehicle noises are recorded, and the signals are retrieved and processed to distinguish between the noise of the vehicle driven on the road in good conditions, as illustrated in Fig. 4.5, and the noise of the vehicle driven on the road in poor conditions, as illustrated in Fig. 4.5. We used the MUSIC algorithm to generate this difference in noises when a vehicle is driven on the terrible road depicted in blue in Fig. 4.5; we used the MUSIC algorithm to make this difference in noises when a vehicle is driven on its two separate roads.

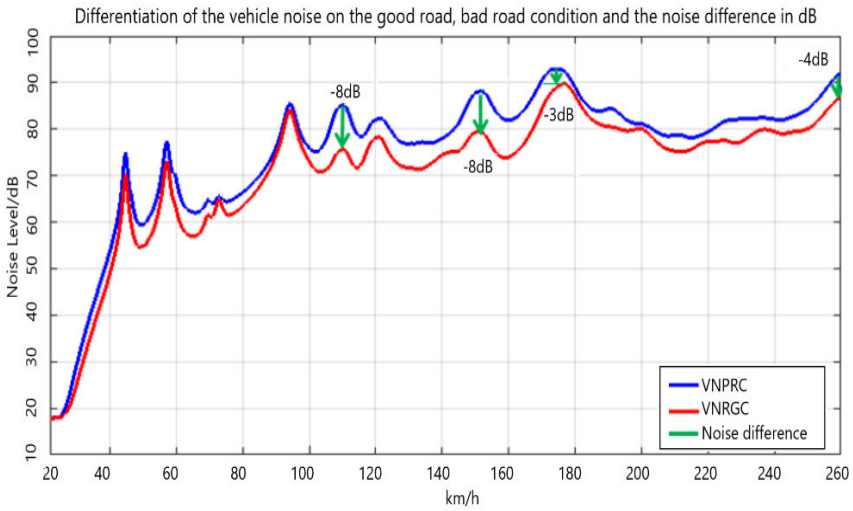

Figure 4-6 Differentiation of the vehicle noise on the good road, bad road condition and the noise difference in dB.

There is a difference in dB between the two noises, which is depicted in Fig. 4.6. As a result, the highest difference is -8dB and the lowest is -3dB, demonstrating that the parts of the road, whether good or bad, can be evaluated in terms of dB differences and conclude that the bad part of the road was not significantly damaged because the difference between the two signals is not too great.

The following section will talk about BF in the detection, suppression, and recovery of the components of a narrow-band signal and an ECG signal.

Part III:
Beamforming-Processing: Detection, Suppression, and Recovering

Chapter 5

5. Algorithms-based beamforming an antenna array: noise and interference characterization for detection and suppression

5.1 Introduction

Maintaining an optimal trajectory and transmitting the signal to its target is a very delicate subject in the field of telecommunications, particularly in wireless transmission, which uses the radio medium, which is very sensitive to interference and other elements harmful to the signal, to guide the trajectory of the wave. This is the most important aspect of radio transmission.

In response to this challenge, we present approaches for combining BF and convolutional neural network (CNN) techniques to a signal received from an antenna array. These approaches involve monitoring and steering the signal trajectory from the antenna output to its target (user device) by detecting and removing all interfaces and noise, which can deviate the signal from the desired direction by rotating it in another direction (approximately 45°), which has a very high sensitivity to even the smallest beam distortions in its direction. The LCMV (linear-constraint minimum-variance) approach, with its superior target detection function, enables the signal to reach its target and prevents self-cancellation by expanding the signal region around the desired direction.

With the objective to optimise signal reception, the LCMV technique can optimise this phase of transmission. When the signal and noise cannot be isolated, a sample covariance matrix is calculated from the data. Constraints are specified using various methods, including amplitude and derivative

constraints. For instance, specifying weights that suppress spurious signals from one direction while transmitting signals from another direction without distorting them. To prevent signal self-cancellation, LCMV allows the positioning of multiple constraints along the target path (directional vector). The final (marginal) approach involves the setup of a 24-layer CNN model, which exploits all the characteristics and components of the D2D (Device-to-Device) signal in depth. Three various convolution kernel sizes (32, 64, and 128) are employed to exploit the noisy original signal, to remove the noise from the signal, and to recover the desired signal.

Due to the rapid growth of the mobile Internet and the Internet of Things (IoT), D2D data exchange, which was the LTE-advanced standard, is no longer the case, and some indicators suggest that the mobile phone network will be unable to satisfy the diverse needs of future location-based applications and D2D interactions [41]. Without this technology, stochastic geometry theory could not adequately study it.

The conventional Wyner model [42]. is the hexagonal grid. Current system simulations can evaluate the Wyner model [42].In a connectivity-variable context, the matrix model scalability and accuracy are debatable [43]. To handle such a circumstance, simulate random point locations and construct the stochastic spatial Poisson model, which is as good as the matrix model [44]. Some researchers [45] use stochastics to estimate matrix network performance. In a study on spectral division on a derivative based on frequency assertions for mobile network data exchange, it was utilised to find the noise-to-interference ratio (NIR). The authors [46], [47] investigated the spatial attribution of network interference noise signal spread ability. The authors [48], [49] used mode and power control on the underlying D2D communication in cellular networks to consider a user on both the length of the link and, more importantly, the distance between the Character-Terminal User Environment (CUE) and the base station (BS). The Rician distribution in [50], [51] addresses small-scale order fading in explicit equipment communication links.

The work [47] discusses purposeful interference in GNSS receiving devices. A schematic for interference cancellation using a double level surrounding antennas is demonstrated. This level detects and reduces interference. All of its

actions occur before GNSS system receiving equipment. The authors wanted to develop a multiple-dimensional signal at the communication system output with a forecast to avert major interference disruptions. This reminds us that the GNSS signal has been regressed to cancel the noise in the regional correlational array. Signal subspace, intensity, and DOA is now easily accessible.

To identify a misleading attack for determining DOA for navigation signals, the cyclic correlation eigenvalue test (CCET) and MUSIC algorithms were tested on real satellite signals via BF to remove erroneous and corrupted signals and increase target signal gain [52]. The BF approach optimises network data transmission using the blind and non-blind processes. Knowing the targeted signal's DOA makes calculating antenna array weight easy [53]. The blind process of BF identifies the targeted signal based on signal characteristics. It has modular oscillations, cyclic redundancy, and more. The Estimation of Signal Parameters via Rational Invariance Techniques (ESPRIT) and MUSIC algorithms can estimate signal parameters via rotational invariant techniques and compute the DOA of the aimed signal [54]. The GNSS receiver antenna array has anti-jamming technology, however multipath interference can compromise its performance. Spatial-only therapy (SOT) and adaptive space-time treatment (STAT) measure this interference, although it may reduce SOT degree of freedom [55].

5.2 A minimal model design wirelessly interconnecting device

Fig. 5.1 represents a basic telecommunications concept with a basic infrastructure connecting user terminals in a cellular perimeter to the network via downlinks. In any telecommunications context, downlinks and uplinks can generate interference when delivering data between devices.

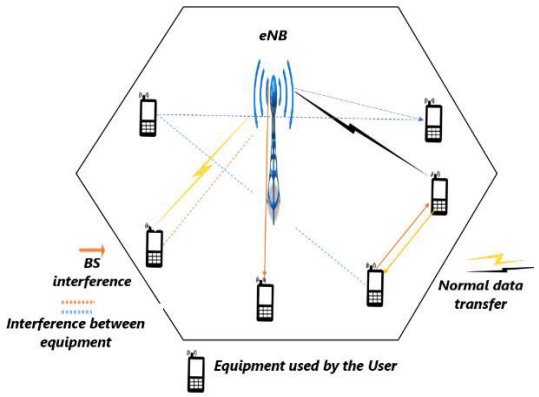

Figure 5-1 A minimal model design wirelessly interconnecting device.

Transmitters, network infrastructure components, the atmosphere, and the climate are all sources of interference that end users encounter in their devices. We also note out that in certain cases, the emitter blocks of user equipment may interfere with the Evolved Node B (eNB), which could imply that better link management will reduce any form of interference. Some sources of interference are given below. Because the research is based on the Noise classification for Detection, Suppression, and Interference, the goal of this part is to highlight and identify specific sources of interference. Here is a group of user terminal equipment connected to the network $U = \{U_1, U_2 ..., U_N\}$. In particular, compared to the previous one, this $(i,c)(i,c \in U)$ shows the individual cellular link of a device to the eNB. The biggest peculiarity is that it revolves within a single cell; equation 1 provides an additional illustration of this:

$$SINR_U = \frac{T_{lglj}}{T_{ehG} + N} \tag{5-1}$$

In (5.1); T_l is the reduced radiation from the junction due to the emission energy contained in the emitter of a user's terminal, $_{glj}$ The capacitive emitting force of the eNB, N , stands for noise from the environment, and $_{hG}$ the gain ratio has been increased by equipment attached to the eNB.

5.3 Beamforming technique

The fundamental approach of the BF technique is radio frequency (RF), which targets wireless communications via an antenna's sensor array with the purpose of reducing interference-containing intruding signals. Because of its unique capacity to concentrate the signal on the chosen receiver, BF has revolutionised signal transfer between transmitter and receiver.

This technology gives BF a considerable advantage over other transmission methods, such as broadcast antennas, which transmit signals in all directions. This approach improves transmission reliability, speed, and, most importantly, stability by focussing the signal on a single receiver.

As mentioned at the beginning of this section, BF employs an antenna array. BF can be carried out in two ways: first, with a physical antenna array (BF hardware); second, with a physical antenna combined with BF algorithms (BF logical); In general, both types can work together or independently without causing complications in directing or concentrating the signal to the intended receiver by suppressing interference and noise.

5.3.1 Fundamental beamforming algorithm

In the context of data processing, what is BF? According to the linear combination of the element outputs, BF can be computationally represented as a beam adopting (5.2).

$$\varsigma(\theta) = \sum_{k=0}^{k=N} a_k(\theta).x_k \tag{5-2}$$

ς : denotes beam reaction.

θ : represents the beam principal lobe angle.

N : the total number of elements,

k : possesses an index property.

a_k : complex coefficient of *k-th* element

x_k : element voltage measurements response.

(5.2) is relatively easy to compute, but we must specify the coefficients use to improve the antenna reception gain in a given direction.

A transmitting station is far from a linear antenna in Fig. 5.2. The emitter is multiple wavelengths from the receiving antenna.

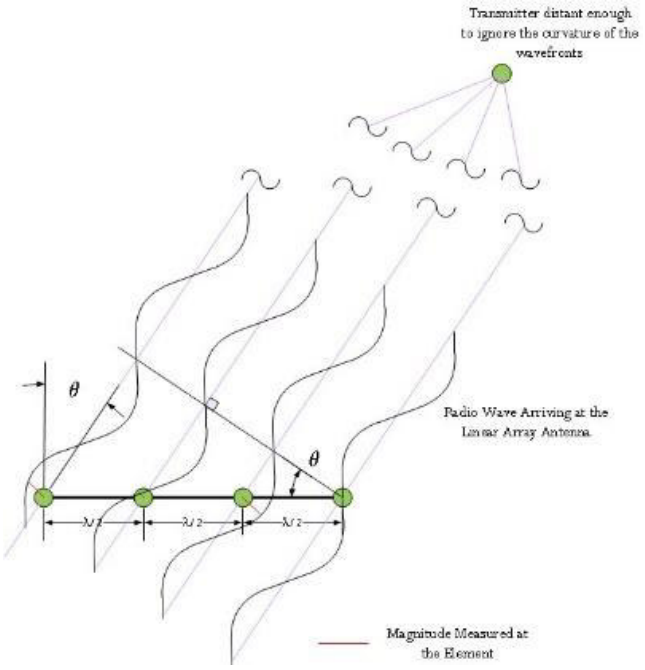

Figure 5-2 Antenna component phase shift.

Wavefronts arriving at the receiving antenna from a remote emitter can be approximated as plane waves. In (5.2) yields the greatest response when all wavefronts impact each element at the same time (perfect constructive interference) for Fig. 5.2, assuming $a_k = 1$. When the transmitter is perpendicular to the linear array, this happens. As the transmitter moves away from the perpendicular, destructive interference occurs, reducing responsiveness.

Fig. 5.2 will allow us to comprehend how to move the beam in various directions. For non-straight-on transmitters, a linearly increasing phase shift is applied along the array's elements. Can we utilise the coefficients to cancel out phase differences and rotate the maximum antenna response direction? It is capable, it turns out. Using (5.2), we can determine the phase shift of the received signal between each piece. The solution to obtaining this equation is to remember that each constituent gets the identical signal at slightly different times.

To summarise this stage, BF maintains signal control between the transmitter and the receiver. Because the amplitude and phase of a signal vary as it moves

across space, BF employs these two components of the g to modify the direction of the signal, which also changes the orientation of the antenna array. The signal finally arrives to the receiving antenna's entrance after completing its path. All of the data from the many sensors must be integrated into a single block in order to orient this set of data (the signal) towards the target. The classic BF, according to convention and the schematic, can alternatively be viewed as a BF with delay and sum. The amplitudes of an antenna's components are proportional to their weights. Let us return to the antenna phase. In other words, the selection of an antenna exact phases is critical to its orientation. This method allows for the reduction of interference. Noise lowers the quality of the signal. Correlated noise causes directional interference, as shown in (5.3): the SNR of a BF with M antennas and F as the possible receiver. Where σ_x^2 represents the noise intensity, it is:

$$\frac{1}{\sigma_x^2} M.F \tag{5-3}$$

There are two ways to improve signal transmission between devices: first, the BF changes its orientation to cancel out the signals from the jammers and increase the signals that are desired; second, the BF changes the way it processes frequencies by treating them as a narrow-band signal by experimenting with the filters, which have very sensitive coefficients in this case.

5.3.2 The computational complexity of antenna array beamforming optimisation

Contemporary cellular radio systems, such as 4G and 5G, employ multi-element antennas, a method known as MIMO, with the objective of increasing radio channel capacity. Evidently, 5G provides even more opportunities, such as massive MIMO, where the transmitting antenna can have hundreds of components, and BF, or beam steering, where the phase of the signals delivered to the antenna elements is modified to concentrate the signal towards the receivers.

Equivalent formulations of the principle of channel formation exist in both the time domain and the frequency domain. Timing representation of 3D free-field track building.

Consider an **H** sensor array. Every sensor h receives $p_h(t), 1 \le h \le H$ timing signals. The ultimate objective of this sensor network is to focus the signal on space. Thus, the focussed signal's amplitude indicates a source at the scanned position. If the wave propagates 3D free field from source to sensor array, the concentrated time signal is:

$$b(t) = \frac{1}{N}\left(\sum_{h=1}^{H} p_h \frac{t + \tau_h}{r_h} \right) \tag{5-4}$$

In 5.4) When r_h represents the geometric distance between each sensor and the position being surveyed, τ_h denotes the delay that must be introduced into the signal from sensor h in order to account for the propagation of the signal. When considering 3D free-field propagation, the parameter $\tau_h = r_h / c_0$ is sufficient, where c_0 represents the wave velocities within the medium. The determinant of standardisation $N = \sum_{h=1}^{H} \frac{1}{r_h^2}$. Suppose a source exists and produce a signal $s(t)$, every sensor receives the propagated signal, as shown in $p_h(t) = s(t - \tau_h) / r_h$, and the focused signal is equal to the source signal $b(t) = s(t)$. As a result, this is a signal processing technology that allows the source signal to be retrieved. The amplitude of the focused signal is often lower than this threshold if the grating focuses at a place where there is no source. We may determine the presence of a source from the readings of a network of sensors by scanning a set of points in space.

5.4 Proposed approaches for signal processing

Dealing with sidelobes and interference in array signal processing is a significant difficulty, particularly in future communication applications such as 5G technology. As a result, we favour the LCMV and MVDR BF methodologies for optimising gearbox. We can cancel or avoid interference and side lobes by

using these strategies. Aside from that, we can improve the beam's directivity. LCMV and MVDR are two separate BF methods. When it comes to obstacles, both systems rely on computed weights. The use of LCMV in particular is becoming more focused on the right signal during transmission [56], [57].

Two famous BF algorithms (MVDR and LCMV) are used to solve the problem. Optimal and adaptive BF are sometimes used interchangeably, but they are not quite the same. Optimal BF applies weights that are determined by optimizing a certain amount. MVDR, for example, determines weights by optimizing a network output's noise to signal ratio and interference rate. MVDR offers several advantages: integration of noise and interference into an optimal solution; MVDR has a higher spatial resolution than conventional BF; MVDR puts zeros in the direction of the interference sources; and the end side lobe levels are smaller and smoother.

To solve the problem of separating the signal with the noise we use LCMV, when the noise is not separable from the signal, we estimate a sample covariance matrix from the data with LCMV. Some approaches are being taken to specify constraints, such as amplitude and derivative constraints. For example, specifying weights that suppress spurious signals from a particular direction while transmitting signals from a different direction without distortion. To avoid signal self-cancellation, we use LCMV, which allows us to put several constraints along the target direction (direction vector). This reduces the risk of either suppressing the target signal or suppressing the signal when it arrives at an angle slightly different from the desired direction. Another important point is that LCMV places the constraints along the specified directions while cancelling the interference signals along 30 and 50 degrees. It is also interesting to note that LCMV is capable of keeping a level performance the area approximately forty-five degrees in azimuth, whereas MVDR cannot.

We have also foreseen the use of convolutional neural network (CNN,) as marginal procedure, that does not affect the substantial contribution of this paper. The CNN possesses the properties of a regional responsive and power exchange. A single neuron is not required to detect every signal, simply the local ones. The different individual neurons acquired through such sensations are capable of being synthesized to get general data at a higher level.

The interchange of parameters among neurons may decrease the number of parameters being sorted out, and the use of multi-layer Fourier allows for the generation of a wide range of map types. Burden exchange is essentially a method of convolution on the data using a single convolution kernel, allowing every neuron at the initial invisible layer to identify signal characteristics and components. CNNs can lower the total number of linkages and extend the network architecture to utilize signal attributes and discover the target signal more effectively.

5.5 Noise cancellation and interference optimisation for D2D communications

At the level of the transmission system, BF and noise reduction (NR) solutions are being evaluated in an effort to improve the equipment-to-equipment link and wireless connection dependability, respectively. The initial analysis of the received signal over interference and noise for the wireless link involves the implementation of interference cancellation (IC) and BF techniques [58].

This strategy has an easiness to analyse and explicitly balance interference cancellation with a desired increase in signal strength. Using PZF, the base station uses L levels of autonomy to reduce its L DUE to interference in a rectangle of size rd centred on the base station, and then utilizes the balance of $M-L$ degrees of flexibility to send the signal it wants to the related CUE receptor. After that, we will talk about the system's efficiency in relation to the interference cancellation strategy (PZF). y_{Co} and y_{Do} represent the signals obtained by an ordinary CUE receiver (R_{CO}) and a typical DUE receiver (R_{DO}), correspondingly. Through

$$y_{Co} = \sum_{n:\Gamma_{Bn}\in\phi_B} \sqrt{P_B} d_{BC,n}^{-a/2} q_{0n} \mu_n x_{Bn} + \sum_{n:\Gamma_{Dn}\in\phi_D}^{n} \sqrt{P_D} d_{DC,n}^{-a/2} f_{0n} x_{Dn} \quad (5\text{-}5)$$

$$y_{Do} = \sum_{n:\Gamma_{Dn}\in\phi_D} \sqrt{P_D} d_{DD,n}^{-a/2} h_{0n} x_{Dn} + \sum_{n:\Gamma_{Bn}\in\phi_B\setminus\{\Gamma_{B0}\}}^{n} \sqrt{P_B} d_{BD,n}^{-a/2} g_{0n} u_n x_{Bn} \quad (5\text{-}6)$$

Let see in (5.5-5.6) $P_n = \left[p_{1n}^T p_{2n}^T ... p_{Ln}^T \right], L \le M-1$, p_{1n}^T is a path in the BS and *Lth* DUE contained within an annulus of size r_d located on the BS, and L is an oval circle function. $\left(E\left[i\right]\right) = (\pi\lambda_{B_d^{r2}})\ E[i] = (\pi\lambda_{B_d^{r2}})\ r_d\ (.)$. u_n is the emission power and is contained in the empty region of G_n to eliminate interfering with the *L DUEs* and to optimize the signal strength. $|q_{nn}u_n|^2$. From, $u_n = q_{nn}^H ss / |q_{nn}^H ss^{HT}|$, where $s \in \sigma\mathbb{C}^{N\times N-L}$ corresponds to the orthonormal foundation of P_n empty area. According to the PZF strategy, the signal-to-interference ratio (SIR) in R_{CO} is:

$$SIR_{CPZF} = \frac{P_B d_{BC}^{-a} |^2\ q_{00n} u_{0n}|^2}{I_{CPZF}} \quad (5\text{-}7)$$

In (5.7) I_{CPZF} means complete interference. In (5.8), one is provided with:

$$I_{CPZF} = \sum_{n:\Gamma_{Bn}\in\phi_B\setminus\{\Gamma_{B0}\}} P_B d_{BC,n}^{-a} |q_{0n}u_n|^2 + \sum_{n:\Gamma_{Dn}\in\phi_D} P_D d_{DC,n}^{-a} |f_{0n}|^2 \quad (5\text{-}8)$$

As it is shown in (5.9), the SIR in R_{D0} based on PZF strategy is:

$$SIR_{D_{PZF}} = \frac{P_D d_{DD}^{-a} |h_{00}|^2}{I_{D_{PZF}}} \quad (5\text{-}9)$$

where $I_{D_{PZF}}$ represents the maximum interference and $I_{D_{PZF,1}}$ indicates interference that comes to BSs. $I_{D_{PZF,2}}$ is also the interference from DUEs. When the CSI of N cellular UEs and M_1 equipment-to-equipment pairs are employed for joint zero-forcing beamforming in the equipment-to-equipment communication underlaying telecom network, as shown in Fig. 5.3, the propagation of beams at the BS will generate no interference on the receiving

antennas of equipment to equipment pairings in set R_{D1}. Since the signals transmitted coming from BS to the E-to-E combinations in set R_{D1}, this configuration eliminates interference.

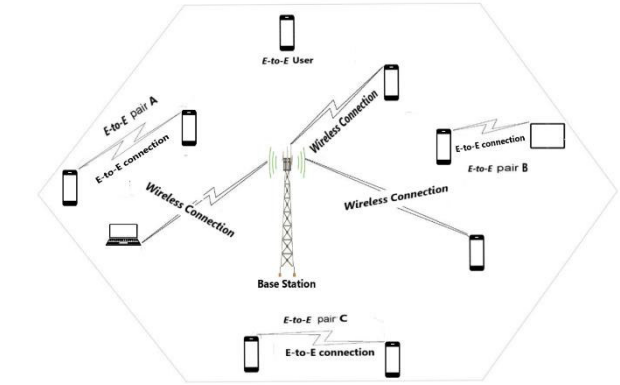

Figure 5-3 E-to-E communication in Cellular network.

When the noise circuits coming from the BS to the audio receivers of equipment-to-equipment combinations in group R_{D2} are entirely aligned with the interference circuits of the BS to the audio receivers of equipment-to-equipment couples in group R_{D1}, the predetermined codes broadcast signals are going to have no influence to the users of equipment-to-equipment combinations in setting R_{D2}. Unfortunately, in a practical system, the likelihood of each of the noise circuits having absolutely identical is approximately zero. If the broadcast signals that travel from the BS towards the users of the equipment-to-equipment combinations in collection R_{D2} are substantially perpendicular and if lines between the BS to the users of E-to-E (Fig. 5.3) pairings in established R_{D2}, i.e., when the number of $\eta_{i,j}$ approaches 1, there will be less interference. The channel parallelism notion enables the development of an equipment-to-equipment screening technique which includes beamforming and noise synchronization [59]- [60].

5.6 LCMV and MVDR approach simulation and outcomes

As depicted in Fig. 5.4, let's apply the adaptive BF to a narrowband signal (NBS) received by an antenna array (AA) via a straightforward rectangular pulse (baseband) for the subsequent portion of the simulation. The carrier wavelength of the signal is approximately 100 MHz, while the receiver consists of a 10 element Uniform Linear Array (ULA) spaced at half wavelength. The signal originates at an angle of 45 degrees with respect to the axis of the ten-column array; each column corresponds to an individual antenna element.
Given that we are addressing disturbance,

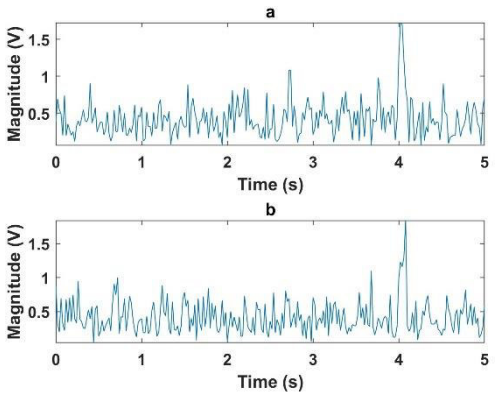

Figure 5-4 Receiving channels.

Two channels (a and b) receive a signal that contains noise, as shown in Fig. 5.4. However, it is difficult to distinguish the desired signal from the noise; therefore, the rectangular wave is very high when examining the pulses prior to applying the BF approach to the signal, as shown in Fig. 5.5.

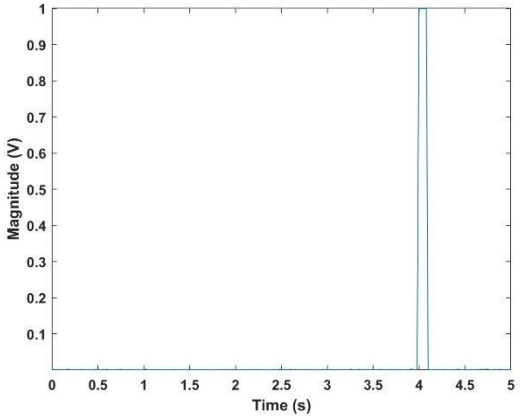

Figure 5-5 Rectangular pulse (right).

Let us first use the standard BF to address the alignment problem so that the signals arrive at the same time. In our example, NBS, we apply a phase factor multiplication to the received signal from each antenna, and Fig. 5.6 and Fig. 5.7 demonstrate the growth in signal power, which becomes greater than the noise. Obviously, if there is any high-intensity interference during the transmission of two devices, the target signal is immediately scrambled or masked by the force of the interference, e.g., the transmitter would fade in their direction.

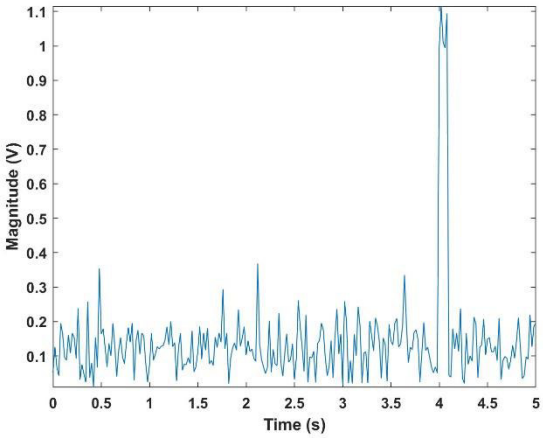

Figure 5-6 Beamforming with phase shift.

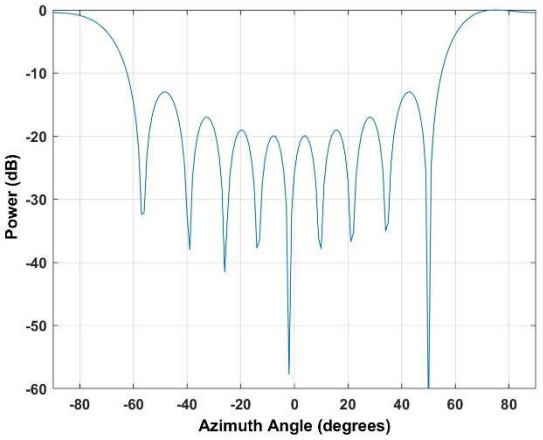

Figure 5-7 Beamforming main beam.

The BF in the LCMV technique places limitations in the directed directions while also cancelling interference along 20 or 50 degrees. LCMV maintains a flat zone approximately 45 degrees in azimuth, while MVDR creates a null.

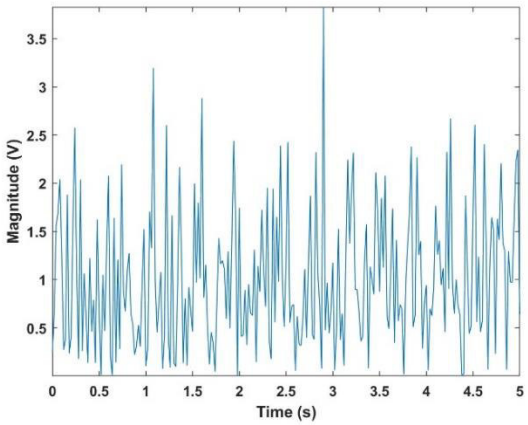

Figure 5-8 The output of the phase-shifting BF with interference.

As a result, for interference cancellation, we added two interference signals with azimuths of 30 and 50 degrees. Fig. 5.8 depicts an interference-filled receiving signal channel. Now, we proceed to solve the interference cancellation problem efficiently using MVDR, which is an adaptive BF, because the first approach is traditional, and this conventional approach may or may not solve the problem correctly due to its flaws.

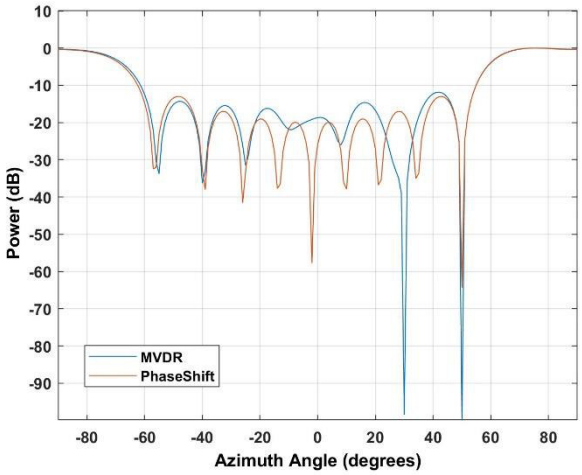

Figure 5-9 Receiving signal channel 1 with interference MVDR BF and phase shift BF.

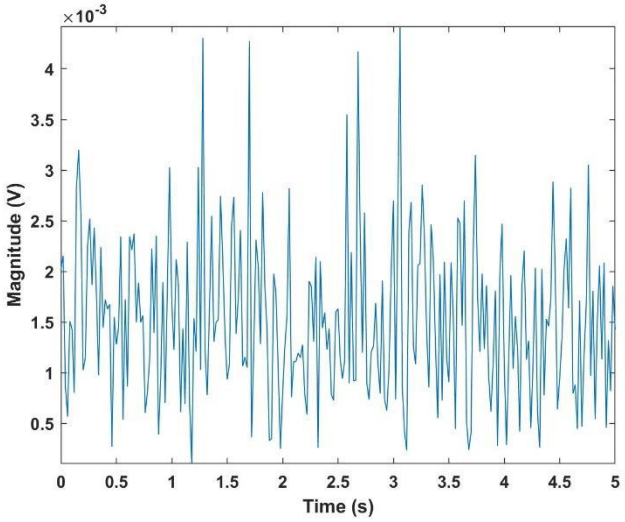

Figure 5-10 Receiving signal channel 2 with.

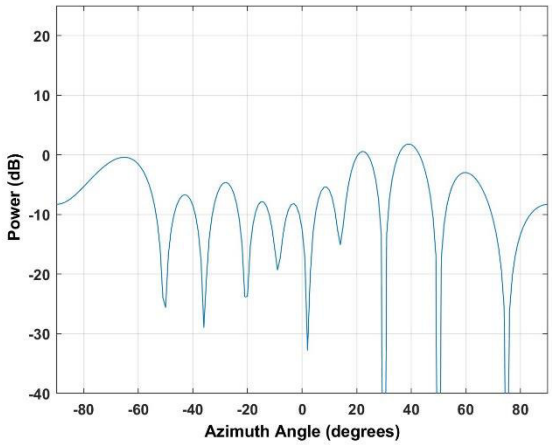

Figure 5-11 Receiving signal channel 2 with interference MVDR BF and phase shift BF.

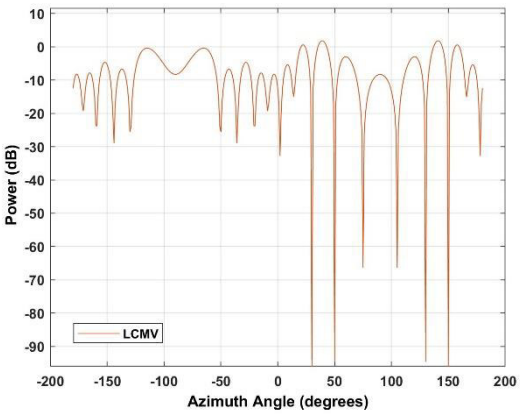

Figure 5-12 Decomposing of LCMV BF with shifted channel detection.

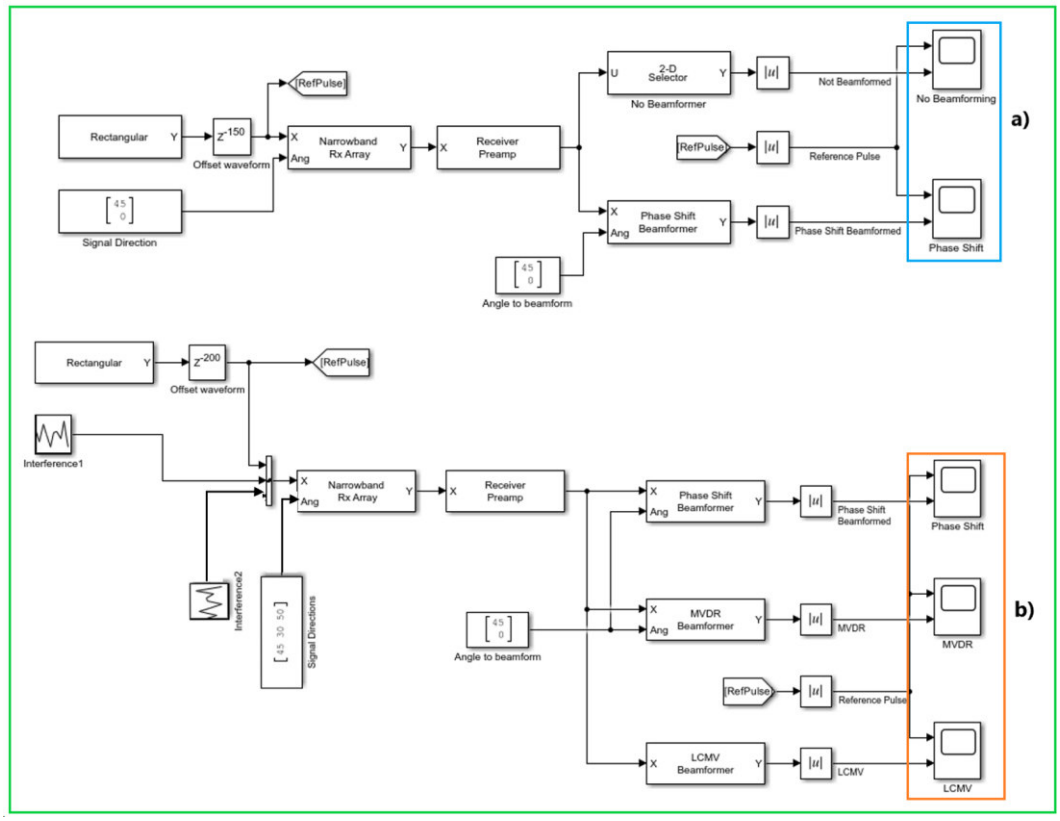

Figure 5-13 Two beamforming architectures: a) conventional on top and b) adaptive on bottom.

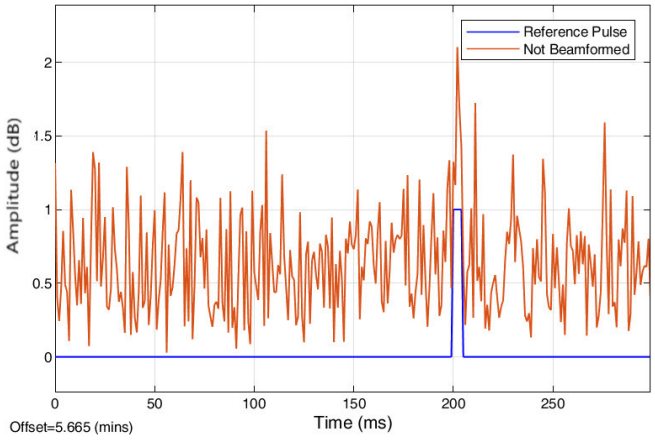

Figure 5-14 Reference pulse not beamformed.

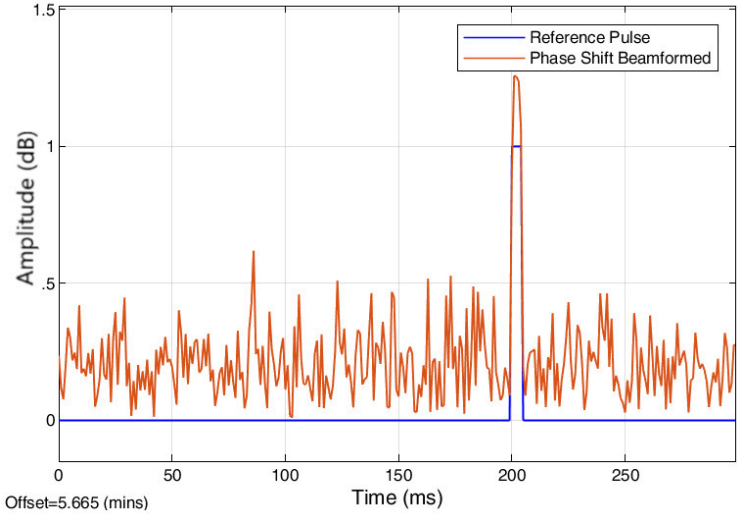

Figure 5-15 Reference impulse with phase shift beamformed.

As seen in Fig. 5. 14 and Fig. 5.15, the algorithm initially displays the signal reference impulse and phase shift beam. The phase-shifting BF is unable to detect pulse signals due to the high pulse intensity of the interfering signals, as illustrated in Fig. 5.16 (output of the phase-shifting BF in the presence of interference).

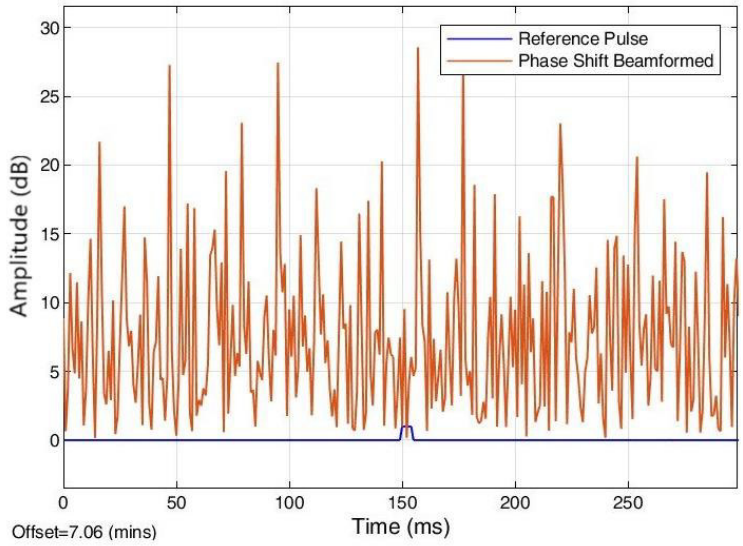

Figure 5-16 BF phase shifter output on a signal containing interference.

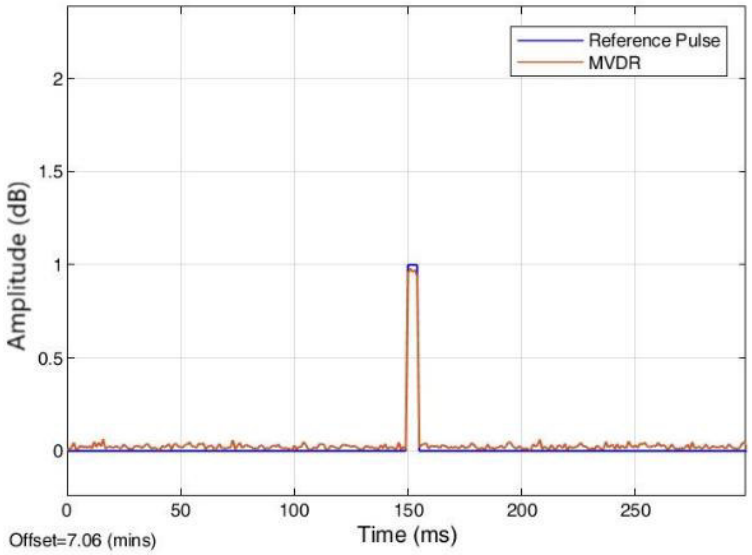

Figure 5-17 : Recovering the targeted signal by MVDR.

With the MVDR BF, we can see how MVDR suppresses signals coming from unexpected directions, including interference (see Fig. 5.17).

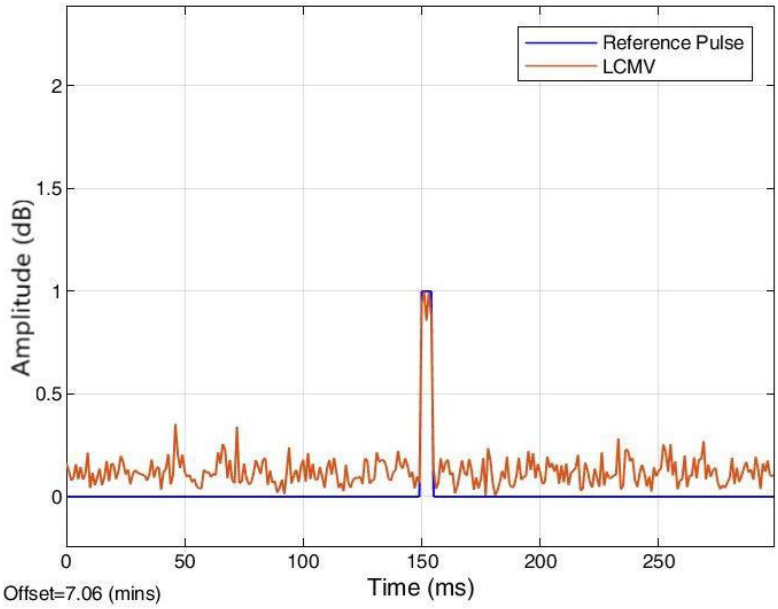

Figure 5-18 The recovery of the signal targeted by LCMV on a different angle of the signal.

Fig. 5.17 and Fig. 5.18 depict how LCMV and MVDR safeguard the signal from self-cancellation by executing the region expanding operation and guarding the target direction, as indicated in the previous paragraphs on signal self-cancellation.

The signal-to-noise ratio, which reveals how the methods reduce noise on the desired signal across the various figures of the outcomes that we observe, demonstrates the success of the BF methodology. The results show the effectiveness of the two approaches (LCMV and MVDR) with different SNR values (% signal to interference + noise), indicating the interference reduction SNR parameters on the target signal.

5.7 Supplemental simulation, results and discussion with CNN approaches

Fig. 5.19 demonstrates the way the second simulation differs from the first in some steps since it is based on CNN [61].

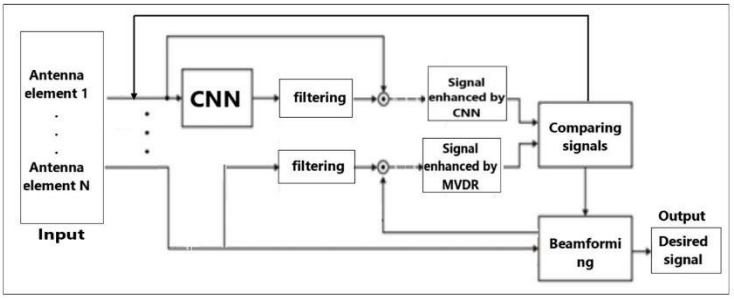

Figure 5-19 Architecture of the proposed signal cancellation system.

As seen in Fig. 5.19, an antenna array transmits the signal at the input. The signal travels through both techniques (CNN and the BF MVDR), and the signal from CNN is compared to the MVDR at the system output.

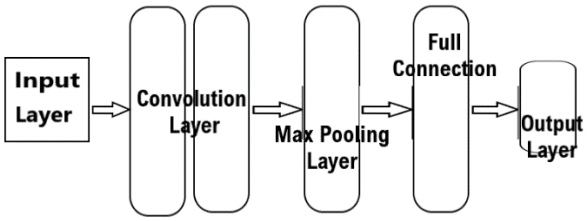

Figure 5-20 CNN architecture.

A CNN is made up of many convolutional layers (Conv). These layers have quadratic unit activation mechanisms that have been corrected (ReLu), the highest or median pooling levels (Max Pool, Avg Pool), and a totally linked layer. Stochastic gradient descent (SGD) and an ongoing standardisation

approach are typically employed to train the models. Unlike popular models like AlexNet and GoogleNet, the proposed CNN model is entirely original.

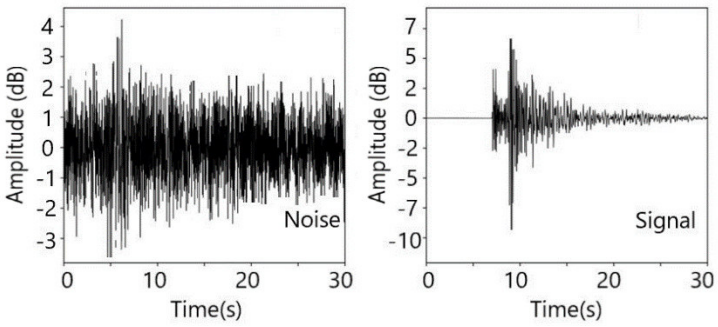

Figure 5-21 Noise (left) and original signal (right) after denoising.

A novel strategy is proposed that attempts to reduce the number of variables used by the algorithm while maintaining its accuracy. This method is based on the total number of convolutional layers and the time it takes to set up and perform the CNN tests, as shown in Fig. 5.21. The model main advantage is that it reduces the parameters and formation time for a CNN [62]. Our three CNN convolutional layers are what allow it to conduct denoising enchantments. Fig. 5.19 and Fig. 5.20 depict the proposed CNN architecture. The received signal covariance is utilised as the input, while the weight vector of the RF antenna network is used as the output. Fig. 5.22 depicts and identifies the desired signal as well as the noise component.

On the same signal, these images show the difference between the CNN technique and the MVDR. When the amplitudes of the CNN and MVDR signals are compared, we can observe that the denoising is quite near to the original signal. After reviewing all of the results, one might conclude that the BF performs admirably in signal rejection. As illustrated in Fig. 5.24, the BF technique detects and suppresses interference and noise better than the CNN technique. The same method improves communication between D2Ds.

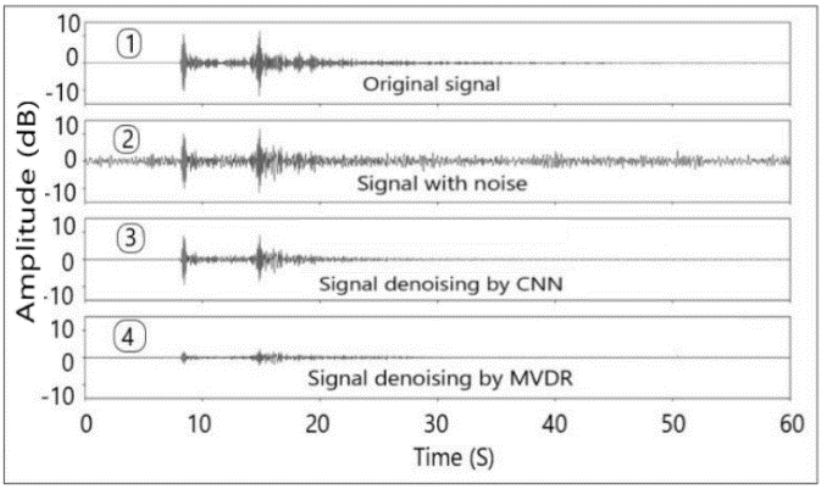

Figure 5-22 Denoising results from different approaches (BF and CNN).

As can be seen in Fig. 5.22, the noise in the signal tends to have a non-fixed frequency with an irregular amplitude. Fortunately, the ability of the MVDR to recognise this type of noise and eliminate it from the original signal with an increase in SNR.

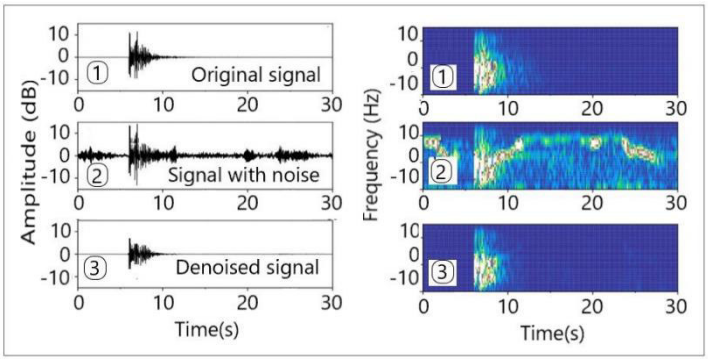

Figure 5-23 Denoising with increase in SNR.

As seen in Fig. 5.23, the green-grey hue symbolises interference and noise (parasites that degrade the quality of service of a signal), while the blue colour represents the desired signal.

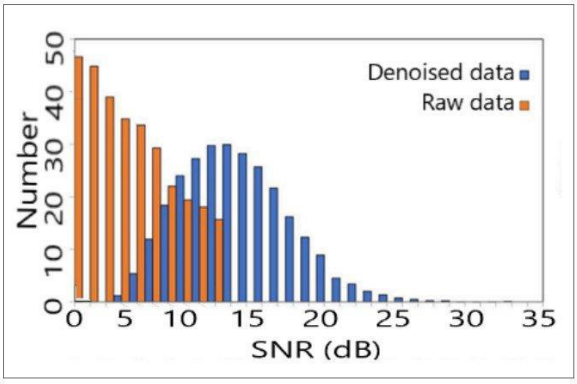

Figure 5-24 Results histogram.

Following signal processing, we used the histogram metric and accurancy to check the signal's denoising. Fig. 5.24 and Fig. 5.25 demonstrate a significant improvement in SNR.

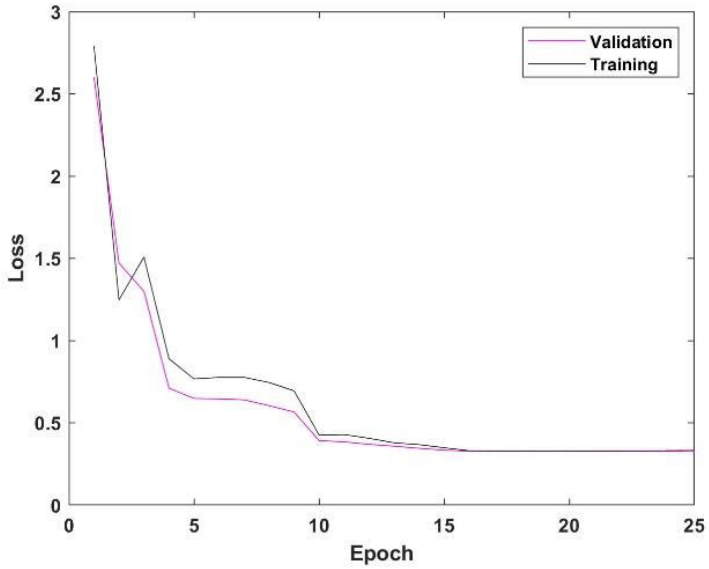

Figure 5-25 Training loss and validation curve.

Table 5-1Comparison of the results of two approaches on signal denoising (SNR).

Approach	SNR (dB)	r
MVRD	8.85	0.3325
CNN	11.60	0.6352

Table 1 demonstrates that, when compared to the MVDR approach, CNN can acquire a higher average SNR and an equally high average correlation coefficient (r), demonstrating that the noise reduction performance in the

transmission of signals between D2D is superior with CNN. The denoising results of CNN and MVDR applied to the same signal are shown in Table 1.

5.8 Conclusion

The BF holds significant importance within multi-element systems. Similar to every engineering challenge, it is possible to make compromises between computational complexity and system performance. Proposed are algorithms for interference detection and suppression, as well as optimisations of the targeted or desired signal direction between a D2D and an antenna array that maximise the rate and quality of communication. Implementing joint zero-forcing the BF on the wireless UEs to ensure that the selected equipment-to-equipment pairings do not conflict with the BS broadcasts.

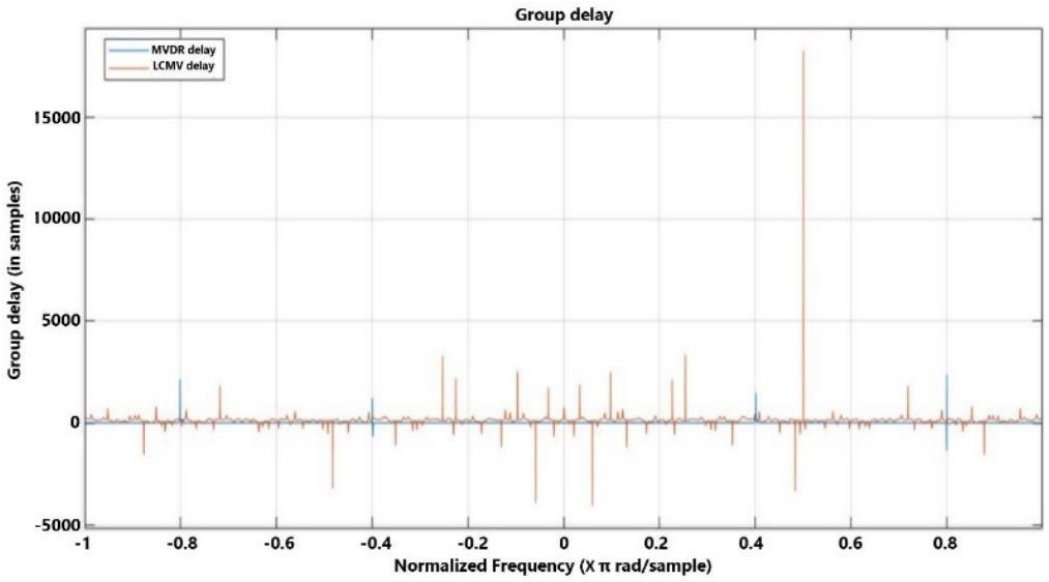

Figure 5-26 Group delay representation of beamformers.

To illustrate the efficacy of our techniques, we initially utilised the identical signal in the simulation while employing the conventional BF technique, which proved inadequate in distinguishing the intended signal from the interference. The application of the LCMV and MVDR methods to the same signal results in a direct separation of the signal from the interference, with extraordinary outcomes. Methods such as LCMV and MVDR are implemented to prevent self-cancellation of the desired signal and to suppress interference. Similarly,

both methodologies aim to maximise the intensity of the intended signal by shielding it from undesirable signals emanating from unintended directions. The suitability of the proposed BF algorithm (MVDR and LCMV) for optimising D2D communication in the antenna array is evident from the simulation results, as illustrated by the various result plots. The utilisation of graphical elements can be beneficial in delineating the comparative analysis of the characteristics documented in this thesis. As illustrated in Fig. 5.26, the group delay is a significant concern.

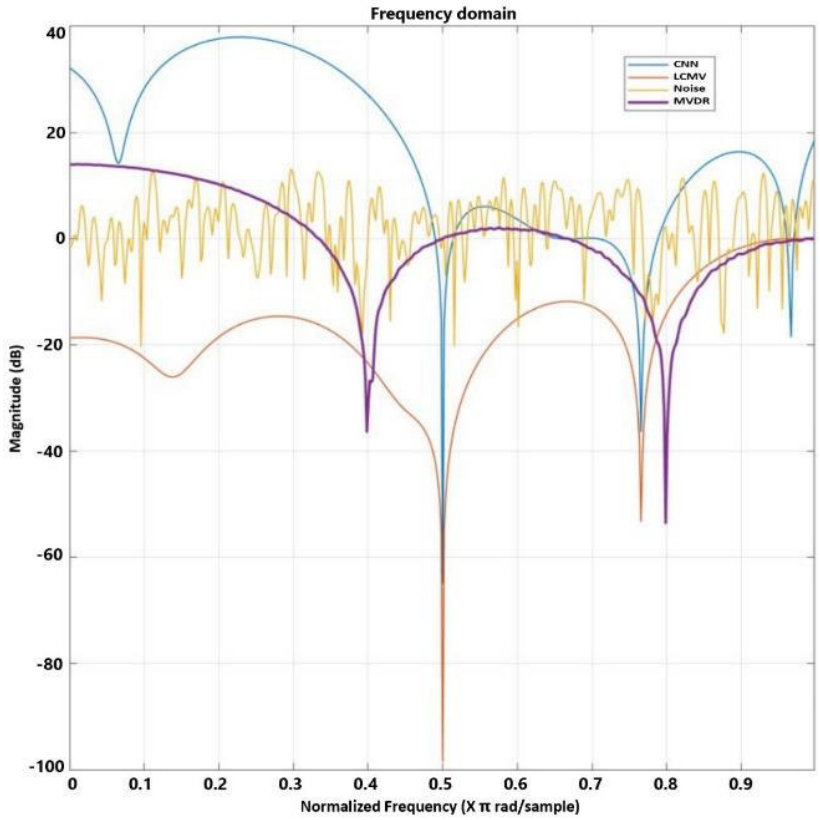

Figure 5-27 Comparative magnitude in frequency domain.

Group delay and phase delay happen during signal processing when a signal traverses a linear time-invariant (LTI) apparatus, such as that of an Ethernet cable, cell phone, microphone, amplifier, or loudspeaker. The group latency of the LCMV is greater than that of the MVDR at 0.5 (Fig.5.26). CNN was compared to the BF technique (LCMV and MVDR) for interference reduction and noise detection. BF is less than 20, whereas the CNN has a magnitude/dB

ratio between 40 and 20 (Fig. 5.27). In short, the BF improves upon CNN. This demonstrates the power of BF and its algorithms in enhancing the quality of signals throughout transmission and reception, thereby rapidly transforming telecommunications antennas (MIMO) (such as those found in base stations and Wi-Fi access points). To make a comparison we can affirm that the traditional approach (BF) technique has displayed a best signal optimization during transmission.

The following chapter will demonstrate how to be recovering and extracting the foetal ECG from a pregnant woman's ECG signal using the BF approach to separate the components of the two signals contained in a single envelope of the signal (ECG of mother).

Chapter 6

6. Beamforming algorithms for recovering signal information

6.1 Introduction

Fatal ECG extraction from a raw maternal ECG (mECG) signal utilising BF-based algorithms is the subject matter in this chapter. Signals containing information about the pregnant woman and the foetus are emitted by foetal ECG (fECG) sensors. Despite the fact that fECG instruments already produce distinct and detailed signals, certain studies pertaining to the child's condition require the signal to be enhanced via explicit processing. Four techniques, each with some modifications, are suggested in this article for carrying out the processing; the following techniques were implemented: The following techniques were implemented: MUSIC a DWT-based technique, and an EWT technique. Additionally, the LMS method was combined with an adaptive noise cancellation technique. The MUSIC and LMS methodologies are associated with the beamforming strategy.

By employing the MEMD (Multivariate Empirical Mode Decomposition) approach, the mECG source signal was decomposed and its individual components were identified. Also, noise was eliminated. Using optimised parameters, LMS, DWT, and MUSIC adaptively decomposed the signal to extract hidden components of the source signal, including foetal characteristics, the quick response system (QRS), pulse rate, and so forth. The outcomes demonstrated that LMS is more effective at identifying and eliminating superfluous noise after undergoing enhancements. By applying the techniques to the electrocardiogram (ECG) signal of a 30-year-old pregnant woman in good health, their applicability was confirmed.

Separating the fECG signal from the mECG and determining the functional condition of the foetal heart rhythm (heart rate and heart beats), which can indicate whether the fECG is malfunctioning, are the primary contributions of this study.

Extensive scientific investigation has been performed or is currently underway regarding the application of computational techniques for the separation or extraction of signals contained within an original envelope. Applied medicine, particularly within the domain of cardiology, is facing specific challenges when it comes to extracting the fECG and mECG signal components. These components are crucial for diagnosing congenital diseases of the foetus or infant, facilitating early treatment by medical professionals, and preventing the birth of malformations or other complications that could significantly disrupt the infant's growth and development. Using the BF method, the objective is to separate the fECG from the original mECG while preserving all essential information [63]- [64].

There are many techniques for processing ECG signals nowadays; however, the transient electromagnetic method, Short-time Fourier Transform (STFT), de-shape Short Time Fourier Transform, and Nonlocal Median have become the preferred methods of ECG signal processing researchers due to their fast signal extraction and decomposition, high efficiency, and great depth of exploration [65]- [66].

By employing entropies and the Support Vector Machine (SVM), the authors distinguished between focal and non-focal EEG signals [67]. The experimental findings demonstrated that the suggested methodology effectively differentiates seizure signals from non-seizure EEG signals by employing performance metrics including sensitivity, accuracy, specificity, score, and the Matthew correlation coefficient (MCC). These metrics were utilised to analyse the single-channel ECG and implement the discrete wavelet transform (DWT) to reconstruct the waveform of the respiratory signal [68].

The MEMD technique was utilised by the author to distinguish mECG from the abdominal ECG, while a wavelet-based technique was implemented to identify foetal R-peaks. By computing the cross-correlation between the detected and actual foetal heart rate signals, the performance was evaluated

[69]. By employing an adaptive noise cancellation method followed by the SWT, the author utilised the Identification of Systems (DaISy) and PhysioNet databases to extract fECG from composite signals. Additionally, in order to detect foetal distress, the heart rate and variability of the foetus have been measured [70]. We have utilised BF in conjunction with its two techniques (LMS and MUSIC) to conduct decomposition and precisely extract the fECG components from the mECG, as opposed to all previous methods: The utilisation of decomposition techniques (MUSIC, MEMD, LMS, and EWT) in conjunction with this combination has undoubtedly produced some of the most favourable outcomes in ECG processing. We implemented some improved techniques for the decomposition and extraction of the concealed components from the source signal as a result of the execution of this research.

6.2 Electrocardiogram

The volume of data in the medical area is continually expanding, forcing scientists to develop effective and appropriate strategies and methods for their speedy treatments in order to save human lives. A variety of approaches have arisen in response to this demand nonetheless, the electrocardiogram (ECG) holds the best position in the field of assessing heart activity. ECG is a test that measures the electrical activity of the heart to study how it works. An electrical impulse (or 'wave') travels through the heart with each beating. This wave causes the heart muscle to contract, causing blood to exit the heart. An ECG monitors and records the electrical activity that occurs in the heart. A doctor can tell you whether the electrical activity you're seeing is normal or not. If you have arrhythmia, chest discomfort, or palpitations, an ECG may be advised. Abnormal ECG findings can be used to diagnose a variety of heart conditions [70].

The ECG is used to detect heart problems such as recent or ongoing heart attacks, arrhythmias (irregular heartbeats), blockages in the coronary arteries, damaged areas of the heart muscle (caused by a previous heart attack), enlargement of the heart, and inflammation of the heart wall (pericarditis). In the event of a pregnant woman, monitoring the foetal heart rate is required in

order to take adequate precautions for therapy before and after birth if the infant has heart abnormalities.

6.3 Heartbeat modelling

The modelling of heartbeats is a critical step in automatically detecting distinctive waves. The goal is to find a mathematical representation of the shape of each wave that makes up the heartbeat that is as basic and compact as feasible. As a result, the most obvious way to characterise waves is to specify the signal's amplitude at each time. As a result, a vector in a space of a few hundred dimensions the recognition of the characteristic waves of the heartbeat is accomplished in two stages: segmentation and labelling. The division of the heart rhythm into zones expected to contain each cardiac wave is referred to as segmentation. Labelling is the process of assigning a medical label (P, Q, R, S, or T) to each of the zones defined during segmentation. As a result, the signal to be decomposed is a single heartbeat.

For example, if we consider the signal s of a beat to be modelled (Fig. 6.1) sampled at 500Hz, it is composed of 342 points. The signal s_0, used for the decomposition, is the vector composed of the signal s preceded by 85 zeros and followed by 84 zeros, which brings the dimension of this vector to 512, or 2^9. S_0 is therefore also a vector S_0 of the 512-dimensional space whose $i-th$ coordinate in the canonical base is the value of the signal at point i. In all that follows, the vectors of this space are noted in bold type.

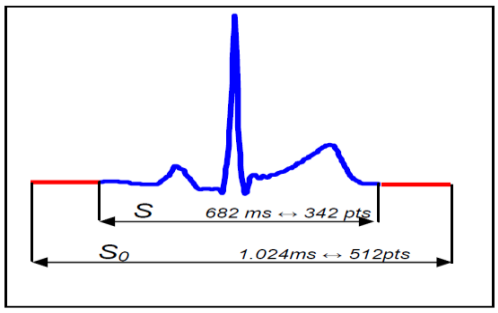

Figure 6-1 The orthogonal wavelet transforms.

The first step, in the decomposition, is the construction of the wavelet basis. If S_0 is the signal, to be decomposed, of length N_p (the number of points), the basis consists of N_p orthogonal wavelets S^I, all of which are deduced from the "mother" wavelet by translations and dilations. Let φ be the mother wavelet; the basis is constructed as follows:

$$B = \left\{ \varphi(2^m \times \pm n), n \in [1..2^{m-2}], m \in [1..\log_2(N_p)] \right\} \quad (6\text{-}1)$$

In (6.1), it is shown that, m and n are the expansion and position coefficients of each wavelet respectively, and N_p the length of the signal to be modelled wavelets. The $N_p - p$ basic functions are denoted $\{\varphi_1\}_{i=[1..N_p-1]}$ in the following. Such a library is shown in Fig. 6.2; wavelets (here Coiflets) that have the same expansion (constant m) are represented on the same line. The modelling of the signal is computationally inexpensive due to the orthogonality property of wavelets mentioned above.

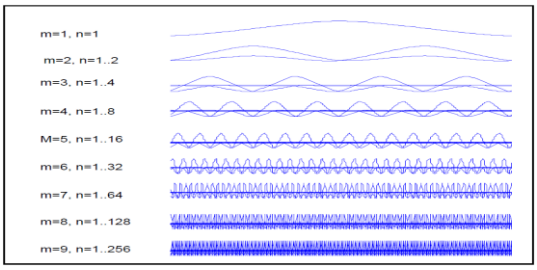

Figure 6-2 Wavelet family used for the decomposition of the S0 signal.

Once the basis is constructed, the decomposition of the signal S_0 is to apply to the vector S_0 the matrix of passage from the canonical basis to the in other terms, to calculate the coordinates of the S_0 vector in wavelet basis wavelet basis:

$$S_0 = \sum_{i=1}^{N_p-1} \langle S_0 | \varphi_i \rangle \varphi_i \quad (6\text{-}2)$$

Also, in (6.2) where $\langle S_0 | \varphi_i \rangle$ represents the *i-th* coordinate of the signal in the wavelet base. Thus, if we decide to choose $N < N_p - 1$ wavelets to model the signal

S_0, the best Y model will be obtained with the N wavelets having the largest scalar product in value. The model Y demonstrated in [71] will be obtained with the wavelets having the largest absolute scalar product with the signal.

$$Y(t) = \sum_{i=\{A\}} \langle S \mid \varphi_i \rangle \varphi_i(t) \tag{6-3}$$

where A represents the indices of the N largest absolute scalar products between the φ_i and S_0, the mean square modelling error is then written in (6.4) as:

$$J = \frac{1}{N_p} \sum_{j=1}^{N_p} \left((S(i) - Y(i)) \right)^2 \tag{6-4}$$

The results of the decomposition the example of an $N = 10$ wavelet model of the previous beat is shown below Fig. 6.3.

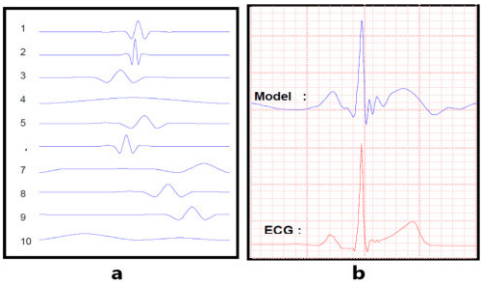

Figure 6-3 The best Y model with N = 10 Coiflets for the signal S0 is shown on the left (a). The decomposition is the weighted sum of the 10 wavelets shown on the right (b).

6.4 Techniques for mECG signal post-processing

In general, there are two methods for obtaining the fECG. The first option is to put an electrode directly to the foetal scalp (head); however, this causes too much discomfort for the mother. The last and second one, for the one we used, consists in the extraction of the fECG using electrodes placed on the mother (Fig. 6.4), implying that we will have both ECGs in a single envelope carrying the signal, which will carry out the objective of our study to carry out the extraction of the fECG from the mECG ECG signal. This approach is

important because it prevents any interaction between the foetus and any external energy.

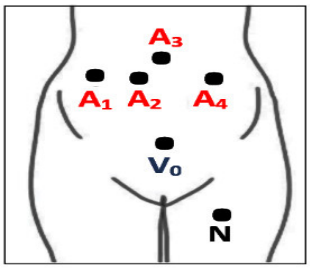

Figure 6-4 Acquisition of the maternal and fetal ECG signal.

A_1 … A_4: abdominal leads, V_0: reference electrode, N: active ground.

It is very important to point out that the ECG technique is a painless, non-invasive procedure, which means that nothing is injected into the body. The technique is carried out by means of electrodes (Fig. 6.4 and Fig. 6.5), usually between 12 and 15, which are attached to various parts of the body such as the arm, leg, and chest, in a particular way its electrodes are attached with small suction cups or adhesive patches, which have sensors that detect the electrical activity of the heart. An ECG normally takes between 5 and 10 minutes [72].

For the adaptive filter unit, the two main parts (blocks) are: first digital filter and last the adaptive algorithm; the filtering is performed by the digital filter and the adaptive algorithm performs a weight adjustment; the operation is carried out automatically, see Fig. 6.6, and see also the adaptive filter with explanation: $d(n)$ desired signal, $y(n)$ output of a digital filter driven by input signal $x(n)$, and the error signal $e(n)$ is the difference between $d(n)$ and $y(n)$.

Figure 6-5 ECG signal collection in a pregnant mother.

A preset cost function associated with $e(n)$ that the adaptive algorithm can optimize by adjusting filter weights [15].

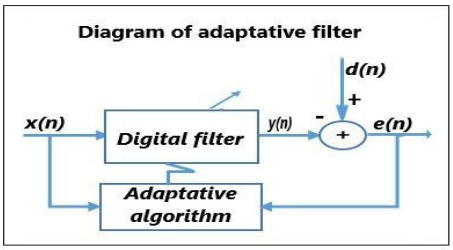

Figure 6-6 Diagram of adaptative filter.

The adaptive filter is implemented with a different number of structures and realization: the calculation, the complexity and the level of performance are decided by the choice of the structure and the number of iterations. In its adaptive implementation: speed of learning or convergence, computational complexity numerical precision and the stability of the algorithm are of the fundamental questions. LMS, is a simple and stable algorithm but, its speed is slow. In the LMS algorithm, the weight update is written in the form below. The relationships of the filter algorithm are displayed in (6.5-6.7).

$$y(n) = w^T(n-1)u(n) \tag{6-5}$$

$$e(n) = d(n) - y(n) \tag{6-6}$$

$$w(n) = \alpha w(n-1) + f(u(n), e(n), u) \tag{6-7}$$

LMS filters allow us to find the filter coefficients, minimizing the difference between the desired signal and the error signal, which formulae are described in from (6.8) up to (6.9)

$$f(u(n), e(n), u) = u(n)u^*(n) \tag{6-8}$$

$$w(i-1) = w(i-1) + ue(i)x(i) \tag{6-9}$$

where $w(i)$ is the error signal, $x(i)$ is the input, $u(n)$ is a step size parameter, and $w(i)$ is the weight function. The parameter μ satisfies the

$$0 < u < (1/\lambda \max) \tag{6-10}$$

Fig.6.7 shows detection and extraction of the fetal heartbeat from the mother's heartbeat (measured signal) by adaptive filtering technique; Fig. 6.8 shows the cancellation and error detection also noise contained in the signal to output reference signal with MEMD.

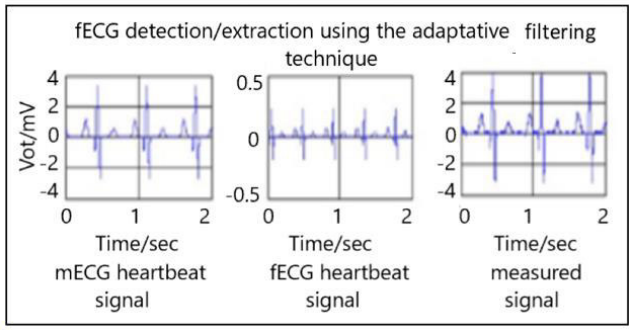

Figure 6-7 Fetal ECG detection/extraction using the adaptative filtering technique.

6.5 Proposed approach for signal processing

We have proposed four joint approaches, including wavelet transformation technique. The wavelet technique is essential in clinical studies to detect the different signals that make up a raw one; the wavelet transformation is a recent technique in non-invasive electrocardiology. Details of the ECG signal is highlighted in time and frequency resolution using wavelet transformation [73]. During our study, we have opted for the wavelet technique to extract up to the minute information of the abdominal signal and knowing that this algorithm remains complex. The goodness of this set of algorithms is the following: the best representation of the signal missed by one member could necessarily be represented by another, to have the fECG signal. We have tried to apply the wavelet (dB10), with the regularity of the wavelet is dB10 (1.25) which is a little higher than that of dB4 (2.90). fECG signal is extracted from the original signal using a two-level wavelet transform. Wavelet transformation technique uses the convolution of the wavelet function $\psi(t)$ with the signal $x(t)$ is the wavelet transform. In this technique, the dyadic orthonormal discrete wavelets will be put together to scaling functions $\varphi(t)$, the coefficient approximation is

produced by convolving the scaling function and the signal. The discrete wavelet transform (DWT) is written in (6.11), [74].

To reconstruct the original signal, we have selected a wavelet base $\psi_{m,n(t)}$ of coefficient approximation, at the scale and in the location as represented by the *m*, *n*, is described in (6.11-6.12)

$$S_{m,n} = \int_{-\infty}^{\infty} x(t)\varphi_{m,n}(t)dt \tag{6-11}$$

N- finite length of the discrete signal. $0 < m < M$ - discrete approximation range scales of the signal, so we can write it:

$$x_0(t) = x_M(t) + \sum_{m=1}^{M} d_m(t) \tag{6-12}$$

The LMS is a search algorithm in which a simplification of the gradient vector computation is made possible by appropriately modifying the objective function. The LMS algorithm, as well as others related to it, is widely used in various applications of adaptive filtering due to its computational simplicity.

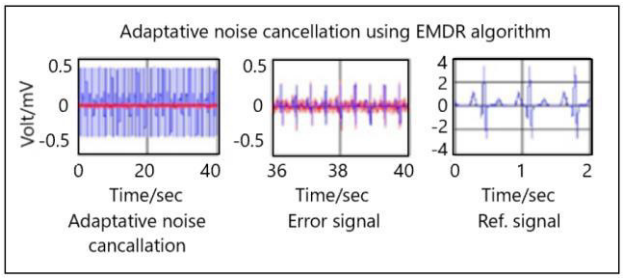

Figure 6-8 Adaptative noise cancellations.

The convergence characteristics of the LMS algorithm are studied in order to establish a range for the convergence factor that will guarantee stability; (difference between the desired and the actual signal), as shown from. (6.13), up to (6.16).

$$W_k(n+1) = W_k(n) - \mu\nabla J \tag{6-13}$$

In (6.13) where, ∇ is the gradient of MSE J, μ is step size, $W_k(n)$ is tap value of k^{th} tap n^{th} iteration , the step size can be variable or constant. In LMS algorithm, it is a constant positive number whose value ranges from

$$0 < \mu < 2/Y\max \tag{6-14}$$

In (6.14) $Y_{\max}$ is maximum eigen value of *R*. If μ exceeds the limit, then the trajectory of W_k becomes unstable.

$$W_k(n+1) = W_k(n) + \mu E[e(n)^* X(n)] \tag{6-15}$$

In (6.15-6.16) of steepest descend algorithm. Now LSM algorithm estimates the gradient as:

$$W_k(n+1) = W_k(n) + \mu^* e_n * X_n \tag{6-16}$$

With this algorithm, calculating the value of the next catch becomes easier. Updating the K^{th} value requires only one multiplication and one addition. Therefore, for a filter of order $P+1, P+1$ multipliers and adders are needed. An adder is needed to find $e(n)$ and a multiplier for $\mu^* e(n)$ [75], [76]. Finally, *P* adders and $P+1$ multipliers are needed to find the output $y(n)$. Thus, a total of $2P+3$ multipliers and $2P+2$ adders are needed. Flowchart of LMS algorithm, the flowchart of is based on the following three equations:

$$y(n) = w(n)^* x(n) \tag{6-17}$$

$$e(n) = d(n) - y(n) \tag{6-18}$$

$$w(n+1) = w(n) + \mu^* e(n)^* X(n) \tag{6-19}$$

The (6.17) calculates the output of filter by multiplying input with the filter weights, the (6.18) calculates error between the desired signal and output. The (6.19) represents filter weight adaption. It denotes the LMS algorithm. The weights are calculated by changing the previous weight and the converging factor. We also used the MUSIC technique; the literature on the MUSIC algorithm is described in [77].

6.5.1 Pre-processing of signal

In general aspects of signal preprocessing (in the field of signal processing it is obvious the signal must be prepared before processing in order to increase its quality. This operation is known as pre-processing. The objective is to remove all kinds of impurities and unwanted elements from the signal as shown in Fig. 6.9. We have used the MEMD technique to pre-process the signal, which has allowed us to detect and remove the noise as shown in Fig. 6.8.

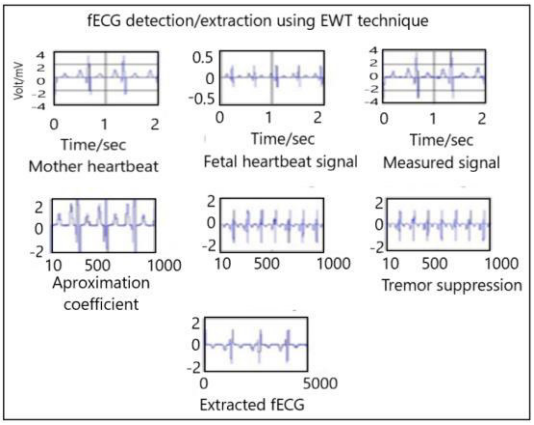

Figure 6-9 Fetal ECG detection/extraction using EWT technique.

6.5.2 Segmentation of the mECG signal

The segmentation of the mECG signal components allows us to identify them. At this point, the components of our fECG signal (peak, QRS, frequency, heartbeat, apnea peak, etc.) will be detected by the MUSIC algorithm (Fig. 6.10).

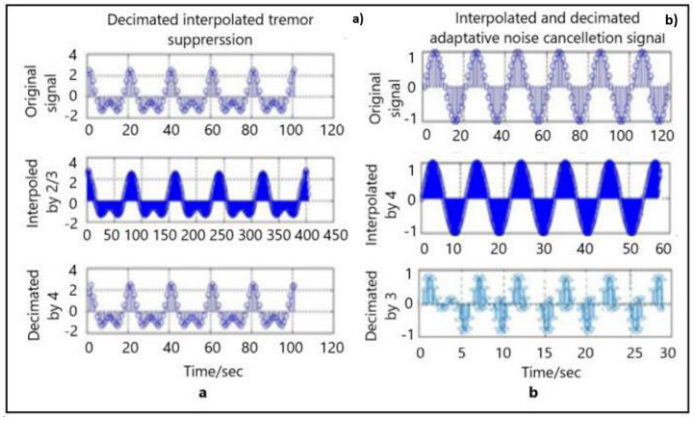

Figure 6-10 Decimated and interpolated tremor suppression (a), Interpolated and Decimated and noise cancellation signal (b)

The use of algorithms saves time in interpreting the ECG signal, particularly for pregnant women who bring the foetal signal within [76].

6.5.3 post-processing of mECG signal

An ECG is a test that measures the electrical activity of the heart to determine how it works. An electrical impulse or wave travels through the heart with each heartbeat. As stated in Section II, this wave causes the heart muscle to contract and expels blood from the heart. We are dealing with a pregnant woman's ECG signal here, not an ordinary ECG signal, therefore by capturing this ECG automatically, we have a double ECG in its components (mother and foetus). As the various results show, the goal of this study is to isolate all of the components of the source signal so that the ECG of the foetus and its internal components can be detected. It is critical to offer information to the cardiologist or paediatrician in order for the cardiologist or paediatrician to diagnose the mother's and, more importantly, the foetus's cardiological state, and to plan for the various outcomes if the foetal heart has abnormalities. The methods provide distinct separation of the two signals' components in terms of frequency, wave peaks, power spectrum, decimations, and interpolations.

6.6 The outcomes

By definition, an ECG is a non-invasive technique that delivers electrical indications of cardiac function. In this research, ECG signal processing with appropriate approaches (MUSIC, MEMD, LMS, and EWT) has resulted in a significant improvement in ECG signal interpretation.

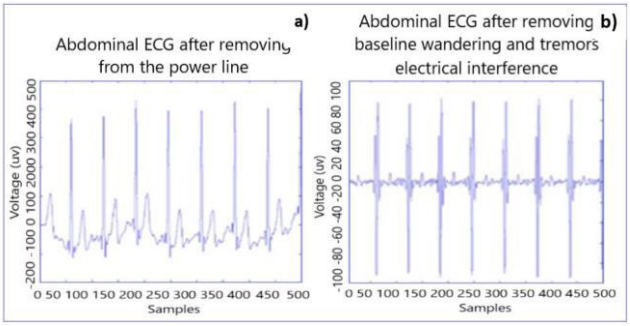

Figure 6-11 a) Abdominal ECG after suppressed power line interference noise at 50 Hz and a) Abdominal ECG after removing interference from the power line, line based on the wandering and trembling.

Especially when it comes to interpreting an ECG signal from a pregnant woman. The most unique advance is the separation of the components of two ECG signals (mother and foetus), which were formerly in one ECG signal, the mother's, as we described at the beginning of our study. That was the context under which we worked. Fig. 6.12 and Figure 6.13 explain how the separation of the two ECG signals was achieved.

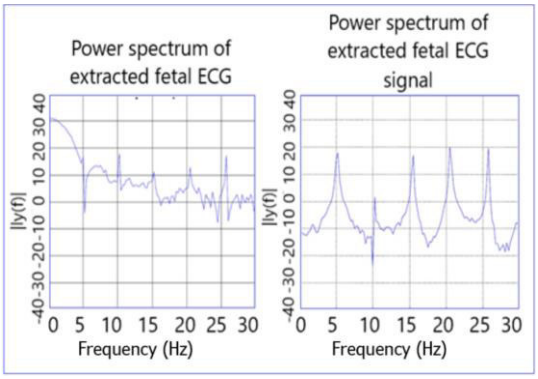

Figure 6-12 Power spectrum of simulated mother ECG signal and power spectrum extracted from fatal ECG signal.

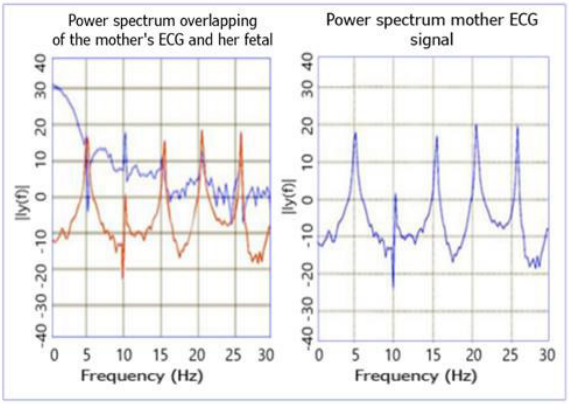

Figure 6-13 Power spectrum overlapping of the mother's ECG signal and her fetal component.

To make it easier for the cardiologist's analysis of the ECG signal from a pregnant woman, thereby enabling time-saving and accurate diagnosis of foetal cardiac activities, assessment of foetal heart health, and prompt preparation of appropriate therapy, the algorithms will highlight detected abnormalities. This will enable the cardiologist to provide a precise prognosis.

The power spectrum of the ECG signals from the mother, shown in red, and from the foetal, shown in blue, overlap in figure 6.13.

The plot suggests that the foetal heart remains reliant on the maternal heart, as evidenced by the nearly identical peaks of the two signals. This reliance is due to the fact that the foetal heart is sustained by the blood of the mother. This enables us to validate the efficacy of the algorithm.

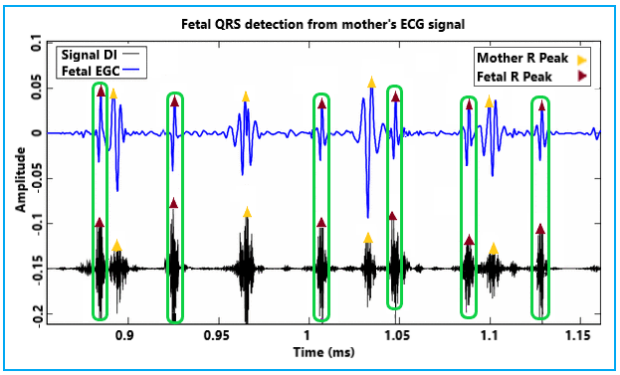

Figure 6-14 Fetal QRS detection from mother's ECG signal.

Fig. 6.14 showed many signals, but they were all contained within a single envelope of origin or source (mECG signal). Each signal's R peaks were distinct. The current result is the result of the MUSIC algorithm, which sorts, separates, and provides reasonable estimations of the number of very small signals. It may also distinguish between signals and noise present during transmission, recording, or dispersion in several channels, sometimes with particular information discovered (see Fig. 6.15 and Fig. 6.16).

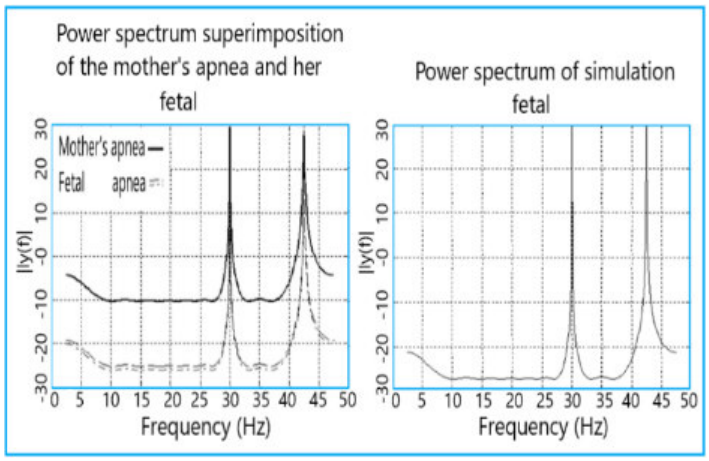

Figure 6-15 Power spectrum overlapping of the monther's apnea and her fetal signal.

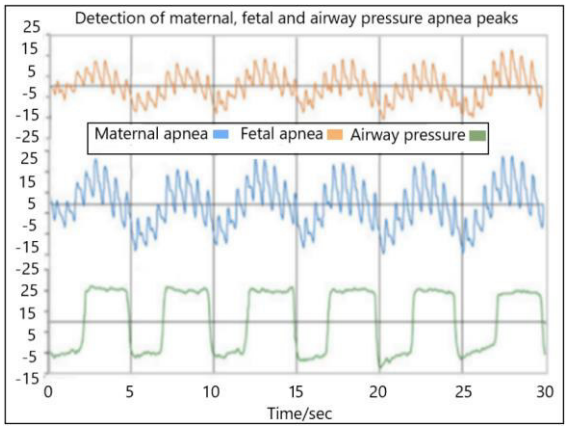

Figure 6-16 Power spectrum overlapping of the mother's apnea and her fetal signal in the bottom, detection of maternal, foetus and airway pressure apnea peaks are represented.

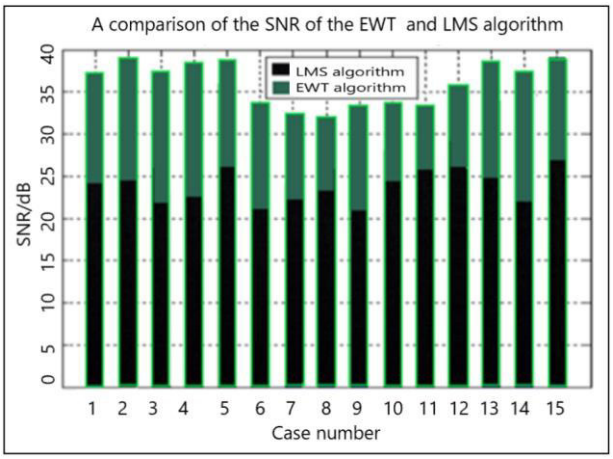

Figure 6-17 A comparison of the SNR of the EWT and LMS algorithm.

We have decided, given the objectives of the paper, to introduce decimation and interpolation for a further interpretation. Decimation and interpolation are two operations that affect the timescale of a signal. For discrete signals, time scaling corresponds to increasing or decreasing the length of the signal. However, we must pay attention to how these operations are carried out. Decimation is the time compression of a signal. This corresponds to speeding up a signal or reducing its sampling rate.

Suppose we have a signal $x[n]$ which corresponds to a continuous signal $x(t)$ samples at t_s intervals. The signal = $y[n]$ is then equivalent to the compressed signal which is sampled at and contains the samples $x[0], x[2], x[4], \ldots$. $y[n]$ can also be obtained directly if the signal $x(t)$ is sampled at intervals of $2t_s$.

Decimating by a factor of N is equivalent to keeping all N samples of a signal. This can lead to information loss.

Fig. 6.17 compares the SNR of the EWT and LMS algorithms, and Fig. 6.18 details the procedure for detecting and labelling the components of the apnoea signal with the MUSIC algorithm on a normal class of apnoea, including hypopnoea, which are shown here in bright colours: red, yellow, and green, as well as other lines labelled in this way with this legend: AF: Airflow, AE: Abdominal Effort, TE: Thoracic Effort SL: Stage Label.

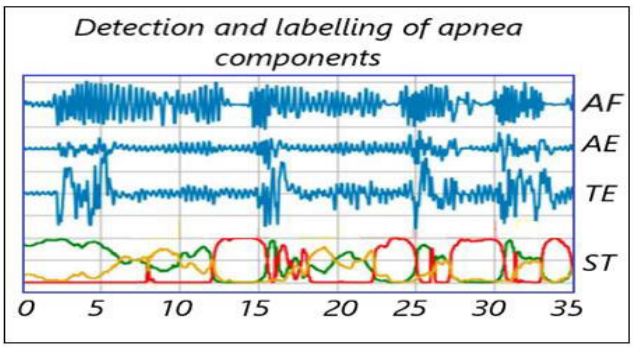

Figure 6-18 Detection and labelling of apnea components.

Another needed operation is the interpolation. It is the stretch over time. This corresponds to slowing down the signal or increasing the sampling rate. Suppose we have a signal $x[n]$ which corresponds to a continuous signal $x(t)$ sampled at intervals t_s. The signal $y[n] = x[n/2]$ is then equivalent to the signal $x(t)$ which is sampled at intervals of $x(t)$ (or at a rate of $S = 2/t_s$). We therefore have twice as many samples: we have stretched the signal (8) in both directions. However, how do you calculate the value of the new samples? Three popular techniques exist for doing the interpolation: 1. Zero interpolation: Implies that each new sample is zero, 2. Step interpolation: We take the previous value for the new sample, and 3. Linear interpolation: The values on each side of the new sample are averaged, Decimation is the reverse of interpolation, but the inverse is not necessarily true. When we apply the decimation, we lose some information; so, we are not able to reproduce the original signal correctly.

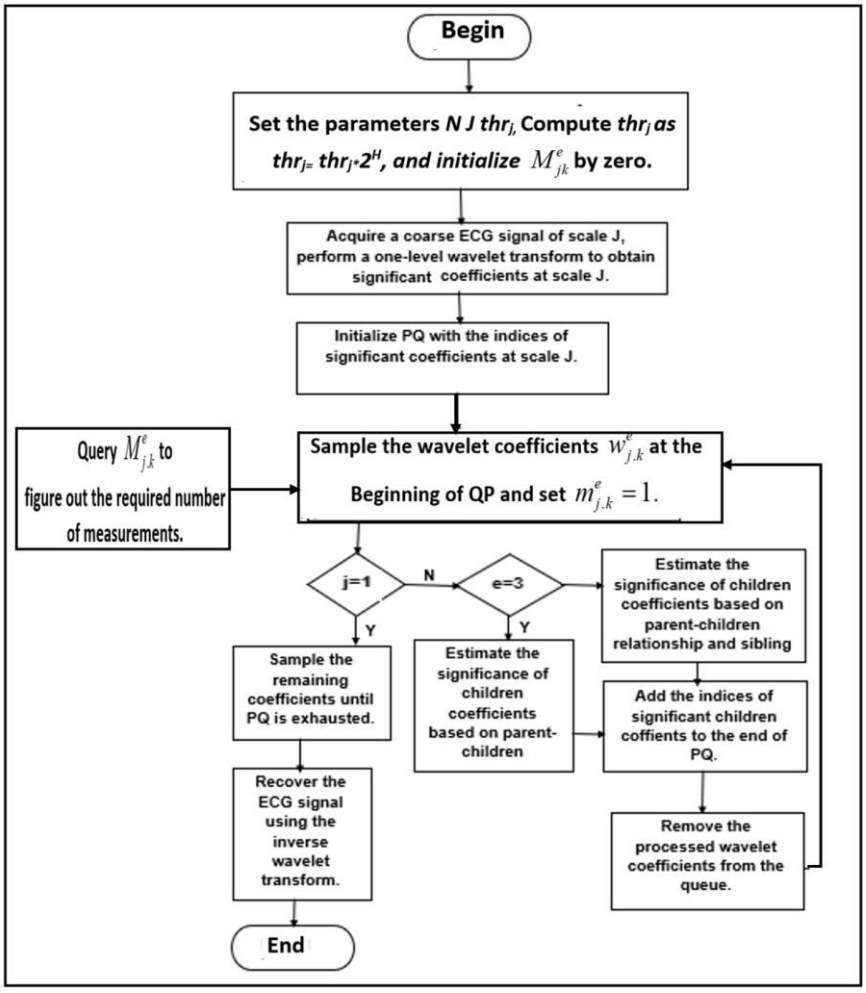

Figure 6-19 EWT Flowchart.

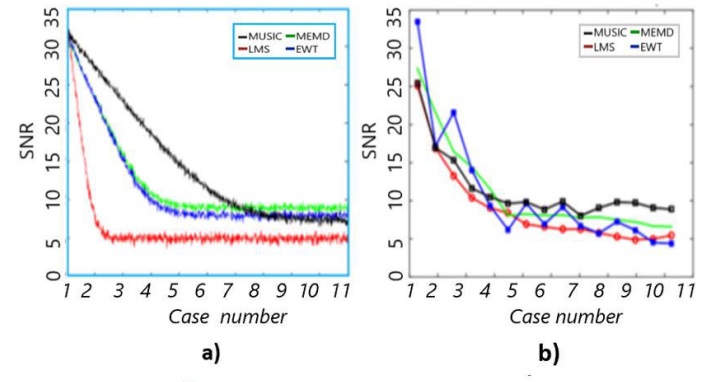

Figure 6-20 A comparison of the SNR of the MUSIC, MEMD, LMS and EWT algorithms for ECG (a) and apneas (b) of the mother and the foetus.

6.7 Conclusion

Significant advancements have been achieved with the BF technique. The BF, also known as spatial filtering or channel formation, is a signal processing technique used for the transmission or directional reception of signals in antenna and sensor networks. As illustrated in Fig. 6.20, several investigations employ four distinct approaches: LMS, MUSIC, MEMD, and EWT.

Deconstructing, visualising, and emphasising the internal components of the ECG signal of an expectant woman is the purpose of this research. As illustrated in Fig. 6.15 - 6.20, a normal decomposition and separation of the internal components of the initial signal (the mECG) were made feasible by the various techniques. The objective is to optimise the time management process for medical practitioners, specifically cardiologists, when interpreting ECG signals, with a particular emphasis on those of pregnant women and the developing foetus.

The main technique employed in this study is still filtering, which is used to separate signal components based on their frequencies and channels. For processing ECG signals, the BF technique (adaptive filtering) works well; each signal source component has been filtered by its correct frequency.

The major goal is to highlight the extraction of the fECG components when the offered techniques are applied to the entire mECG signal to extract the fECG. The BF technology allows visibility and observation of foetal cardiac function due to the separation of the components.

The next chapter characterises delay and sum motion to determine hydrodynamic signal components. The BF approach is used to extract hydrodynamic data from river channel footage, including flow velocity, temperature, depth, wave motion, and riverbed recognition.

Part IV:
Beamforming: Delay and Sum for Motion Characterization

Chapter 7

7. Delay and sum beamforming: characterizing objects in motion

7.1 Introduction

At the local level, environmental factors must often be monitored using low-cost monitoring techniques and technologies because they must be assessed on a regular basis. Stream flow in riverbeds or canals is a hydrological variable that must be monitored in order to control run-off patterns and predict flooding, thereby protecting people and infrastructure. Furthermore, measuring such a variable is always critical for understanding the environmental state of connected aquatic ecosystems. This chapter discusses a new way to examine the hydrodynamic properties of a specific channel utilising a BF technique used for video detection. Several parameters, including flow velocity, temperature, and riverbed displacement, have been estimated.

The adopted BF method operates on a modified Delay and Sum (DaS) approach, incorporating the MUSIC and functioning as post-processing for synthetic aperture radar (SAR). The results are extremely intriguing, particularly when compared to the data collected on-site, and they support the implementation of inexpensive video sensors along the channel or river course for monitoring purposes.

Additionally, the study demonstrates how BF measurements can be calibrated utilising traditional approaches in order to obtain more precise data. While the results are certainly capable of improvement, they do suggest that there is opportunity for updating and enhancement. The greyscale/pixel histogram was selected as the metric for evaluation, with consideration given to the

illustrations of curves and layers. Variations are evident in the presentations contingent upon the locations where the collaborative videos were filmed.

The European Union's Water Framework Directive (WFD) explicitly acknowledges the importance of the flow regime for the quantitative and qualitative evolution dynamics of natural water systems.

The River Basin Management Plan (RBMP) can be implemented using credible indicators of hydrological impact on aquatic systems and ecology derived from flow component analysis and change [78]. However, statistical, or physically based models must handle enormous data sets and long-time series for such analysis. For smaller watercourses, when streamflow observations are limited or lacking, this data demand is a weakness [79]. Monitoring programs should be modified to better understand hydrological changes and their effects on qualitative and morphological watercourse features, including smaller ones.

The International Association of Hydrological Sciences (IAHS) declared 2003–2012 the "decade of the ungauged basin" [80], promoting science and technology to provide hydrological data where ground-based observations are lacking. The best solution and cost-effectiveness must be balanced while creating a hydrological monitoring network [81]. Due to hydrogeological and climatic reasons, Mediterranean basins have substantial regional and temporal hydrological regime fluctuation, which increases monitoring requirements and expenditures. Characterizing riverbed infiltration under diverse hydrologic, hydraulic, and sediment-load regimes is important in arid land hydrology. In such circumstances, streamflow-vadose zone interaction must be thoroughly researched for flow measurement network design and development.

Aquifers supply most water in dry and semi-arid locations, and streambed infiltration during floods is the predominant recharge source [82], [83]. General groundwater recharge review studies exist [84], [85], but not for ephemeral and intermittent streams in dry settings. Shanafield and Cook [86] present a simple method to estimate streambed infiltration into groundwater using differential discharge data between upstream and downstream portions. In ephemeral watercourses with unstable flow, loss rates must be calculated by integrating upstream and downstream flow rates over the flow event [87].

Rating curves are used to automatically quantify flow depth and discharge rate, but ephemeral streams are difficult to rate again. Ephemeral and intermittent stream basins have rapid water runoff, which causes erosion and deposition, streambed geometry changes, and flowrate inaccuracies [88]. An novel and dependable alternative to standard riverbed assessment methods is utilizing sensing devices that can monitor flow conditions and other geo-environmental parameters using still or video images [89], [90].

The digital BF synthetic aperture radar technique is one approach utilized to generate a beam capable of aggregating data from a multitude of sensors. BF finds application in numerous domains that are pertinent to the subject matter of this work [91], [92], [93], [94]. BF is founded on the notion of array processing, which comprises the subsequent primary concerns: array configuration, temporal and spatial properties of the signal and interference, and ultimately, the intended purpose of the array processing. Radar systems predominantly operate through the utilization of antenna arrays; in fact, they represent the initial implementation of BF. These arrays serve the purpose of determining the trajectory of beams or signals, including the DOA [95], [96].

The overarching objective of the suggested methodology is to develop a proficient surveillance system that can conduct measurements distributed across the channel and is consistent across various seasonal flow regimes.

7.2 Materials and procedures

An algorithm utilised for frequency estimation and transmitter localization is MUSIC [27, 28]. Even with an extremely low SNR, this algorithm enables the direction of incident signals on a sensor network to be determined. The MUSIC algorithm implemented in the work to detect and separate peaks for nearby signals is illustrated in Fig. 7.1.

We assume that a signal vector, consists of complex exponentials, whose frequencies are unknown, in the presence of white Gaussian noise (WGN) as given by the linear model (7.1)

$$X = As + n \tag{7-1}$$

Here $A = [a(\omega_1), \dots, a(\omega_p)]$ is an $M \times p$ Vandermonde matrix of steering vectors $a(\omega) = \left[+1, e^{-j\omega} e^{-j2\omega}, \dots, e^{-j(M-1)\omega}\right]^T$ and $S = \left[s_1, \dots, s_p\right]$ is the amplitude vector. A crucial assumption is that the number of sources P, is less than the number of elements in the measurement vector, $M,\ i.e. P < M$.

The $M \times M$ autocorrelation matrix of X is then given (7.2) by $R_x = AR_sR^H + \sigma^2 I$, where $\sigma^2$is the noise variance, I is the $M \times M$ identity matrix, and R_s is the $p \times p$ autocorrelation matrix of S.

$$\widehat{\boldsymbol{R}}_{\boldsymbol{x}} = \frac{\mathbf{1}}{\boldsymbol{N}} \boldsymbol{X}\boldsymbol{X}^{\boldsymbol{H}}, \tag{7-2}$$

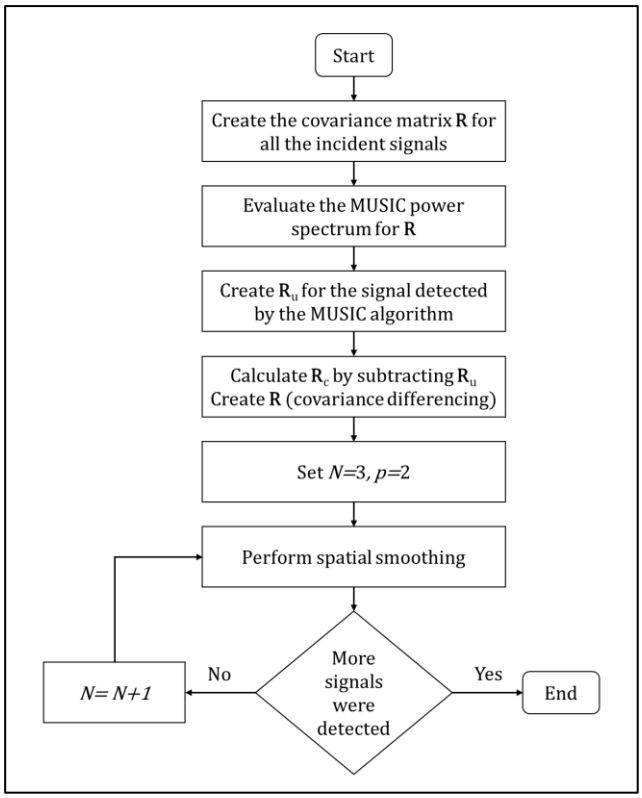

Figure 7-1 MUSIC algorithm carried out in the work for detecting and separating peaks for close signals.

where $N > N$ is the number of vector observations and $X = [X_1, X_2, \dots, X_3]$. Given the estimation of R_x, MUSIC estimates the frequency content of the signal or autocorrelation matrix using an eigenspace method. Since R_x is a Hermitian matrix, all its **M** eigenvectors $\{V_1, V_2, \dots, V_M\}$ are orthogonal to each other. If the eigenvalues of R_x are sorted in decreasing order, the eigenvectors

$\{V_1, V_2, \ldots, V_p\}$ corresponding to the p largest eigenvalues (i.e., directions of largest variability) span the signal subspace $\mu_s \perp \mu_N$.

7.2.1 Estimating the exact number of targets and minimum description length

For MUSIC algorithm to produce or give an accurate estimate of the DOA [97], [98], the total number of targets in each range bin must be known. One algorithm that estimates the number of targets is called the minimum description length (MDL). MDL uses the eigenvalues of the correlation matrix and maximizes the following log likelihood ratio.

$$L\Theta = -Nlog\ det\ R - tr[R]^{-1}\hat{R}, \tag{7-3}$$

In (7.3-7.4), where $\hat{R}$ is the sample covariance matrix:

$$\hat{R} = \frac{1}{N}\sum_{i=1}^{N}(t_i) \times (t_i)^H, \tag{7-4}$$

By substituting in maximum likelihood estimates, the log likelihood ratio is reduced to (7.5)

$$L(k) = (p-k)Nlog\left(\frac{\prod_{i=k+1}^{P} l_i^{1/(p-k)}}{\frac{1}{p-k}\sum_{i=k+1}^{p} l_i}\right), \tag{7-5}$$

where p is the number of array elements, k is the number of targets and l_i are the eigenvalues with $l_i \geq l_2, \ldots, l_p$. Using this maximum likelihood estimate and adding in the free parameter calculation, the resulting criterion is:

$$MDK(k) = L(k) + \frac{1}{2}k(2p-k)logN, \tag{7-6}$$

In (7.6), where N is the number of observations of the signal for our radar, the correlation matrix is made from the average of 6 pulses, so $N = 6$. To solve the maximum likelihood estimation, L should be maximized. The number of targets is value of k minimizes the MDK. Once this has been done, the $p-k$ eigenvectors corresponding to the $p-k$ smallest eigenvalues can be used from a noise matrix as explained above.

7.2.2 Eigenvalue gradients

In the gradients of the eigenvalues are used to estimate the number of targets. Given that the eigenvalue decomposition of the correlation matrix, where (7.7) L is the number of antenna elements, results in eigenvalues [99], [100]

$$\lambda_1 \geq \lambda_2 \geq \cdots \geq \lambda_p \geq \cdots \geq \lambda_L, \tag{7-7}$$

$$\Delta\lambda = \lambda_1 - \frac{\lambda_L}{L-1}, \tag{7-8}$$

$$\Delta = \lambda_1 - \lambda_{i+1},\ for\ i = 1, \ldots, L-1, \tag{7-9}$$

Next you find i that satisfies:

$$\Delta\lambda_i \leq \Delta\lambda, \tag{7-10}$$

In (7.10), then take the i that first one of the last continuous blocks and the estimated signal number is

$$p = i_0 - 1. \tag{7-11}$$

7.3 Detecting moving targets and measuring velocity

One of the most fundamental tasks of a radar is to be able to detect targets accurately and to measure its velocity if the target is moving. To do this accurately we have used the Array Digital Beamforming Algorithms technique in its specification called Doppler Procession [34, 35].

Several simultaneous criteria are required for a signal to be considered a detection. It is an adaptive process that automatically adjusts to background noise and environmental influences. There is a test cell, where the surrounding cells are summed, multiplied by a constant and used to establish a threshold, as shown in (7.12).

$$\boldsymbol{Threshold\ criteria}\left\{\begin{array}{c}\{\boldsymbol{Cell(n)} > [\boldsymbol{Cell(n-2)} + \\ \boldsymbol{Cell(n-1)} + \\ \boldsymbol{Cell(n+1)} + \\ \boldsymbol{Cell(n+2)}] \times \\ \boldsymbol{constant}\}\end{array}\right. \tag{7-12}$$

The detection only covers speeds that exceed the speed rejection setting. As an example of speed rejection, if speed rejection is set to 75 mph, hailstones travelling at 50 mph in a thunderstorm will not be detected, but an aircraft travelling at 100 mph will be, as illustrated in (7.13-7.14).

$$Peak\ criteria \begin{Bmatrix} \left(\frac{\Delta Amplitude}{\Delta Frequency}\right) Cell(n-1) < 0 \\ \left(\frac{\Delta Amplitude}{\Delta Frequency}\right) Cell(n-1) > 0 \end{Bmatrix} \tag{7-13}$$

$$Speed\ criteria \left\{\left(\frac{C \times Doppler\ Frequency}{2 \times Transmit\ Frequency}\right)\right\} > Rejection \tag{7-14}$$

This involves minimizing the probabilities of false alarm (reporting a detection when there is no target) and missed detection (not reporting a detection when there is a target).

7.3.1 Doppler Processing

Doppler processing (DP) is another important technique that uses Doppler information to detect targets and measure their speed [101]. This technique can detect targets when clutter is the dominant interference [102]. This is applicable in environments where echoes and clutter (buildings, trees, the movement of water waves and other objects) can drown out the return signal. Increasing the transmit power does not help the detection of targets in clutter, as the power returned from the clutter is also increased. Fig. 7.2 shows the DP for characterizing physical features of the water channel.

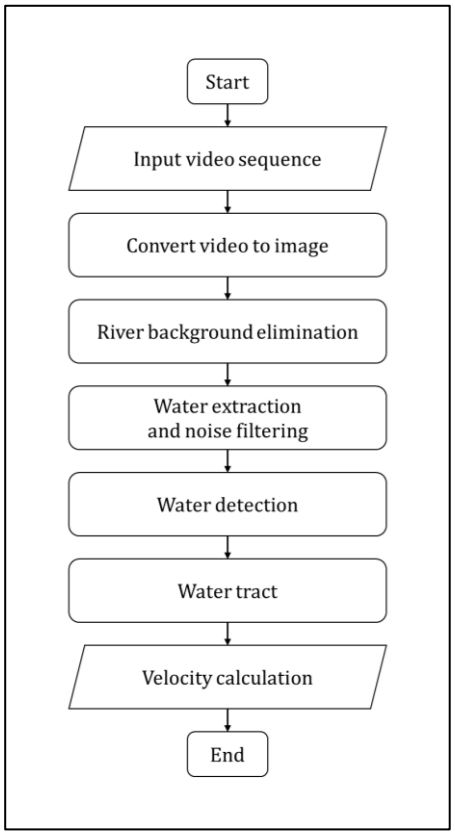

Figure 7-2 Doppler processing for characterizing physical features of the water channel.

DP is the main technique for increasing the signal to clutter ratio (SCR). To increase the SCR, the signals must be frequency separable. The moving target signal can be separated from the clutter echoes in the frequency domain. The clutter is relatively stationary (wind moving trees, flowing water, etc.) and therefore contributes little or nothing to the Doppler shift of the return echo. Thus, we can apply DP to detect significant clutter. DP has two general cases: moving target indication (MTI) and pulse DP. MTI requires fewer calculations but can only detect the presence of a moving target, MTI cannot identify if there is more than one target per range bin or what the speed of that target is. The main advantage of an MTI is less complexity and fewer calculations. On the other side, pulsed DP can detect a target likewise, but it can also measure the Doppler shift and, from this, determine the velocity of the target. A further advantage with pulsed DP is the detection of multiple targets, with the only condition that they are separated by a sufficiently large Doppler shift. These advantages bring with them the trade-off of increased computation and

complexity. An MTI may only be implemented by making use of temporal data on many coherent, i.e., slow time, pulses, so its consecutive slow time intervals will be filtered out in the internal composition of digital beamforming using a high pass filter. This attenuates the clutter that is confined to around 0Hz. Finally, a threshold is applied to the time data and a decision is made on the detection.

7.3.2 Beamforming delay and sum technique

The traditional beamformer, referred to as the Bartlett beamformer or DaS BF, is one of the most used and robust FB algorithms. The DaS beamformer applies delay and intensity filtering to each sensor output and then sums the outcome of the signals.

The delays are set to improve the array sensitivity to incoming waves from a specific direction. The network search direction can be oriented towards the source by altering the delays, and the waveforms caught by the various sensors add up constructively. This means that signals at certain angles are subjected to constructive interference, while others are subjected to destructive interference. Think about an array of M sensors situated at various points in space $\overrightarrow{x_m} = [x_m, y_m, z_m]$ and monitoring a wavefront of $f\left(\overrightarrow{x}, t\right)$. The mth sensor spatially sampled waveform is $y_m(t) = f\left(\overrightarrow{x_m}, t\right)$. The DaS beamformer works by adding a delay Δ_m and an amplitude weight w_m to each sensor's result and then totalling the resulting signals, as illustrated in Fig. 7.3.

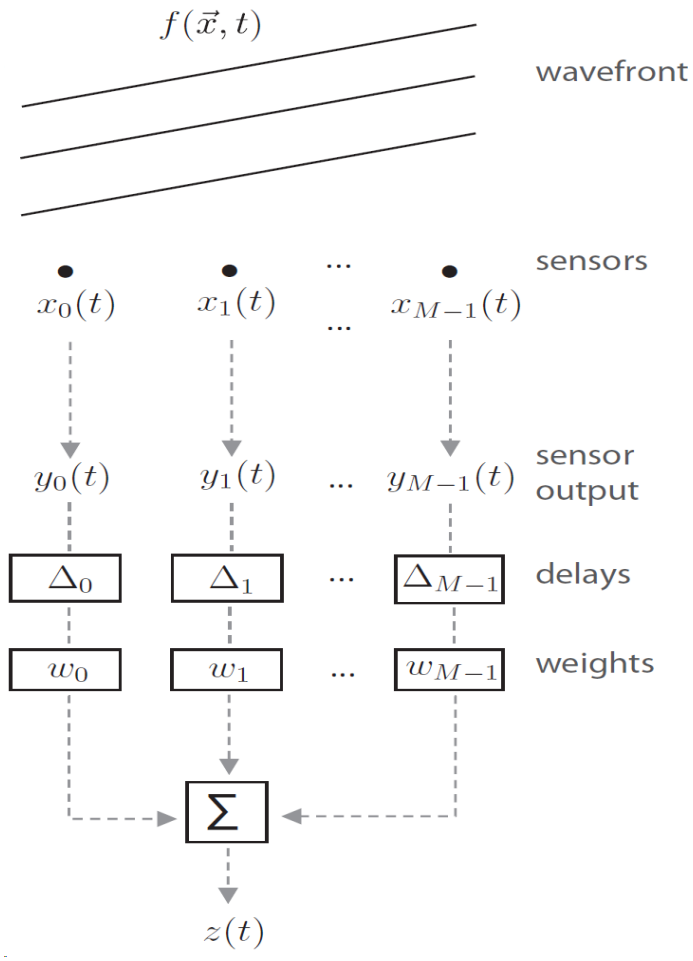

Figure 7-3 Conventional DaS beamforming.

To enhance array sensitivity to waves propagating in a particular direction, delays are used. Adjusting delays aligns the array view with the source and enhances the sensor waveforms. This is stacking. Weighting the array sensors differentially improves their shape and lowers the secondary lobes of the listening beam.

$$z(t)=\sum_{m=0}^{M-1} w_m.y_m\left(t-\Delta_m\right) \tag{7-15}$$

DaS BF sensor weights are chosen before the waveform, unlike adaptive techniques. In (7.15) shows BF DaS time-domain output.

BF uses delays to guide the array in different directions or scan plane spots. Maximum power is observed when steering direction matches a source.

Interpolating the observed output power from all scan points colours spatial power and gives a signal a desired characteristic [103], [104]
In additional DaS BF for the image or video is often reconstructed (processed) using the BF DaS technique, which is defined in the (7.16) as follows:

$$S_{DaS}(t) = \sum_{i=1}^{N} a_i s_i^{'}(t + \Delta t_i) = \sum_{i=1}^{N} s_i(t + \Delta t_i) \tag{7-16}$$

Where DaS beamformer results is S_{DaS}, collecting aperture size is N, a_i represents the apodization factor. The signal recorded by the ith element, denoted as $s_i^{'}(t + \Delta t_i)$, is accompanied by a time delay, Δt_i
Large side lobes, nevertheless, contribute to the BF DaS comparatively limited lateral resolution. In order to address this side-lobe issue, a non-linear weighting function known as a coherence element (CE) was implemented. In the equation, the DaS is combined with the coherence element as follows in the (7.17-7.18):

$$S_{DaS-CE}(t) = S_{DaS}(t) \times CE_{S_{DaS}}(t), \tag{7-17}$$

where:

$$CE_{S_{DaS}}(t) = \frac{\sum_{i=1}^{N} s_i(t + \Delta t_i)^2}{N \sum_{i=1}^{N} (s_i(t + \Delta t_i)^2} \tag{7-18}$$

In addition to increase the resolution of space, the CE can enhance SNR by eliminating sidelobes and noise [105]- [106].

7.4 The study area

The proposed approach for determining the hydrodynamic characteristics of a river on the Canale Reale, a significantly modified river located in the southeastern region of Apulia, Italy, has been evaluated by researchers (Fig. 7.4). The discharge characteristics of this river exhibit a transient and irregular pattern. As a result of the 210 km2 expansion of its catchment area, it signifies the preeminent watercourse in the southern region of Apulia. The purified effluents from the wastewater treatment plants (WWTPs) of four municipalities—Ceglie Messapica, Francavilla Fontana, Latiano, and

Carovigno—are transported along its nearly 50 km of length (Fig. 7.4). A portion of the Canale Reale that empties into the Natural State Reserve of Torre Guaceto supplies water to a saline wetland along the coast.

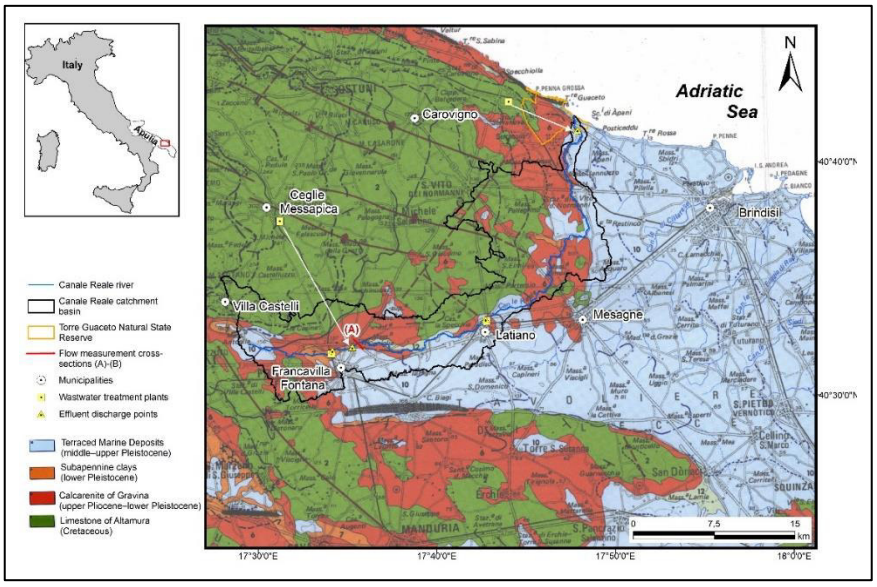

Figure 7-4 Study location and geological map (modified after Ciaranfi et al., 1988 [38]).

7.4.1 Groundwater

According to [107]- [108] (Fig. 7.4), the area has two distinct aquifer structures: a deep one in the Cretaceous carbonate rock succession and a shallow porous one in Terraced Marine deposits (sand-calcarenite levels) [109].

The latter, intensively used for local irrigation, only receives rainwater recharge and supplies the Canale Reale river and other topographically depressed areas. Rainfall infiltrating the innermost section recharges the karst-affected deep carbonate aquifer. Groundwater runs freely near the coast, forming underwater and subaerial springs in morphologically depressed zones. Mixed deep and shallow aquifers have been found in the Torre Guaceto wetland [110]. Since the mid-1990s, regional aquifers have been monitored in space and time, and groundwater quality and quantity have been studied for decades [111].

7.4.2 Climate

In the study area is typical of the dry-sub-humid Mediterranean climate seen across the region [112], [113]. More specifically, precipitation is limited (600 mm/year) and temperatures are pleasant most of the year. Summers are lengthy, dry, and hot, with two or three months of rainfall and temperatures above 40°C. Winter temperatures rarely drop below 10°C and precipitation is variable. The area under investigation's 20-year hydrological balance is shown in Fig. 7.5.

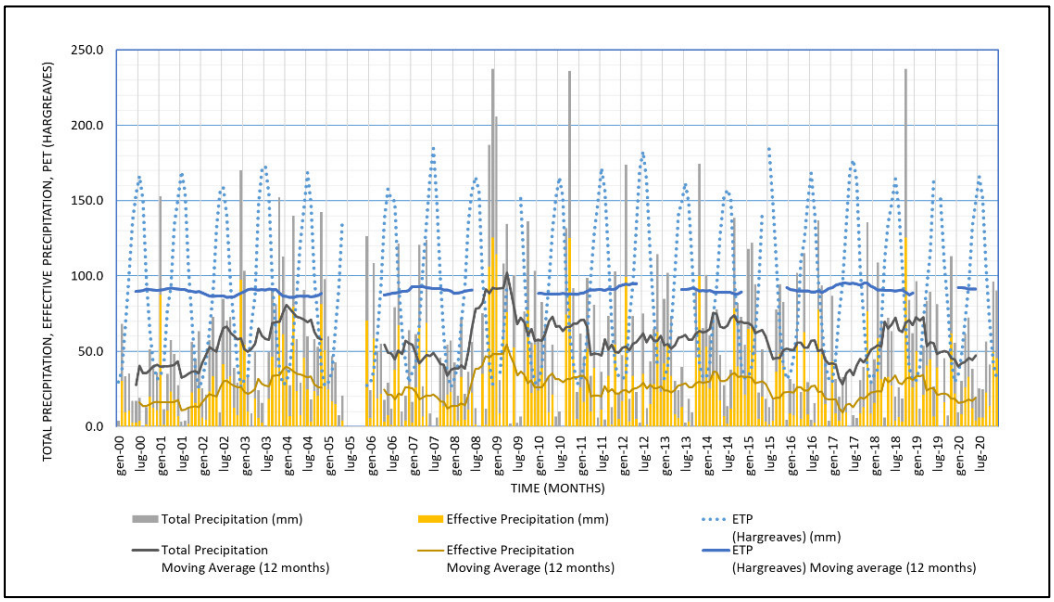

Figure 7-5 Monthly elements of the hydrological balance in the area under investigation. Effective precipita-tion and the potential evapotranspiration (PET) have been assessed based [114] and the Har-greaves formula [115], respectively. Precipitation and temperature data have been downloaded by the Hydrological Annals published by the Apulian Civil Protection [116]

At the meteorological station in Latiano, in the middle of the research region, monthly measured total and estimated effective precipitation and estimated monthly potential evapotranspiration are depicted. The estimated PET was 1000 mm/year throughout the study. The WMO-recommended non-parametric Mann-Kendall test for monotonic trend [117], [118] showed no monotonic trends in any meteo-climatic parameters during the period.

7.4.3 The most important environmental issues

The area flat topology allowed intensive agricultural exploitation, mostly of olives, grapes, and vegetables. Over the last 50 years, intensive farming and the progressive spread of water-demanding crops have resulted in an increase in water uptake for irrigation purposes, with a significant anthropogenic impact on local groundwater resources, particularly those hosted in the deep aquifer, both quantitatively and qualitatively. Indeed, the massive withdrawals have created an imbalance between fresh groundwater and underlying salt water, resulting in localised saltwater contamination along the coast and even in the interior [119]. This problem is exacerbated by the consequences of climate change, which result in a succession of severe rainfall events and dry intervals marked by high evapotranspiration rates, limiting natural aquifer recharge [120]. Furthermore, because surface watercourses are few or have intermittent regimes, the water balance is heavily skewed towards groundwater overexploitation.

7.5 Video measurements in the study area

To apply and validate the proposed methodology, on-field flow video recording and measurements have been carried out in a river cross-section located less than 100 m downstream at the Ceglie Messapica WWTP effluent discharge point. Fig 7.6 shows the location and the surveyed geometry of the cross-section, while Fig. 7.7 shows a still image of the water flow video through it.

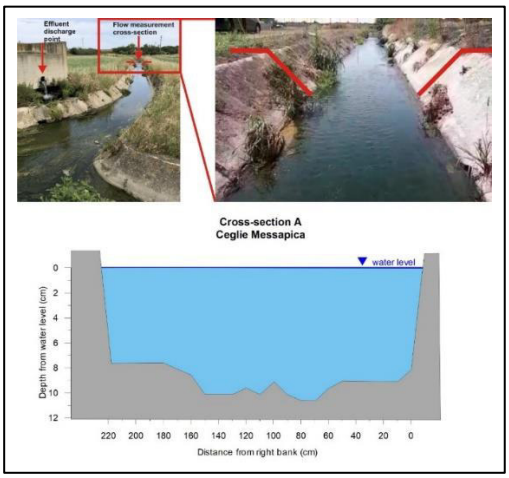

Figure 7-6 Flow measurement cross-section of Ceglie Messapica (A) (for location see Fig. 7.4).

Concerning the on-site flow measurements methods, an exhaustive account of the related advantages and disadvantages. In recent work [121], compared two measurement methods, which are the more reliable current meters method (CM method) and the float method (F method). It resulted that the F method overestimates the water flow rate of the CM by about 11%.

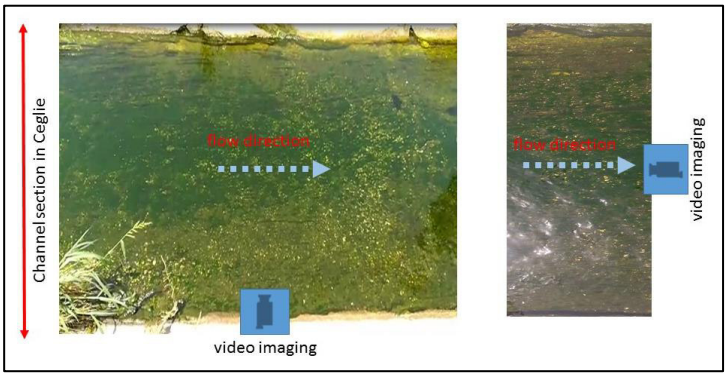

Figure 7-7 Example of channel photos serving for processing.

This relative error can be considered widely acceptable compared to the more rigorous, but much more time-consuming CM method, especially when measurements need to be repeated in time. In this study, both methods were used, and the flow rate measurements were carried out on 27 July 2021.

7.6 The outcomes and methodology

The proposed technique, as stated in the previous section, has been applied to a river cross-section near the municipality of Ceglie Messapica. The video was recorded using a camera placed up between 1.2 and 1.4 metres high, perpendicular to and parallel to the flow direction (Fig. 7.7).

The techniques described in the subsection 7.3 are reported here in terms of the case study outcomes. The first result is the detection of the temperature distribution using the MUSIC technique to retrieve the channel hyperthermia, similar to how UWB (ultra-wideband) radar seeks the reaction of the human tissue and its permittivity.

In our scenario, the channel bed is regarded a tissue, and the water flow is similar to blood flow within the arteries. Because the channel bed is reinforced concrete, important temperature readings are retrieved while the temperature fall is indicated in depth. These heat values are consistent with seasonal and local datasets.

The MUSIC algorithm distinguishes between close values of the same quantity, such as the temperature values in Fig. 7.8 and the wave motions (displacements) inside the channel in Fig. 7.9. The intensity of the waves along the flow direction as a function of channel depth is represented by such wave displacements.

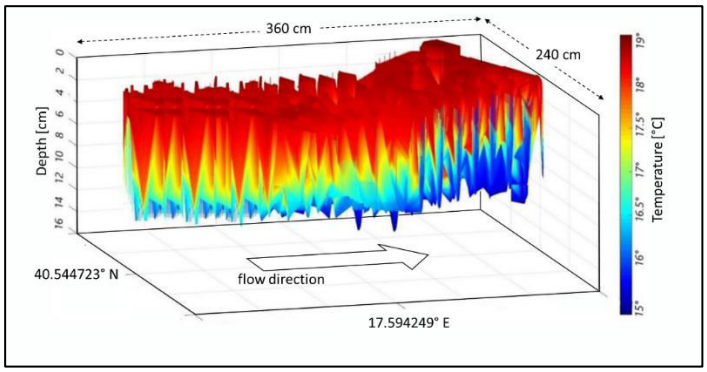

Figure 7-8 Temperature values retrieved by means of beamforming-based technique vs depth and GPS.

Both of these metrics, as calculated by the MUSIC approaches, can be useful in assessing river hydrodynamics.

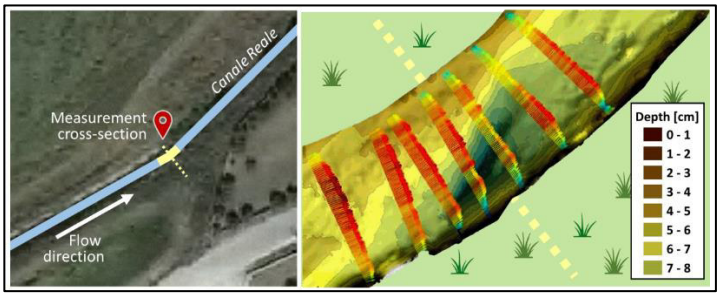

Figure 7-9 Detection of different layers and waves of the channel at certain portion vs depth.

Aside with MUSIC, the plan is to apply the diffusion method in conjunction with radar sensors to extract additional elements, such as water waving.

Doppler processing is related to the speed or diffusion of the parameter under test, as stated in subsection (beamforming imaging-based algorithms). Fig. 7.10 depicts the expression of the identical waves as a function of depth. In terms of vectors, the field of waves inside the riverbed can be utilised as a first metric (indicator) to examine the dynamics of getting-born phenomena in the channel capable of causing extreme hydrological events such as flooding. Finally, we were able to determine the water velocity as a function of temperature (i.e., hot and cold water) using the Doppler processing of the video imaging (Fig. 7.11).

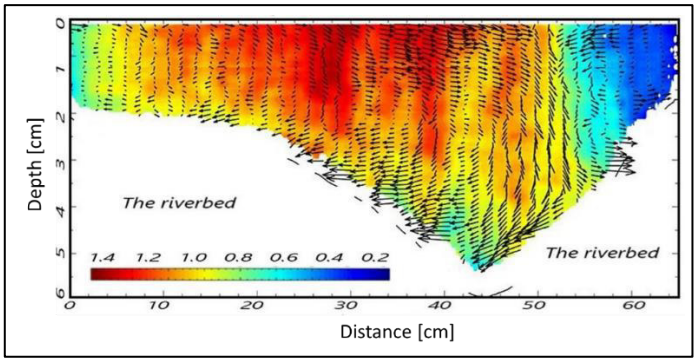

Figure 7-10 Detection of the riverbed and wave movements along the of the considered channel portion with Doppler processing.

The detected water velocities reported in Fig. 7.11 range between 0.2 m/s and 1.4 m/s that, given the measured area of the considered section equal to 0.2m^2, correspond to flow rates between 40 and 280 l/s.

As is known in the literature, the more the considered variable values fall in the upper side of the range of possible values, the more the DaS BF performs better, providing more reliable results in terms of uncertainty.

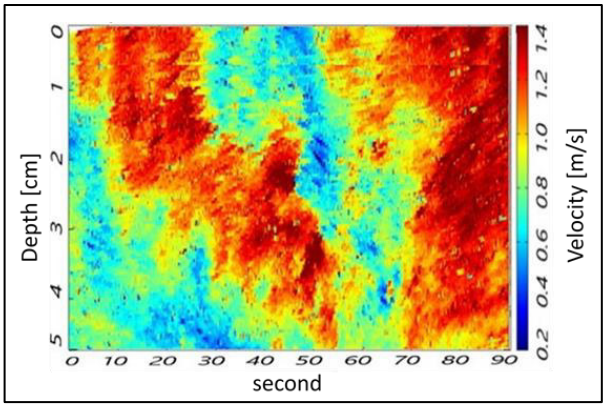

Figure 7-11 Detection of water velocity as function of the temperature by Doppler processing: cold water – bottom; hot water - surface.

Moreover, in the case at hand the loss of reliability of DaS is also due to unfavorable environmental Condit ghosts such as the presence of a concrete riverbed, causing problems such as ghost or multiple sources that appear to arrive from different directions, due to successive reflections in walls.

For trying to understand the efficiency and stability of the proposed procedures, the same features/outcomes were reproduced for two more sections of the same channel. However, the graphs are organized by the comparative parameters. Fig. 7.12 and Fig. 7.13 depict the temperatures. There is a little difference in temperature distribution between them that differs from the prior site (Fig. 7.8).

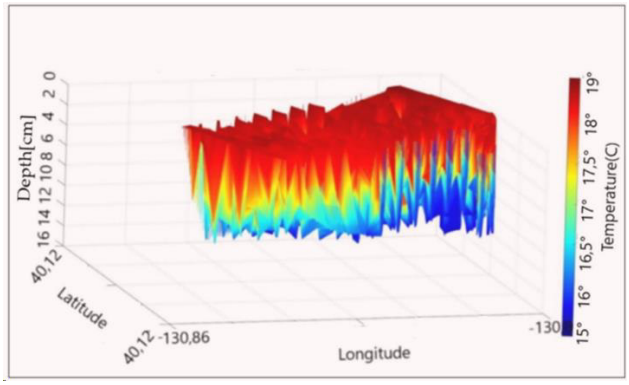

Figure 7-12 Temperature values retrieved by means of beamforming-based technique vs depth and GPS references for site 2.

For all processed figures by the BF included in this work, the flow direction is the same, that is, from left to right. The plots of layers and waves, on the other hand, represent a distinct picture. Fig. 7.13 and Fig. 7.14 exhibit the layers and waves discovered in the same context as Fig. 7.9, but with a different and more artistic substratum (black letters) to better emphasise the contrast.

For the riverbed and wave movement, we can observe from the related figures that the depth is different; that is, Fig. 7.17 displays around 5.5 cm, Fig. 7.15 exhibits around 6 cm, and Fig. 7. 13 depicts 5.3 cm.

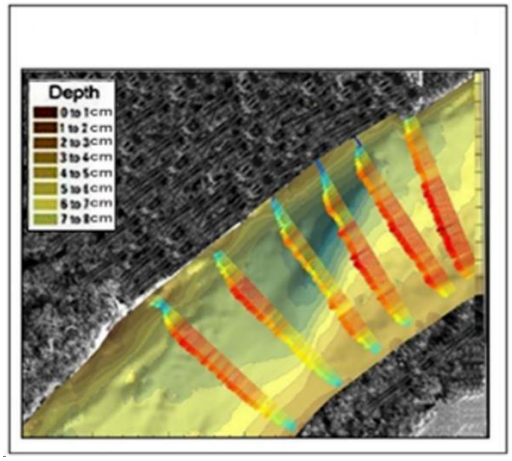

Figure 7-13 Detection of different layers and waves of the channel at certain portion vs depth for site 2.

These little differences are due to material deposition on the channel bed. Furthermore, given the same channel and flow, the wave movement field is the same everywhere, with no notable differences.

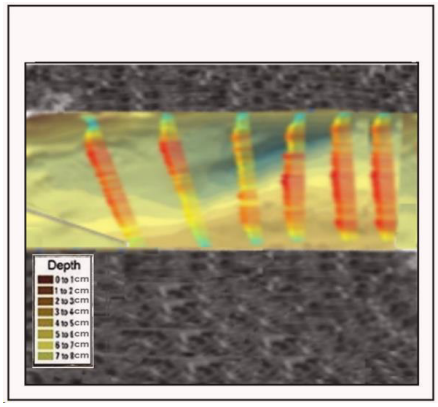

Figure 7-14. Detection of different layers and waves of the channel at certain portion vs depth for site 3.

Fig. 7.16 and Fig. 7.17 show that there are no differences in water velocity as a function of temperature. These results correspond to those shown in Fig. 7.11. As a last note on this part, we can emphasise the proposed technique's stability at all three sites.

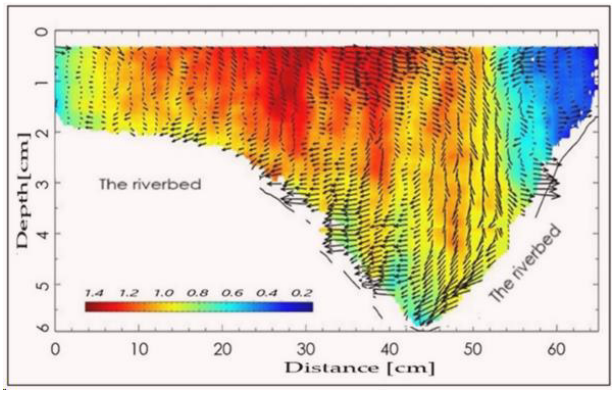

Figure 7-15 Detection of the riverbed and wave movements along of the considered channel portion with Doppler processing for site 2.

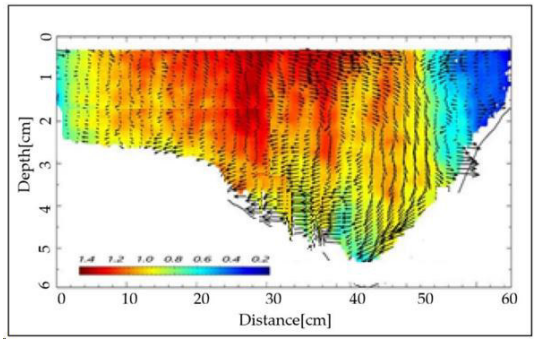

Figure 7-16 Detection of the riverbed and wave movements along of the considered channel portion with Doppler processing for site 3.

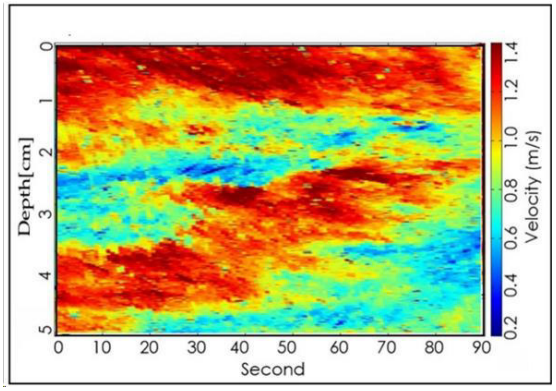

Figure 7-17 Detection of water velocity as function of the temperature by Doppler processing: cold water – bottom; hot water – surface, for site 2.

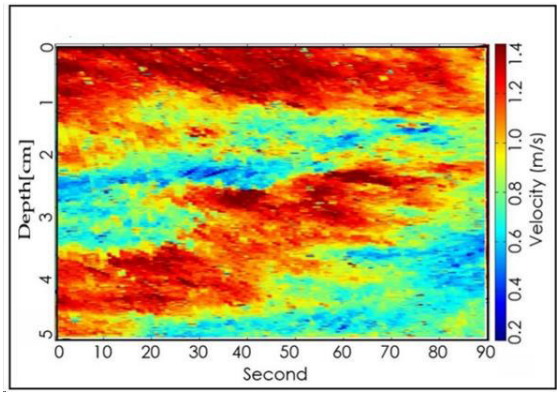

Figure 7-18 Detection of water velocity as function of the temperature by Doppler processing: cold water – bottom; hot water – surface, for site 3.

7.6.1 Measurements of field flow and method validation

To carry out the riverbed flow measurements by the F method, a cylinder float, 10 cm long and 3 cm in diameter, closed at its ends and filled out with little pebbles to make it travel horizontally and partially submerged, was used. Four measurements of the float travel time were taken, and the average value was used to estimate the surface speed *(Vs)* representative of the investigated cross-section. By applying a quadratic corrective coefficient *(F)* [122], the average sectional velocity (Vm) was calculated and, finally, the transit flow rate (Q) was obtained by multiplying Vm by the average cross-section area between the ones upstream and downstream.

Measurements by the CM method was carried out by a Miniwater ®20 water-flow velocity meter. Punctual velocity measurements were taken starting from the right bank of the river to the left one at a step of 10 cm and a depth of 60% of the water level, to approximate the segment "i" average velocity (Vmi) [123]. The total transit flow rate Q was then defined as the sum of the segment flow rates computed multiplying each segment area (Ai) by the related Vmi.

Table 7.1 reports the calculated Q values by both the CM and F methods. As expected, the F method overestimates the CM method by about 11% in accordance with [124].

Table 7-1 Values of the transit flow rate (Q) measured in the cross-section A.

Cross-section	CM method (l/s)	F method (l/s)
A	93.74	104

By comparing the transit flow rates obtained with the last two methods, there is an apparent discrepancy amongst these and DaS ones (40-280 l/s). As already said, the DaS measures tend to evaluate the maximum values. Therefore, a direct comparison between the values is not possible, while it is possible to verify that both the values obtained by CM and F methods fall within the range of the radar.

Major accuracy can be obtained in three ways: (i) repetition of the measurement in higher flow rates conditions, that is major velocity over 50% of the range; (ii) implementation of a weighted DaS, able to overcome the loss of reliability of DaS due to unfavorable environmental conditions (iii) using a delay-multiply-sum-to-standard-deviation-factor (DMSSF). This latter approach allows improving all kinds of drawbacks like, lateral resolution, SNR, and reduces side lobes of the reconstructed image in comparison to the other conventional methods, like DaS. DMSSF technique will be implemented in a further activity.

Certification is performed using the proposed methodology, which is based on BF as a detecting radar; in other words, the CM and F methods are employed to calibrate the indicated technology. We chose the layers and wave outputs represented in Fig. 7.9 for site 1, Fig. 7.13 for site 2, and Fig. 7.14 for site 3 to analyze the impact of the DaS BF technique on the three sites, because there are interesting fluctuations in these figures. A quick summary shows that in Fig. 7.9, the radar detected 7 portions (as cross-sections) of the channel in a clear way, 6 portions in Fig. 7.13, and 6 portions in Fig. 7.14, but with background in apparent foggy conditions, possibly due to the quality of the riverbed including sedimentary deposition.

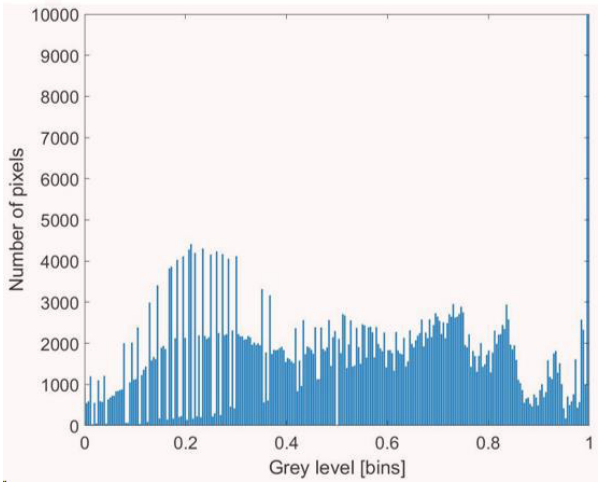

Figure 7-19 Histogram of grey scale vs number of pixels for the first acquisition (site 1) concerning layers and waves.

The previously mentioned issues are clearly explained in the histograms; for example, Fig. 7.19, derived from Fig. 7.9, shows a large number of peaks along the abscissa; the same can be said for Fig. 7.20 (for Fig. 7.13), while Fig. 7.21 shows a low content of peaks due to the foggy background.

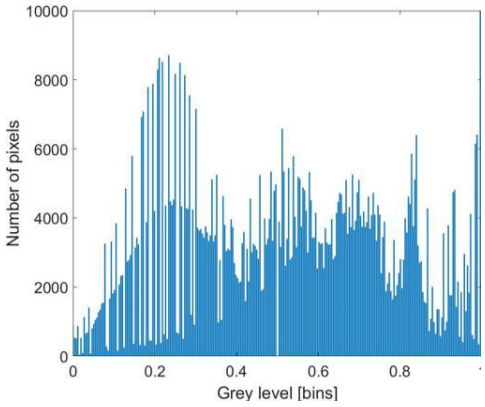

Figure 7-20 Histogram of grey scale vs number of pixels for the second acquisition (site 2) concerning layers and waves.

We can confirm the promising results of the proposed technique once more.

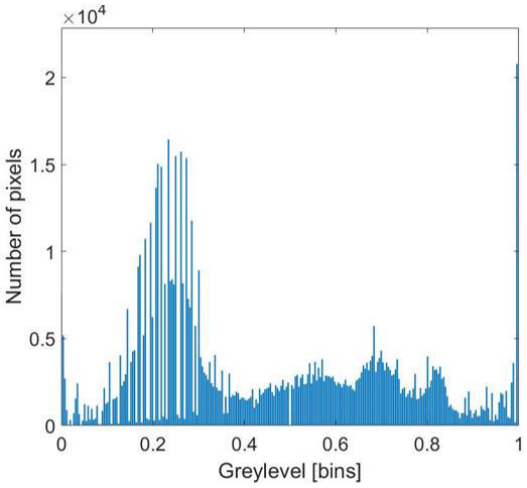

Figure 7-21 Histogram of grey scale vs number of pixels for the third acquisition (site 3) concerning layers and waves.

7.7 Conclusion

The advancement of technology in video sensors, particularly mobile video cameras, has enabled us to employ these devices for a wide range of applications due to their strong embedded electronics. They arrive to assist with signal processing techniques. These devices can therefore be used to manage the hydrodynamics of channels instead of large facilities. Video sensors, on the other hand, can be positioned along the channels. By considering the use of radar to monitor ground features, two major strategies based on DaS BF can be adopted and customised suitably. MUSIC has been utilised to extract near metrics such as temperature and water wave vectors within the channel based on its properties. The second approach, also known as Doppler processing, uses Doppler radar to extract diffusion of the quantity under test within the channel; in this situation, we are dealing with hot or cold waves in the water.
The results obtained are promising, given that they were obtained using a standard smartphone video sensor, albeit with sophisticated post-processing.
The study highlighted the significance of applying the BF algorithm to hydrological observations.

8. General conclusion

It is worth noting that telecommunications extend beyond the mere transmission and reception of messages, as it may also be employed to address environmental and biomedical challenges through the utilisation of its algorithms.

The scope of the research does not encompass the comprehensive use of the BF in the realm of telecommunications, namely in terms of its capabilities as a transmitter/receiver for the purpose of verbal communication or visual content consumption.

The primary objective of this study was to illustrate the significant and advantageous influence of telecommunications in addressing environmental and biological challenges.

In the present setting, algorithms rooted in telecommunications offer a novel and enlightening perspective on the field of telecommunications.

The success of the research objective is evident from the high quality of the results obtained in various domains, including environmental signal processing, medical signal processing, telecommunications signal optimization, wireless link transmission, and environmental monitoring using beamforming technology. Nonetheless, BF is not without its limitations: BF possesses the following limitations, as BF is a technique and all techniques have limitations or constraints: For BF calculations, the technique occasionally necessitates additional computing power and resources; vast digital and MIMO BF systems can be more complicated, particularly when the number of antennas and other equipment utilized is considered, and they are typically more expensive than conventional systems. In spite of its present constraints, this methodology is exceptionally effective and possesses significant potential that has established it as a paradigm shifter in the domain of wireless signal processing and transmission. It is crucial to promote for the implementation of BF technology in applications involving radar, medicine, environmental monitoring, and aerospace. Moreover, BF technology can concentrate sensor network

transmissions in a particular direction. By utilizing the beamformer technique, signals received by a sensor array can be concentrated in a particular direction.

9. References

[1] S. Yandong, X. Jian, H. Chuang, L. Wang e T. Mingliang, «A polarization-sensitive array reconfiguration technique resorting to antenna selection for navigation interference mitigation,» *Digital Signal Processing,* vol. 129, p. 103661, 2022.

[2] H. T. Sediq, «Miniaturized MIMO antenna design based on octagonal-shaped SRR metamaterial for UWB applications,» *AEU - International Journal of Electronics and Communications,* vol. 172, p. 154946, 2023.

[3] G. P. Kumar, V. S. Tallapragada e N. A. Manga, «Optimized transmit antenna selection and self-attention based convolutional resource allocation model for massive MIMO technology,» *Computer Networks,* vol. 235, p. 109948, 2023.

[4] X. Zhang, X. Wang, J. Huang e H. C. So, «Joint design of antenna selection and transmit linear array beamformer for integrated radar and communications,» *Digital Signal Processing,* vol. 144, p. 10428, 2024.

[5] M. V. Rao, D. Mondal, J. Malik, M. Kartikeyan e S. Yuvaraj, «Series-feed UCA antenna for generating highly azimuthal symmetric OAM Beam for unmanned aerial vehicles,» *AEU - International Journal of Electronics and Communications,* vol. 171, p. 154917, 2023.

[6] A. Massoud, A. Osman e A. Noureldin, «DOA estimation based on fourth order cumulant beamforming for nonuniform linear array of DIFAR sonobuoys,» *Computers & Electrical Engineering,* vol. 38, n. 4, pp. 986-993, 2012.

[7] M. Asghari, M. Zareinejad, S. M. Rezaei e H. Amindavar, «ECF-MUSIC: An empirical characteristic function based direction of arrival (DOA) estimation in the presence of impulsive noise,» *Digital Signal Processing,* vol. 123, p. 103440, 2022.

[8] M. Asghari, M. Zareinejad, S. M. Rezaei e H. Amindavar, «DOA estimation of coherently and incoherently distributed sources using a characteristic function based ESPRIT algorithm with heavy-tailed signals and noises,» *Physical Communication,* vol. 59, p. 102089, 2023.

[9] L. Wan, Z. Guo-long, X. Wang, Z. Le-an, L. Tian e Z. Qi-xing, «Tiny crystalline grain nanocrystal NiCo2O4/N-doped graphene composite for efficient oxygen reduction reaction,» *Journal of Power Sources,* vol. 345, pp. 41-49, 2017.

[10] C. Gregory, McLaskey, D. Steven, Glaser, U. Christian e Grosse, «Beamforming array techniques for acoustic emission monitoring of

large concrete structures,» *Journal of Sound and Vibration,* vol. 329, n. 12, pp. 2384-2394, 2010.

[11] H. Jochen, Kurz, U. Christian, Grosse e R. Hans-Wolf, «Strategies for reliable automatic onset time picking of acoustic emissions and of ultrasound signals in concrete,» *Ultrasonic,* vol. 43, n. 7, pp. 538-546, 2005.

[12] E. Baidoo, H. Jurong, B. Zeng e B. D. Kwakye, «Joint DOD and DOA estimation using tensor reconstruction based sparse representation approach for bistatic MIMO radar with unknown noise effect,» *Signal Processing,* vol. 182, p. 107912, 2021.

[13] Y. Arjoune e S. Faruque, «Experience-driven learning-based intelligent hybrid beamforming for massive MIMO mmWave communications,» *Physical Communication,* vol. 51, p. 101534, 2022.

[14] Z. Fang, Q. Li, L. Jianhua, J. Zhou e S. Shen, «Beamforming design for multi-antenna multi-tag symbiotic radio backscatter systems,» *AEU - International Journal of Electronics and Communications,* vol. 170, p. 154820, 2023.

[15] B. Zhao, Y. Guo, B. Xu, M. Cheng, M. Biao e L. Min, «Combined UAV positioning with robust beamforming and IRS-enhanced NOMA transmission in cognitive UAV networks,» *AEU - International Journal of Electronics and Communications,* vol. 168, p. 154727, 2023.

[16] A. Ayman, Althuwayb, M. Alibakhshikenari, S. Bal, Virdee, H. Benetatos, N. Rashid, K. Kaaniche, A. B. Atitallah, Osama e I. Elhamrawy, «Design technique to mitigate unwanted coupling in densely packed radiating elements of an antenna array for electronic devices and wireless communication systems operating in the millimeter-wave band,» *AEU - International Journal of Electronics and Communications,* vol. 159, p. 154464, 2023.

[17] L. Yang, Y. Wang, Y. Yang e Y. Mengling, «Robust broadband adaptive beamforming with constant beamwidth using frequency difference technique,» *Digital Signal Processing,* vol. 140, p. 104108, 2023.

[18] G. Jenkinson, M. A. B. Abbasi, A. M. Molaei, O. Yurduseven e V. Fusco, «Deep Learning-Enabled Improved Direction-of-Arrival Estimation Technique,» *Electronics,* vol. 12, p. 3505, 2023.

[19] A. Naghavi, M. S. Fazel, M. Beheshti e E. Yazdian, «A sequential MUSIC algorithm for scatterers detection in SAR tomography enhanced by a robust covariance estimator,» *Digital Signal Processing,* vol. 128, p. 103621, 2022.

[20] G. Zheng, Y. Song e C. Chen, «Height Measurement with Meter Wave Polarimetric MIMO Radar: Signal Model and MUSIC-like Algorithm,» *Signal Processing,* vol. 190, p. 108344, 2022.

[21] T. Wang, L. Shi, S. Qiu, Z. Sun e Y. Duan, «Continuous broadband lightning VHF mapping array using MUSIC algorithm,» *Atmospheric Research,* vol. 231, p. 104647, 2020.

[22] J. P. D. Okitadiowo, A. Lay-Ekuakille, T. Isernia e A. Massaro, «Design of a beamforming antenna sensor for environmental noise detection to discriminate vehicle emission according to road conditions,» *Measurement: Sensors,* vol. 23, p. 100389, 2022.

[23] Y. Xiao, W. Yan, K. Doğançay, H. Ni e W. Wang, «Multikernel adaptive filtering over graphs based on normalized LMS algorithm,» *Signal Processing,* vol. 214, p. 109230, 2024.

[24] X. Guangbo, Z. Bingting, H. Yuan, Z. Zheng e H. Zhang, «Underwater four-quadrant dual-beam circumferential scanning laser fuze using nonlinear adaptive backscatter filter based on pauseable SAF-LMS algorithm,» *Defence Technology,* p. 2214, 2023.

[25] L. Zhu, X. Qiu, M. Dongxing, S. Wu e X. Zhong, «Efficient segment-update block LMS-Newton algorithm for active control of road noise,» *Mechanical Systems and Signal Processing,* vol. 198, p. 110436, 2023.

[26] Z. Yang, L. Huo, J. Wang e J. Zhou, «Denoising low SNR percussion acoustic signal in the marine environment based on the LMS algorithm,» *Measurement,* vol. 202, p. 111848, 2022.

[27] B. Ye, G. Fang, J. Hu, H. Wang, Y. Fu, S. Zhang e A. K. Dwivedi, «A novel positioning method for magnetic spiral-type capsule endoscope using an adaptive LMS algorithm,» *Journal of Magnetism and Magnetic Materials,* vol. 563, p. 169939, 2022.

[28] M. J. M. Spelta e W. A. Martins, «Normalized LMS algorithm and data-selective strategies for adaptive graph signal estimation,» *Signal Processing,* vol. 167, p. 107326, 2020.

[29] C. Xiwang, Y. Gao, Y. Ma, F. Liu e H. Wang, «Time delay estimation using cascaded LMS filters fused by correlation coefficient for pipeline leak localization,» *Mechanical Systems and Signal Processing,* vol. 199, p. 110500, 2023.

[30] C. Zhang, Y. Mao, X. Zhou, Y. Chen e G. Ren, «Adaptive intensity noise suppression of fiber optic gyroscopes based on period LMS algorithm,» *Optik,* vol. 251, p. 168033, 2022.

[31] R. S. A. Araújo, J. C. Tironi, W. D. Parreira, R. C. Borges, J. F. D. P. Santana e V. R. Q. Leithardt, «Analysis of Adaptive Algorithms Based on Least Mean Square Applied to Hand Tremor Suppression Control,» *Appl. Sci,* vol. 13, p. 3199, 2023.

[32] D. Bismor, «Leaky Partial Update LMS Algorithms in Application to Structural Active Noise Control,» *Sensors,* vol. 23, p. 1169, 2023.

[33] R. P. Lorente, R. M. Ferrer, A. F. Martínez e G. Palacios-Navarro, «An Alternative Approach to Obtain a New Gain in Step-Size of LMS Filters Dealing with Periodic Signals,» *Appl. Sci,* vol. 11, p. 5618, 2021.

[34] Q. Lu, H. Qin, F. He, Y. Zhang, Q. Wang e J. Meng, «Wideband Interference Cancellation System Based on a Fast and Robust LMS Algorithm,» *Sensors,* vol. 23, p. 7871, 2023.

[35] J. Capon, «High-resolution frequency-wavenumber spectrum analysis,» *Proceedings of the IEEE,* vol. 8, p. 1408–1418, 1969.

[36] V. Nagaraju, A. Sethy, R. S. K. Boddu, S. Balambigai e K. Sakthisudhan, «Diagnosed image of breast cancer by antenna MVDR beamforming algorithm with composites,» *Materials Today: Proceedings,* vol. 46, n. 9, pp. 4207-4211, 2021.

[37] Y. Yao, K. Zhao e Z. Zheng, «An improved TOA estimation algorithm based on denoised MVDR for B5G positioning,» *Physical Communication,* p. 101992, 2023.

[38] S. Jiang, S. Liu e M. Jin, «High-dimensional MVDR beamforming based on a second unitary transformation,» *Signal Processing,* vol. 205, p. 108869, 2023.

[39] U. J. Kidav, N. M. Sivamangai, M. P. Pillai e S. G. Sreejeesh, «A broadband MVDR beamforming core for ultrasound imaging,» *Integration,* vol. 81, pp. 221-233, 2021.

[40] S. Dioline, M. Arunkumar, V. Dinesh, T. Nagarjuna e S. Karuppanan, «Radiology: Clinical trials implemented by composite test-beds via MVDR beamformer system,» *Materials Today: Proceedings,* vol. 46, pp. 4295-4297, 2021.

[41] C. Jhih-Chung, «Combining GA and iterative MVDR for DOA estimation in space-time CDMA systems,» *Computers & Electrical Engineering,* vol. 38, n. 6, pp. 1399-1408, 2012.

[42] Z. Fang, Q. Li, J. Liu, J. Zhou e S. Shen, «Beamforming design for multi-antenna multi-tag symbiotic radio backscatter systems,» *AEU - International Journal of Electronics and Communications,* vol. 170, p. 154820, 2023.

[43] U. Fırat e T. Akgül, «Compressive beamforming for direction-of-arrival estimation of cyclostationary propeller noise,» *Signal Processing,* vol. 214, p. 109221, 2024.

[44] J. P. D. Okitadiowo, A. Lay-Ekuakille, T. Isernia e A. Massaro, «Design of a beamforming antenna sensor for environmental noise detection to discriminate vehicle emission according to road conditions,» *Measurement: Sensors,* vol. 23, p. 100389, 2022.

[45] H. K.-c. Ho, T. Kah-chye e A. Nehorai, «Estimating Directions-of-Arrival of Completely and Incompletely Polarized Signals with Electromagnetic Vector Sensors,» *IFAC Proceedings Volumes,* vol. 30, n. 11, pp. 513-518, 1997.

[46] A. Bakhtiar, Karim e H. K. Ali, «A novel beamforming technique using mmWave antenna arrays for 5G wireless communication networks,» *Digital Signal Processing,* vol. 134, p. 103917, 2023.

[47] A. Bakhtiar, Karim e H. K. Ali, «Computationally efficient MUSIC based DOA estimation algorithm for FMCW radar,» *Journal of Electronic Science and Technology,* vol. 21, n. 1, p. 100192, 2023.

[48] Y. Yue, Z. Wu, S. Wang, L. Wan, P. Wang, X. Yang, Y. Cui, K. Zhang e L. Deng, «Identification and extraction of lateral target signals in tunnel geological prediction with the Karhunen-Loéve beamforming method,» *Journal of Applied Geophysics,* vol. 217, p. 105167, 2023.

[49] M. Karimi e L. Maxit, «Acoustic source localisation using vibroacoustic beamforming,» *Mechanical Systems and Signal Processing,* vol. 199, p. 110454, 2023.

[50] S. Seoni, G. Matrone, M. Kristen e Meiburger, «Texture analysis of ultrasound images obtained with different beamforming techniques and dynamic ranges – A robustness study,» *Ultrasonics,* vol. 131, p. 106940, 2023.

[51] C. Zizheng, M. Qian, A. B. Smolders, Y. Jiao, J. Michael, C. O. Wan, W. Hequan e A. M. J. Koonen, «Advanced Integration Techniques on BroadbandMillimeter-Wave Beam Steering for5G Wireless Networks and Beyond,» *IEEE JOURNAL OF QUANTUM ELECTRONICS,* vol. 52, p. 0600620, 2016.

[52] J. Wang, Q. Feng, R. Wu e Z. Su, «A constant-beamwidth beamforming method for acoustic imaging,» *Antennas and Propagation International Symposium, IEEE,* pp. 9-15, 2007.

[53] C. Albaladejo, P. Sánchez, A. Iborra, F. Soto, J. López e R. Torres, «Wireless sensor networks for oceanographic monitoring: a systematic review,» *Sensors,* vol. 10, pp. 6948-6968, 2010.

[54] P. Vergallo, A. Lay-Ekuakille, N. I. Giannoccaro, A. Massaro, S. Urooj, D. Caratelli e A. Trabacca, «Processing EEG signals through beamforming techniques for seizure diagnosis,» in *ICST 2012, 6th International Conference on Sensing Technology*, Kolkata, India, 2012.

[55] M. G. D. Giorgi, A. Ficarella e A. Lay-Ekuakille, «Monitoring cavitation regime from pressure and optical sensors: comparing methods using wavelet decomposition for signal processing,» *IEEE Sonsor Journal,* vol. 15, pp. 4684-4691, 2015.

[56] P. John, M. Supriya e P. S. Pillai, «Cost effective sensor buoy for ocean environmental monitoring,» *Proceedings of the MTS/IEEE Oceans Conference,* pp. 1-5, 2010.

[57] A. Lay-Ekuakille, P. Vergallo, D. Saracino e A. Trotta, «Optimizing and post processing of aSmart beamformer for obstacle retrieval,» *IEEE Sensor Jouenal,* vol. 12, pp. 1294-1299, 2012.

[58] N. I. Giannoccaro, L. Spedicato, A. Messina e A. Lay-Ekuakille, «Ultrasonic visibility tests and estimation of specular target plane orientation through a robotic scanning,» in *IEEE SSD*, Castelldefels-Barcelona, Spain, 2014.

[59] A. K. Sharma, M. Sharma, A. K. Sharma, M. Sharma e M. Sharma, «Mapping the impact of environmental pollutants on human health and environment: A systematic review and meta-analysis,» *Journal of Geochemical Exploration,* vol. 255, p. 107325, 2023.

[60] J. Wang, M. Agrawala e M. F. Cohen, «Soft scissors: An interactive tool for realtime high quality matting,» *34th Annual Meeting of the Association for Computing Machinery's Special Interest Group on Graphics; San Diego, CA,* p. 70691, 5-9 August 2007.

[61] M. Merenda, F. G. Praticò, R. Fedele, R. Carotenuto e F. G. D. Corte, «A Real-Time Decision Platform for the Management of Structures and Infrastructures,» *Electronics,* vol. 8, p. 1180, 2019.

[62] N. Sengupta, M. Sahidullah e G. Saha, «Lung sound classification using cepstral-based statistical features,» *Computers in Biology and Medicine,* vol. 75, pp. 118-129, 2016.

[63] W. J. Song e C. Dong-Jin, «Signal-processing-based characterization of thermoacoustic coupling in a lean premix swirling gas turbine combustor,» *International Communications in Heat and Mass Transfer,* vol. 147, p. 106954, 2023.

[64] K. Ma, A. Chang'an, A. Zhan e F. Yang, «Corrigendum to "Multi-classification of arrhythmias using ResNet with CBAM on CWGAN-GP augmented ECG Angular Summation Field,» *Biomedical Signal Processing and Control,* vol. 77, p. 103834, 2022.

[65] M. H. e Hayes, Statistical Digital Signal Processing and Modeling, John Wiley & Sons Inc, 1996.

[66] J. Xin, Q. Zhu, G. Liang e T. Zhang, «Performance Analysis of D2D Communication with Retransmission Mechanism in Cellular Networks,» *Applied Sciences,* vol. 10, p. 1097, 2020.

[67] S. Akoum e R. W. Heath, «Interference coordination: random clustering and adaptive limited feedback,» *IEEE Transactions on Signal Processing,* vol. 61, p. 1822–1834, 2018.

[68] J. Zhang, X. Cui, H. Xu e M. Lu, «A tractable approach to coverage and rate in cellular networks,» *IEEE Transactions on Communication,* vol. 59, n. 11, p. 3122–3134, 2011.

[69] M. C. Erturk, S. Mukherjee, H. Ishii e H. Arslan, «Distributions of transmit power and SINR in device-to-device networks,» *IEEE Communications Letters,* vol. 17, n. 2, p. 273–276 , 2012.

[70] H. ElSawy, E. Hossain e M.-S. Alouini, «Analytical modeling of mode selection and power control for underlay D2D communication in cellular networks,» *IEEE Transactions on Communications ,* vol. 62, pp. 4147–4161, , , 2014.

[71] J. Zhang, X. Cui, H. Xu e M. Lu, «A Two-Stage Interference Suppression Scheme Based,» *Sensors MDPI,* vol. 19, p. 3870, 2019 .

[72] Y. Z. Cui, Z. Xu e J. Lu, « A Two-Stage Interference Suppression Scheme Based on Antenna Array for GNSS Jamming and Spoofing,» *Sensors,* vol. 3870, p. 19, 2019.

[73] O. Sharifi-Tehrani, M. F. Sabahi e M. Danaee, «Null broadened–deepened array antenna beamforming for GNSS jamming mitigation in moving platforms,» *ICT Express,* vol. 8, pp. 161-165, 2022.

[74] C. Fernande-Prades, J. Arribas e P. Closas, «Robust GNSS receivers by array signal processing: theory and implementation,» *Proc. IEEE,* vol. 104, p. 1207–1220, 2016.

[75] L. Huang, Z. Lu, Z. Xiao, C. Ren, J. Song e B. Li, «Suppression of Jammer Multipath in GNSS Antenna Array Receiver,» *Remote Sens,* vol. 14, p. 350, 2022.

[76] H. Kaibin, J. G. Andrews, G. Dongning, J. Heath e R. A. Berry, «Spatial interference cancellation for multiantenna mobile ad hoc networks,» *IEEE Transactions on Information Theory,* vol. 58, p. 1660–1676, 2012.

[77] Y. Jian, Z. Yue, B. Qinlong e C. Zengping, «Frequency Broadband Signal MVDR Adaptive Beamforming Method and Application,» in *2nd International Conference on Signal Processing Systems (ICSPS)*, 2010.

[78] L. Thalluri, V. N. V. Sai-Divya e P. Gone, «Deepthi, Optimized Beam Forming by Using LCMV, MVDR and PSO for Advanced 5G Applications,» in *International Conference of Advance Research & Innovation (ICARI)*, January 19, 2020 .

[79] R. M. Maina, P. K. Lang e P. K. Kihato, «Collaborative beamforming in wireless sensor networks using a novel particle swarm optimization algorithm variant,» *Heliyon,* vol. 7, p. 08247, 2021.

[80] M. Khodier e G. Saleh, «Beamforming and power control for interference reduction in wireless communications using particle swarm optimization,» *AEU - International Journal of Electronics and Communications,* vol. 64, pp. 489-502, 2010 .

[81] N. N. Van, «Optimal Interference for Device-to-Device Communication Underlaying Cellular Network,» *Journal of Communications ,* vol. 3, p. 17, 2022.

[82] O. A. Amodu, M. Othman, N. K. Noordin e I. Ahmad, «Transmission capacity analysis of relay assisted D2D cellular networks with interference cancellation,» *Ad Hoc Networks,* vol. 117, p. 102400, 2021.

[83] J. Han, B. P. Ng e M. Hwa, «Adaptive orientational beamforming techniques for narrowband interference rejection,» *Signal Processing,* vol. 196, p. 108495, 2022.

[84] J. Xin, Q. Zhu, G. Liang e T. Zhang, «Performance Analysis of D2D Communication with Retransmission Mechanism in Cellular Networks,» *Applied Sciences,* vol. 10, p. 1097, 2020.

[85] M. Noura e R. Nordin, «A survey on interference management for Device-to-Device (D2D) communication and its challenges in 5G networks,» *Journal of Network and Computer Applications,* vol. 71, pp. 130-150, 2016.

[86] M. K. Awad, W. M. Baidas, A. A. El-Amine e N. Al-Mubarak, «A matching-theoretic approach to resource allocation in D2D-enabled downlink NOMA cellular networks,» *Physical Communication,* vol. 54, p. 101837, 2022.

[87] A. Massaro, A. Panarese, S. Selicato e A. Galiano, «CNN-LSTM Neural Network Applied for Thermal Infrared Underground Water Leakage,» in *IEEE International Workshop on Metrology for Industry 4.0 & IoT* , 219-224, 2021 .

[88] B. Claudia, C. Casavola, G. Pappalettera, V. P. Kannan e D. K. Mpoyi, «Acoustic Emission and Deep Learning for the Classification of the Mechanical Behavior of AlSi10Mg AM-SLM Specimens,» *Applied Sciences ,* vol. 13, p. 189, 2023.

[89] A. K. Rahmati, S. K. Setarehdan e B. N. Araabi, «A PCA/ICA based Fetal ECG Extraction from Mother Abdominal Recordings by Means of a Novel Data-driven Approach to Fetal ECG Quality Assessment,» *J Biomed Phys Eng,* vol. 7, pp. 37-50, 2017.

[90] N. Widatalla, A. Khandoker, M. Alkhodari, K. Koide, C. Yoshida, Y. Kasahara, Y. Kimura e M. Saito, «Similarities between maternal and fetal RR interval tachograms and their association with fetal development,» *Front Physiol ,* vol. 13, p. 21, 2022.

[91] J. Zöllkau, E. M. Dölker, A. Schmidt, U. Schneider e D. Hoyer, «Dependencies between maternal and fetal autonomic tone,» *J Perinat Med,* vol. 24 , pp. 323-330, 2019.

[92] A. Schmidt, R. Witte, L. Swiderski, J. Zöllkau, U. Schneider e D. Hoyer, «Advanced automatic detection of fetal body movements from multichannel magnetocardiographic signals,» *Physiol Meas,* vol. 40, p. 085005, 2019.

[93] L. E. May, R. R. Suminski, A. Berry, M. .. Langaker e K. M. Gustafson, «Maternal physical activity mode and fetal heart outcome,» *Early Hum Dev,* vol. 65, p. 90, 2014 .

[94] R. Li, M. G. Frasch e H. T. Wu, «Efficient Fetal-Maternal ECG Signal Separation from Two Channel Maternal Abdominal ECG via Diffusion-Based Channel Selection,» *Front Physiol ,* vol. 16, p. 277, 2017.

[95] L. Su e H. T. Wu, «Extract Fetal ECG from Single-Lead Abdominal ECG by De-Shape Short Time Fourier Transform and Non local Median,» *Front. Appl. Math. Stat,* vol. 10, p. 338, 2017.

[96] N. Arunkumar, K. Ramkumar, V. Venkatraman, E. Abdulhay, S. L. Fernandes, S. Kadry e S. Segal, «Classification of focal and non-focal EEG using entropies,» *Pattern Recogn. Lett,* vol. 94, p. 112–117, 2017.

[97] K. Ashima, K. Padmavati e T. Chand, «A comparative analysis of signal processing and classification methods for different applications based on EEG signals,» *Biocybernetics and Biomedical Engineering,* vol. 40, pp. 649-690, 2020.

[98] D. Labate, F. L. Foresta, G. Occhiuto, F. C. Morabito, A. Lay-Ekuakille e P. Vergallo, «Empirical Mode Decomposition vs. Wavelet Decomposition for the Extraction of Respiratory Signal From Single-Channel ECG: A Comparison,» *IEEE Sensors Journal,* vol. 13, pp. 2666-2674, 2013.

[99] P. Gupta, K. K. Sharma e S. D. Joshi, «Fetal heart rate extraction from abdominal electrocardiograms through multivariate empirical mode decomposition,» *Comput. Biol. Med,* vol. 11, p. 1016, 2016.

[100] S. L. Lima-Herrera, C. Alvarado-Serrano e H. R. Rodriguez, «Fetal ECG extraction based on adaptive filters and Wavelet Transform: Validation and application in fetal heart rate variability analysis,» in *13th International Conference on Electrical Engineering, Computing Science and Automatic Control (CCE)*, 2016.

[101] N. Siti, R. U. Partan, W. Caesarendra, T. Dewi, M. N. Rahmatullah, A. Darmawahyuni, V. Bhayyu e F. Firdaus, «An Automated ECG Beat Classification System Using Deep Neural Networks with an Unsupervised Feat,» *Applied Sciences,* vol. 14, p. 2921, 2019 .

[102] B. Widrow, «Adaptive noise cancelling: Principles and applications,» *Proceedings of the IEEE,* vol. 63, pp. 1692-1716, 1975 .

[103] J. D. Bie, I. Diemberger e J. Mason, «Comparison of PR, QRS, and QT interval measurements by seven ECG interpretation programs,» *Journal of Electrocardiology,* vol. 63, pp. 75-82, 2020.

[104] J. D. Bie, I. Diemberger e I. W. Mason, «Comparison of PR, QRS, and QT interval measurements by seven ECG interpretation programs,» *Journal of Electrocardiology,* vol. 63, pp. 75-82, 2020.

[105] S. Pratik, P. Gayadhar e S. Shahnawazuddin, «Denoising of ECG signal by non-local estimation of approximation coefficients in DWT,» *Biocybernetics and Biomedical Engineering,* vol. 37, pp. 599-610, 2017.

[106] Z. Guimei, S. Yuwei e C. Chen, «Height Measurement with Meter Wave Polarimetric MIMO Radar: Signal Model and MUSIC-like Algorithm,» *Signal Processing,* vol. 190, pp. 165-1684, , 202.

[107] A. Jitendra, I. McCowan e B. Hervé, «Speech/music segmentation using entropy and dynamism features in a HMM classification framework,» *Speech Communication,* vol. 40, pp. 351-363, 2003.

[108] D. C. Bradley, D. Cadman e N. J. Milner, «Ecological indicators of the effects of abstraction and flow regulation and optimisation of flow releases from water storage reservoirs. Project WFD21d Final Report SNIFFER, Edinburgh,» 2012. [Online]. Available: https://www.wfduk.org/sites/default/files/Media/Assessing%20the%20status%20of%20the%20water%20environment/WFD21D%20Final%20Report_30%2008%2012.pdf. [Consultato il giorno 8 February 2022].

[109] M. Rinaldi, B. Belletti, W. V. d. Bund, W. Bertoldi, A. Gurnell, T. Buijse e E. Mosselman, «Review on eco-hydromorphological methods. Deliverable of the EU FP7 REFORM project,» 2013. [Online]. [Consultato il giorno 8 February 2022].

[110] M. 3. Sivapalan, K. Takeuchi, S. Franks, V. Gupta, H. Karambiri, V. Lakshmi, X. Liang, J. J. McDonnell, E. M. Mendiondo, P. E. O'Connell, T. Oki, J. W. Pomeroy, D. Schertzer, S. Uhlenbrook e E. Zehe, «IAHS Decade on Predictions in Ungauged Basins (PUB) 2003-2012: Shaping an exciting future for the hydrological sciences,» *Hydrolog Sci J ,* vol. 48, pp. 857-880, 2003.

[111] M. Fiorentino, D. Carriero, V. Lacobellis, S. Manfreda e I. Portoghese, «MEDCLUB - starting line and first activities. In: Predictions in Ungauged Basins: Promises and Progress,» *Wallingford UK,* vol. 2006, pp. 463-476, 2006.

[112] A. U. Sorman e M. J. Abdulrazzak, «Infiltration-recharge through wadi beds in arid regions,» *Hydrolog Sci J ,* vol. 38, pp. 173-186, 2013.

[113] I. Shentsis e E. Rosenthal, «Recharge of aquifers by flood events in an arid region,» *Hydrol Process,* vol. 17, pp. 695-712, 2003 .

[114] J. J. D. Vries e I. Simmers, «Groundwater recharge: an overview of processes and challenges,» *Hydrogeol J,* vol. 10, pp. 5-17, 2002 .

[115] B. R. Scanlon, R. W. Healy e P. G. Cook, «Choosing appropriate techniques for quantifying groundwater recharge,» *Hydrogeol J,* vol. 10, pp. 18-39, 2002 .

[116] M. Shanafield e P. G. Cook, «Transmission losses, infiltration and groundwater recharge through ephemeral and intermittent streambeds: A review of applied methods,» *J Hydrol,* vol. 511, pp. 518-529, 2014 .

[117] M. J. Abdulrazzak, «Losses of flood water from alluvial channels,» *Arid Soil Res Rehabil ,* vol. 9, pp. 15-24, 1995.

[118] J. Constantz e C. L. Thomas, «Stream bed temperature profiles as indicators of percolation characteristics beneath arroyos in the middle Rio Grande Basin, USA,» *Hydrol Process ,* vol. 11, pp. 1621-1634, 1997.

[119] A. Lay-Ekuakille, M. A. Ugwiri, V. Telesca, R. Velazquez, G. Passarella e S. Maggi, «Detection of river flow slow-down through sensing system and quasi-real time imaging,» *Flow Meas Instrum ,* vol. 81, p. 102042, 2021 .

[120] A. Lay-Ekuakille, J. P. D. Okitadiowo, M. A. Ugwiri, S. Maggi, R. Masciale e G. Passarella, « Video-Sensing Characterization for Hydrodynamic Features: Particle Tracking-Based Algorithm Supported by a Machine Learning Approach,» *Sensors,* vol. 21, p. 419, 2021.

[121] R. A. Monzingo, R. L. Haupt e T. W. Miller, «Introduction to Adaptive Arrays,» *SciTech Pub. Inc. Raleigh, NC, US ,* p. 544, 2011.

[122] M. Suess, M. Zubler e R. Zahn, «Performance investigation on the high resolution, wide swath SAR system,» in *Proceedings of EUSAR*, Cologne, Germany, 2002, June 4-6, 2002;187–191.

[123] A. Lay-Ekuakille, G. Vendramin e A. Trotta, «Implementation and characterization of a novel acoustic imaging through beamformers for automotive applications,» *Smart Sensors and Sensing Technology; Springer,* vol. 20, 2008.

[124] A. G. Rad, A. Dehghani e M. R. Karim, «Vehicle speed detection in video image sequences using CVS method,» *Int J Phys Sci ,* vol. 5, p. 2555 – 2563, 2010.

[125] M. Devendra e K. Manjunathachari, «DOA estimation of a system using MUSIC method,» in *International Conference on Signal Pro-cessing and Communication Engineering Systems* , Guntur, India, 2015 January 2-3.

[126] A. Lay-Ekuakille, N. Giannoccaro, S. Casciaro, F. Conversano e R. Velazquez, «Modeling and Designing a Full Beamformer for Acoustic Sensing and Measurement,» *Int J Smart Sens Intell Syst ,* vol. 10, pp. 718-734, 2017 .

[127] E. M. A. Ardi, R. M. Shubair e M. E. A. Mualla, «Computationally Efficient High-Resolution DOA Estimation in a Multipath Environment,» *IEE Electron Lett,* vol. 40, p. 908–909., 2004.

[128] P. K. Mvemba, A. Lay-Ekuakille, S. Kidiamboko e M. Z. U. Rahman, «An Embedded Beamformer for a Pid Based-Trajectory Sensing Autonomous Vehicle,» *Metrol Meas Syst ,* vol. 25, p. 561–575, 2018 .

[129] P. Kumar, A. Singhal, S. Mehta e A. Mittal, «Real-time moving object detection algorithm on high-resolution videos using GPUs,» *J Real-Time Image Process ,* vol. 11, p. 93 – 109, 2016 .

[130] A. Abbass, «Estimating vehicle speed using image processing,» *Al-Mansour Journal,* vol. 14, p. 127–140, 2010 .

[131] T. Yardibi, J. Li e P. Stoica, «Nonparametric and sparse signal representations in array processing via iterative adaptive approaches,» in *42nd Asilomar Conference on Signals, Systems and Computers*, Pacific Grove, CA, USA, 26-29 Oct. 2008.

[132] W. Chen, Y. Zhao e J. Gao, «Improved capon beamforming algorithm by using inverse covariance matrix calculation,» in *IET International Radar Conference* , Xi'an, China , 4-16 April 2013, 1–6.

[133] S. Jeon, P. Eun-Yeong, W. Choi, R. Managuli, K. j. Lee e C. Kim, «Real-time delay-multiply-and-sum beamforming with coherence factor for in vivo clinical photoacoustic imaging of humans,» *Photoacoustics,* vol. 15, p. 100136, 2019.

[134] G. Matrone, A. S. Savoia, G. Caliano e G. Magenes, «The delay multiply and sum beamforming algorithm in ultrasound B-mode medical imaging,» *IEEE Trans. Med. Imaging,* vol. 34, pp. 940-949, 2015.

[135] J. Park, S. Jeon, J. Meng, L. Song, J. S. Lee e C. Kim, «Delay-multiply-and-sum-based synthetic aperture focusing in photoacoustic microscopy,» *J. Biomed. Opt,* vol. 21, p. 036010, 2016.

[136] M. L. Li, H. F. Zhang, K. Maslov, G. Stoica e L. Wang, «Improved in vivo photoacoustic microscopy based on a virtual-detector concept,» *Opt. Lett,* vol. 31, pp. 474-476, 2006.

[137] K. Hollman, K. Rigby e M. O'donnell, «Coherence factor of speckle from a multi-row probe,» *IEEE Int. Ultrason. Symp,* vol. 2, pp. 1257-1260, 1999.

[138] N. Ciaranfi, P. Pieri e G. Ricchetti, «Note alla carta geologica delle Murge e del Salento (Puglia Centro Meridionale),» *Mem Soc Geol It ,* vol. 41, pp. 449-460., 1988 .

[139] M. Spizzico, N. Lopez e D. Sciannamblo, «Analysis of the potential contamination risk of groundwater resources circulating in areas with anthropogenic activities,» *Nat Hazards Earth Syst Sci ,* vol. 5, pp. 109-116, 2005 .

[140] M. Tozzi, «Assetto tettonico dell'avampaese apulo meridionale (Murge meridionali - Salento) sulla base di dati strutturali,» *Geol Rom ,* vol. 29, pp. 95-111, 1993.

[141] M. Maggiore e P. Pagliarulo, «Circolazione idrica ed equilibri idrogeologici negli acquiferi della Puglia,» *Geologi e Territorio,* vol. 1, p. 13–35, 2004.

[142] D. Sciannamblo, M. Spizzico, T. Tadolini e R. Tinelli, «Lineamenti idrogeologici della zona umida di Torre Guaceto (Br),» *Geol Rom ,* vol. 30, pp. 754-760., 1994.

[143] R. Masciale, S. Amalfitano, E. Frollini, S. Ghergo, M. Melita, D. Parrone e G. Passarella, «Assessing natural background levels in the groundwater bodies of the Apulia Region (Southern Italy),» *Water ,* vol. 13, p. 958, 2021.

[144] R. W. Herschy, Streamflow Measurement, London UK: 3rd ed.; CRC Press, 2008.

[145] W. M. Organization, «Meteorological Organization Geneva, Switzerland,» [Online]. Available: https://library.wmo.int/doc_num.php?explnum_id=10473 . [Consultato il giorno 8 Feb 2022].

[146] C. Brouwer e M. Heibloem, «Irrigation water management: Irrigation water needs. Train. Man,» [Online]. Available: https://www.fao.org/3/s2022e/s2022e00.htm#Contents . [Consultato il giorno 8 February 2022].

[147] G. H. Hargreaves e Z. A. Samani, «Estimating potential evapotranspiration,» *J Irri. Drain Div ,* vol. 108, pp. 225-230, 1982 .

[148] A. C. Protection, «Hydrological Annals,» [Online]. Available: https://protezionecivile.puglia.it/ . [Consultato il giorno 8 February 2022].

[149] H. B. Mann, «Nonparametric tests against trend,» *Econometrica ,* vol. 13, pp. 245-259, 1945 .

[150] S. Yue, P. Pilon e G. Cavadias, «Power of Mann-Kendall and Spearman's rho tests for detecting monotonic trends in hydro-logical series,» *J Hydrol ,* vol. 259, p. 254–271, 2002 .

[151] D. Zaccaria, G. Passarella e D. R. D. Giordano, «Sandoval-Solis Risk Assessment of Aquifer Salinization in a Large-Scale Coastal Irrigation Scheme, Italy,» *Clean - Soil Air Water,* vol. 44, pp. 371-382., 2016.

[152] A. Doglioni e V. Simeone, «Effects of Climatic Changes on Groundwater Availability in a Semi-arid Mediterranean Region,» in *In: Shakoor, A.; Cato, K. Eds; IAEG/AEG Annual Meeting Proceeding* , San Francisco. California, 2019, 4, 105-110.

[153] I. Portoghese, R. Masciale, M. C. Caputo, L. D. Carlo e D. Malcangio, «Combined Discharge and Thermo-Salinity Measure-ments for the Characterization of a Karst Spring System in Southern Italy,» *Sustainability ,* vol. 12, p. 3311, 2020.

[154] W. M. Organization, «Guide to Hydrological Practices vol. I: Hydrology—From Measurement to Hydrological Information, 6th ed.; WMO No.168; World Meteorological Organization Geneva, Switzerland,» 2008. [Online]. Available:

https://library.wmo.int/doc_num.php?explnum_id=10473 . [Consultato il giorno 8 February 2022].

[155] I. Portoghese, E. Bruno, P. Dumas, N. Guyennon, S. Hallegatte, J. H. Hourcade, H. Nassopoulos, G. Pisacane, M. V. Struglia e M. Vurro, «Impacts of climate change on fresh water bodies: Quantitative aspects In Regional Assessment of Climate Change in the Mediterranean; Navarra, A., Tubiana, L., Eds,» *Springer,* vol. 2, pp. 241-306, 2013.

[156] R. W. Herschy, Streamflow Measurement, London, UK: 3rd ed.; CRC Press, 2008; p. 536.